Climate Data Record (CDR) Program

Climate Algorithm Theoretical Basis Document (C-ATBD)

Total Solar Irradiance and Solar Spectral Irradiance

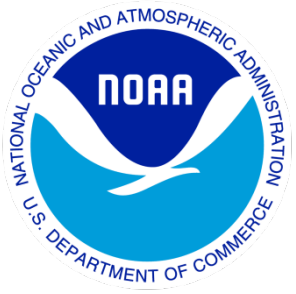

CDR Program Document Number: CDRP-ATBD-0612
Configuration Item Number: 01B-32, 01B-33
Revision 3 / September 09, 2024

REVISION HISTORY

Rev.	Author	DSR No.	Description	Date
1	Odele Coddington, LASP Judith Lean, NRL	DSR-788	Initial Submission to CDR Program	04/07/2015
2	Odele Coddington, LASP Judith Lean, NRL	DSR-1171	Revised Submission to CDR Program, accompanying v02r01 release; affects solar irradiance estimates prior to 1976.	06/15/2017
3	Odele Coddington & Judith Lean, LASP	DSR-1970	Revised Submission to CDR Program, accompanying V03 release	09/09/2024

TABLE of CONTENTS

1. INTRODUCTION 8
1.1 Purpose 8
1.2 Definitions 9
1.3 Referencing this Document 10
1.4 Document Maintenance 10

2. OVERVIEW OF SOLAR IRRADIANCE CLIMATE DATA RECORD 13
2.1 Products Generated 13
2.2 Instrument and Model Characteristics 15

3. ALGORITHM DESCRIPTION 18
3.1 Algorithm Overview 18
3.2 Processing Outline 18
3.3 Algorithm Input 22
3.3.1 Primary Input Data 22
3.3.2 Ancillary Data 26
3.3.3 Derived Data 28
3.3.4 Forward Models 32
3.4 Theoretical Description 32
3.4.1 Physical and Mathematical Description 41
3.4.2 Data Merging Strategy 45
3.4.3 Numerical Strategy 46
3.4.4 Calculations 46
3.4.5 Look-Up Table Description 46
3.4.6 Parameterization 46
3.4.7 Algorithm Output 46

4. TEST DATASETS AND OUTPUTS 51
4.1 Test Input Datasets 51
4.2 Test Output Analysis 55
4.2.1 Reproducibility 55
4.2.2 Precision and Accuracy 55
4.2.3 Error Budget 55

5. PRACTICAL CONSIDERATIONS 62
5.1 Numerical Computation Considerations 62
5.2 Programming and Procedural Considerations 62
5.3 Quality Assessment and Diagnostics 62
5.4 Exception Handling 63
5.5 Algorithm Validation 63
5.6 Processing Environment and Resources 68

6. ASSUMPTIONS AND LIMITATIONS 69

6.1 Algorithm Performance 72
6.2 Sensor Performance 72

7. FUTURE ENHANCEMENTS 75
7.1 Enhancement 1: Improved Facular Brightening Index 75
7.2 Enhancement 2: Improved Model Formulation 76
7.3 Enhancement 3: Improved Exception Handling 76
7.4 Enhancement 4: Improved Quality Flagging 76

8. REFERENCES 78

APPENDIX A. ACRONYMS AND ABBREVIATIONS 83

LIST of FIGURES

Figure 1: Flow diagram of the algorithm processing. 22

Figure 2: Solar white light images made by the GONG instrument at the Big Bear Solar Observatory during solar cycle maximum in 2002 (left) and during solar cycle minimum in 2009. In the bottom panels, the intensity of each pixel is plotted as a function of the radial position of that pixel from disk center... 23

Figure 3: Sunspot darkening indices calculated from six difference GONG sites. 24

Figure 4: Time series of the DRAO Penticton F10.7 cm solar radio flux (proxy of coronal facular brightening), the bolometric facular brightening composite and the bolometric sunspot darkening composite (inverted to be shown as a positive value) as input to the algorithm during the space-era. ... 26

Figure 5: As in Figure 2 but during solar rotation during a period of high solar activity. 26

Figure 6: The adopted baseline reference spectra of the CDR V3 (NNLSSI1) and CDR V2 (NRLSSI2) irradiance variability models and their wavelength-dependent absolute and relative differences. 27

Figure 7: Shown are the model scaling coefficients that convert changes in the bolometric facular brightening and sunspot darkening functions and the F10.7 cm solar radio flux to SSI change, in energy units. 27

Figure 8: Total solar irradiance reconstructed with the NNLTSI1 model algorithm (upper), and the corresponding bolometric facular and sunspot contributions to the total solar irradiance variations (lower). The reference baseline total solar irradiance is 1361.2549 W m^{-2}. 29

Figure 9: An example solar spectral irradiance spectrum from 115-500 nm calculated by the NNLSSI1 model in 1- nm bins (purple) and the high-resolution NNLSSI1h model, after the online algorithm normalizing has been applied to scale the high-resolution output to the match the irradiance scale and variability of the higher accuracy NNLSSI1 output (green). 29

Figure 10: As in Figure 8 but for solar spectral irradiance reconstructed with the NNLSSI1 model algorithm. Shown are time series of SSI in eight broad bands spanning the full spectral range of the model output from the far ultraviolet through the far-infrared. The reference baseline solar spectrum is shown in Figure 6. 30

Figure 11: The wavelength-dependence of solar cycle energy change (shown as a percentage) between moderately high activity levels in June 2023 and low solar activity levels in December 2019 as estimated by the NNLSSI1 and NNLSSI1h models. 31

Figure 12: Comparison of solar rotational variability in TSIS-1 SIM measurements and the NRLSSI2 and NNLSSI1 models over the same 3 year period. 37

Figure 13: Shown in the upper panel are daily values of the bolometric facular index, in the middle panel of the bolometric sunspot index and in the bottom panel their respective uncertainties, since 1874. 40

Figure 14: Shown in the upper panel are annual values of the bolometric facular index, in the middle panel of the bolometric sunspot index and in the bottom panel their respective uncertainties, since 1610. 40

Figure 15: Projections of TSI and bolometric facular brightening and sunspot darkening indices (blue curves) are shown from 2023 to 2100, compared with the observations (red curves) from 1980 to 2023. The assumed period of the Schwabe cycle is 10.9 years; grey lines indicate uncertainties associated with Schwabe cycle periods from 10.7 to 11.1 years. 41

Figure 16: Comparison of NNLTSI1 total solar irradiance variations calculated by the algorithm with the earlier NRLTSI2 model of the Solar Irradiance CDR V02. At bottom is the residual difference between the datasets, after NRLTSI2 output is scaled to the more accurate NNLTSI1 level during solar minimum conditions in December 2019. NRLTSI2 scaling factor is listed in the plot title. 52

Figure 17: As in Figure 16, but for the period 1880-2023 and after 365-day smoothing applied to each data set to highlight the solar cycle variability. 52

Figure 18: As in Figure 16 but for comparisons of NNLSSI1 solar spectral irradiance variation calculated by the algorithm and binned in selected broad wavelength bands with the earlier model, NRLSSI2. On the left are the time series in energy units. On the right are the residual differences between NNLSSI1 and NRLSSI2 (after NRLSSI2 offsets as listed in the subtitles); the mean and standard deviation of the residual differences from 1978-2023 are listed on each plot. 53

Figure 19: As in Figure 18, but for the period 1880-2023 and after 365-day smoothing applied to each data set to highlight the solar cycle variability. 54

Figure 20: Examples of NNLTSI1 total solar irradiance variations and estimated uncertainties in the relative changes (i.e., excluding the ±0.27 W m^{-2} uncertainty in the total solar irradiance absolute scale) that the algorithm calculates during epochs of high solar activity (left) and moderate solar activity (right). 57

Figure 21: Wavelength dependence of percent uncertainties of the facular brightening and sunspot darkening coefficients, that the algorithm uses to calculate solar spectral irradiance variability. 59

Figure 22: NNLSSI1 modeled solar spectral irradiance change typical of high solar activity and percentage uncertainties. Uncertainties shown are relative and exclude the additional uncertainty in the solar spectral irradiance absolute scale. 60

Figure 23: Solar spectral irradiance variations calculated by the algorithm during an epoch of relatively high solar activity for the four wavelengths listed in Table 7. Uncertainties shown are relative. 60

Figure 24: (top) The total solar irradiance time series calculated by the algorithm (NNLTSI1 model), the earlier CDR V2 (NRLTSI2 model), and the original NRLTSI2 model are compared with the CDR V3 TSI observational composite comprised of the LASP TSI composite since 2003 and the PMOD composite prior to 2003 after adjustment to the absolute irradiance scale of the LASP TSI composite. The

comparisons are shown on the native scales of the dataset and after normalization to the LASP TSI composite (normalization factors are listed in legend). (bottom) The comparisons are shown during solar rotation at high and moderate activity conditions. 64

Figure 25: Differences in daily total solar irradiance that the algorithm calculates (according to NNLTSI1) with the CDR V3 TSI composite (upper) and the NRLTSI2 model of the CDR V2 (lower). 65

Figure 26: Shown are time series of solar spectral irradiance variations that the algorithm calculates (i.e., the NNLSSI1 model) and binned in broad wavelength bands compared with TSIS SIM (V12) observations from 2022 to 2024. For comparison, also shown are NRLSSI2 model output of the CDR V2. The primary variations are associated with the Sun's 27-day rotation. 66

Figure 27: Shown are the solar spectral irradiance changes during the descending phase of solar cycle 24, in both energy units (upper) and percentages (lower), that the algorithm calculates (using the NNLSSI1 model) from solar minimum at the end of 2019 to high solar activity at the start of 2013, compared with corresponding changes estimated using the NRLSSI2 model. 67

LIST of TABLES

Table 1: Definitions of symbols used in the C-ATBD. 11

Table 2: Solar irradiance products that this CDR provides. 16

Table 3: Structure of the algorithm (NNLTSI1) output of Total Solar Irradiance (TSI). 47

Table 4: Structure of the algorithm (NNLSSI1) output for values of Solar Spectral Irradiance (SSI). 49

Table 5: Structure of the algorithm (NNLSSI1h) output for values of High-resolution Solar Spectral Irradiance (SSI), scaled to NNLSSI1 absolute level and variability. 50

Table 6: Representative quantities and their uncertainties, used to estimate 1-σ relative uncertainties in the daily value of total solar irradiance produced by the algorithm on 30th October 2003, when facular brightening and sunspot darkening values were relatively high. 58

Table 7: Representative quantities and their uncertainties, used to estimate 1-σ uncertainties in daily values of solar spectral irradiance produced by the algorithm on 30th October 2003, when bolometric facular brightening and sunspot darkening indices were relatively high and equal to the values specified in Table 6. 61

Table 8: Summary of assumptions in the theoretical basis for modeled solar irradiance, model inputs and the potential validation approaches. Validation approaches that can be monitored over time (i.e. statistical) to provide an estimate in the uncertainty in the modeled solar irradiance are labeled '*Operational*'. 69

1. Introduction

1.1 Purpose

This document describes the algorithm that is used to create Version 3 of the Total Solar Irradiance and Solar Spectral Irradiance Climate Data Records (CDR), submitted to the National Centers for Environmental Information (NCEI) by Odele Coddington and Judith Lean (Laboratory for Atmospheric and Space Physics, University of Colorado). Also described are the solar activity indices of sunspot darkening, $S(t)$, facular brightening, $F(t)$, and the coronal component of facular brightening, the F10.7 cm solar radio flux, $F_{10.7}(t)$, that are input to the algorithm. The algorithm's calculations of solar irradiance augment direct measurements made by the SOlar Radiation and Climate Experiment (SORCE), Total and Spectral Solar Irradiance Sensor (TSIS-1), the Thermosphere Ionosphere Mesosphere Energetics and Dynamics (TIMED), and Solar Dynamics Observatory (SDO) missions. The actual algorithm is defined by the computer program (code) that accompanies this document. This C-ATBD provides a guide to understanding that algorithm, from both a scientific perspective and to assist software engineers or end-users to evaluate the code. Two accompanying publications describe in detail the updated NASA NOAA LASP (NNL) (Lean et al., 2024, Earth and Space Science, *in prep*) and the implementation of these updated models that prescribe the CDR V3 (Coddington et al., BAMS, *in prep*). These accompanying publications provide additional descriptions of the algorithms, comparisons with the previous algorithms of the Version 2 Solar Irradiance CDRs, and of the modeled irradiance variability with the current NASA TSIS-1 and TIMED observations and with the earlier SORCE observations that ended in 2020.

The NNL solar irradiance variability models were previously known as the Naval Research Laboratory (NRL) solar irradiance variability models, which have shown great utility over their long history of usage by the Earth science community. The new name reflects the current agency support and evolving heritage of the models.

The first Solar Irradiance CDR, designated v02r00, was submitted to NOAA in 2015. A revision submitted in June 2017, designated v02r01, revised the historical estimates of total and spectral irradiance variability prior to 1976 by inputting a revised sunspot darkening index to the algorithm. This revised sunspot index was determined using a new cross calibration of the current sunspot region observations made by the Solar Observing Optical Network (SOON) with the historical records of the Royal Greenwich Observatory (RGO). The numerical algorithm, and the facular and sunspot indices input to the algorithm after 1976 are the same in v02r01 as in v02r00; the v02r01 revision thus did not affect the Solar Irradiance CDR record of v02r00 after 1976. The v02r01 CDR was updated regularly from 2017 through fall, 2024. More than 20,000 website "hits" of the Solar Irradiance CDR occurred during this period, illustrating the importance of these Climate Data Records to the Earth science research communities.

This C-ATBD describes the procedures, algorithms and input datasets used to construct the new Version 3 of the Solar Irradiance CDR that specifies total solar irradiance and the concurrent solar spectral irradiance variations during recent decades and in historical time periods since 1610. The CDR V3 incorporates new understanding of solar irradiance variability obtained from

measurements and models, extended and advanced since the original submission in 2015. Also described are the output files of daily-, monthly- and annually-averaged solar irradiance, and their validation procedures. The solar irradiance reconstructions that this C-ATBD describes complement the direct measurements made of total (TSI) and spectral solar irradiance (SSI) by the TSIS-1 mission, documented in the separate TSIS ATBD, and the extreme ultraviolet measurements of SSI by the TIMED Solar EUV Experiment (SEE) and SDO Extreme Ultraviolet Variability Experiment (EVE) instruments.

Version 3 of the CDR, designated v03r00, was transitioned to NCEI operations in August 2024; preliminary updates occur quarterly, with final data replacing the preliminary updates following year end. The numerous research advances embodied in v03r00 of the CDR include:

- an expanded spectral range from ~0 nm to 200,000 nm to provide SSI useful for the space weather and space climate, earth chemistry/climate and Sun-Earth system communities
- revised model coefficients derived at wavelengths longer than 115 nm from higher-quality TSIS-1 SSI observations and a longer record of SSI and TSI
- new model coefficients derived at wavelengths shorter than 115 nm from SDO EVE and TIMED SEE observations
- a new absolute irradiance scale for total and spectral irradiance based on TSIS-1 Spectral Irradiance Monitor (SIM), Total Irradiance Monitor (TIM) and the Compact TIM (CTIM) measurement records
- the determination of new bolometric facular and sunspot indices from the separate Geostationary Operational Environment series (GOES) and National Science Foundation (NSF) Global Oscillations Network Group (GONG) operational programs
- revised reconstructions of facular brightness, sunspot darkening and solar irradiance since the seventeenth century Maunder Minimum based on new, improved, magnetic flux transport calculations and a longer composite total solar irradiance record
- a new separate, high spectral resolution (0.1 to 0.5 nm) SSI product between 115 and 500 nm, that is numerically consistent with the standard SSI product in 1-nm bins
- a new TSI observational composite comprising measurements made by TIM instruments on SORCE, the TSI Continuity Transfer Experiment (TCTE), TSIS-1, and CTIM observations on a revised absolute irradiance scale (average of TSIS-1 and CTIM).
- updated modeled solar reference spectra for varying solar activity levels, including the Maunder Minimum period, based on the numerous advances summarized above.
- projections of annual solar total and spectral irradiance from the present to 2100.

1.2 Definitions

Table 1 provides definitions of symbols used in this C-ATBD.

1.3 Referencing this Document

This document should be referenced as follows:

Total Solar Irradiance and Solar Spectral Irradiance - Climate Algorithm Theoretical Basis Document, NOAA Climate Data Record Program CDRP-ATBD-0612 by CDRP Document Manager> Rev. 3 (2024). Available at https://www.ncei.noaa.gov/products/climate-data-records/atmospheric

1.4 Document Maintenance

The algorithm that calculates TSI for the Solar Irradiance Climate Data Record v03r00 (hereafter, the CDR V3) uses coefficients to, firstly, convert the two time-varying operationally produced facular brightening, $F(t)$ and sunspot darkening, $S(t)$, indices to their respective modulations of a reference total solar irradiance value. The linearly-transformed input indices are termed the bolometric facular brightening index, $T_F(t)$, and the bolometric sunspot darkening index, $T_S(t)$. The bolometric facular brightening and sunspot darkening indices specify the change in TSI from a reference value (in units of Watts per square meter, W m^{-2}) due to facular brightening, $T_F(t)$, and sunspot darkening, $T_S(t)$. The bolometric facular brightening and sunspot darkening indices are used to calculate the contributions to TSI variability and the corresponding SSI irradiance changes in 1 nm wavelength intervals from 0 to 200,000 nm. In the wavelength range from 115 nm to 200,000 nm, the CDR V3 algorithm uses wavelength-dependent coefficients to convert the two time-varying bolometric inputs into their wavelength-dependent modulations of a reference solar irradiance spectrum. The SSI for the CDR V3 in the extreme ultraviolet (EUV) (wavelengths shorter than 115 nm) uses wavelength-dependent coefficients to convert *three* time-varying inputs into their wavelength-dependent modulations of the reference solar irradiance spectrum. The three inputs are the bolometric facular brightening index, $T_F(t)$, an 81-day temporally smoothed bolometric facular brightening index, $T_F^{sm}(t)$, and the F10.7 cm solar radio flux, $F_{10.7}(t)$. Faculae contribute strongly to net irradiance change at EUV wavelengths, but sunspots have negligible effect. The bolometric facular index and the F10.7 cm solar radio flux are proxies of chromospheric and coronal faculae emission, and adding the temporally smoothed bolometric facular brightening index has been shown to better reproduce EUV solar cycle change (Lean et al., 2011).

The starting point for the algorithm is a reference (time-invariant) value of total, T_{ref}, and spectral, $I_{ref}(\lambda)$ solar irradiance. In the CDR V3, the magnitude of TSI and SSI in the solar cycle minimum between solar cycles 24 and 25 (specifically, 1-7 December 2019) defines T_{ref} and $I_{ref}(\lambda)$. In the CDR V3, $I_{ref}(\lambda)$ from 115 nm to 200,000 nm is solar line data normalized to the space-based irradiance observed by the high-accuracy TSIS-1 instrument during the 2019 solar cycle minimum and extended with theory to wavelengths not directly observed (Coddington et al., 2021; 2023). At wavelengths from 0 to 115 nm, $I_{ref}(\lambda)$ is determined from the direct NASA EVE and SEE observations in this period. A small wavelength-independent adjustment ensures that the integral of $I_{ref}(\lambda)$ equals the corresponding TSI reference value (Harber et al., Earth and

Space Science, *in prep*) defined (average of TSIS-1 and CTIM TSI). The CTIM flight detectors were used in the re-validation of a new, room-temperature, absolute standard called NACR5 in the LASP total solar irradiance radiometer facility (TRF) against the NIST Primary Optical Watt Radiometer (POWR) in power mode (White et al., 2022). Observed TSIS-1 TSI is within 2-σ uncertainty of the CTIM TSI value. For comparison, the scale of the CDR V2 was defined by total solar irradiance during the 2008-2009 solar minimum (~1360.8 Wm^{-2}), consistent with the SORCE TIM measurements.

The numerical values of the coefficients that determine the TSI modulation imposed by sunspots and faculae, when these features are present on the solar disk, are determined from analysis of variability in extant TSI datasets measured by instruments onboard the SORCE, TCTE, TSIS-1, and CTIM spacecrafts. Similarly, the numerical values of the wavelength-dependent coefficients that determine the corresponding SSI modulation imposed by sunspots and faculae, are determined from analysis of variability in extant SSI datasets measured directly by instruments onboard the NASA TIMED, SDO, SORCE, and TSIS-1 spacecrafts and the relative SSI variability measured by the NASA Aura spacecraft.

Both the reference irradiance values and the coefficients that calculate the irradiance modulation with time are constant values in the algorithm; future updates of these quantities are not expected for approximately another decade, until new information accrues from ongoing TSIS-1 measurements and the follow-on TSIS-2 mission with a planned launch in 2025. For this reason, it is expected that the algorithm will evolve slowly, if at all, and that frequent synchronization will not be needed. The initial version of the Solar Irradiance CDR, v02r00, was provided to the public in 2015 and the first revision, v02r01, in mid 2017. This new version, v03r00, was released in late 2024 and replaces the earlier versions.

Table 1: Definitions of symbols used in the C-ATBD.

Symbol	Definition	Units
t	time	day, month, year
λ	wavelength	nm
$T(t)$	total solar irradiance (TSI) at time t	W m^{-2}
T_{ref}	TSI of the reference (nominally “quiet”) Sun; invariant with time	W m^{-2}
$I(\lambda, t)$	solar spectral irradiance (SSI) at wavelength λ and time t	W m^{-2} nm^{-1}
$I_{ref}(\lambda)$	SSI of the reference (nominally “quiet”) Sun at wavelength λ	W m^{-2} nm^{-1}

$I_{hires}(\lambda, t)$	High spectral resolution (hires) SSI at wavelength λ and time t	W m^{-2} nm^{-1}
$F(t)$	facular brightening index at time t	units of the GOES Mg index
$S(t)$	Bolometric sunspot darkening index at time t	W m^{-2}
$F_{10.7}(t)$	Solar radio flux at 10.7 cm	Solar Flux Units (SFU)
$T_F(t)$	Bolometric change in TSI due to faculae	W m^{-2}
$T_S(t)$	Bolometric change in TSI due to sunspots	W m^{-2}
$T_F^{sm}(t)$	81-day smoothed bolometric facular index	W m^{-2}
F_{ref}	facular brightening index of the reference (invariant) Sun, corresponding to I_{ref} and S_{ref}	units of the GOES Mg index
$F_{10\mathrm{ref}}$	10.7 cm flux reference (invariant) Sun, corresponding to I_{ref} and S_{ref}	Solar Flux Units (SFU)
S_{ref}	sunspot darkening of the reference (invariant) Sun, corresponding to I_{ref} and F_{ref}	Millionths of a solar hemisphere
A_{S}	sunspot area	millionths of solar hemisphere
μ	sunspot location in radial heliocentric coordinates	
$Mg(t)$	The MgII index at time, t, determined as the ratio of core to wing emission in the Mg II Fraunhofer line	units of the GOES Mg index

2. Overview of Solar Irradiance Climate Data Record

2.1 Products Generated

The Solar Irradiance Climate Data Record provides values of the Sun's total and spectral irradiance as functions of time, over different epochs as listed in Table 2. Total solar irradiance, $T(t)$, is the total, spectrally integrated (i.e., bolometric) energy input to the top of the Earth's atmosphere, at a standard (invariant) distance of one Astronomical Unit (1AU) from the Sun. Its units are W m^{-2}. Solar spectral irradiance, $I(\lambda,t)$, is the corresponding spectrum that integrates self-consistently to the total, $T(t)$. Values of solar spectral irradiance are provided in 4,300 (variable width) wavelength bands from 0.5 $\pm$ 0.5 nm to 199,875 $\pm$ 125 nm, in units of W m^{-2} nm^{-1}. A separate high spectral resolution (hires) SSI dataset, $I_{hires}(\lambda,t)$, is also delivered. $I_{hires}(\lambda,t)$ is the spectrum from 115-500 nm at 0.1 to 0.5 nm spectral resolution that is consistent in magnitude and variability with the 1-nm binned $I(\lambda,t)$. Values of $I_{hires}(\lambda,t)$ are provided in 9,700 (variable width) wavelength bands from 115.0125 $\pm$ 0.0125 nm to 499.9 $\pm$ 0.100 nm, in units of W m^{-2} nm^{-1}.

Both direct observations and model calculations contribute to the Solar Irradiance Climate Data record. The Total and Spectral Irradiance Sensor (TSIS-1) is the corresponding observing system that directly measures the total solar irradiance and solar spectral irradiance, beginning in 2018. The predecessor SORCE mission ended in 2020. A separate ATBD describes TSIS-1 (Coddington et al., 2015). The follow-on TSIS-2 mission has a planned 2025 launch and will be accompanied by its own ATBD. Whereas the predecessor CDR V2 specified solar irradiance using the NRLTSI2 and NRLSSI2 models constructed from SORCE observations, CDR V3 utilizes a new NASA NOAA LASP (NNL) solar irradiance variability model constructed primarily from TSIS-1 observations as part of the NASA-funded Solar Irradiance Science Team (SIST).

Version 1 of the NASA NOAA LASP (NNL) total solar irradiance (NNLTSI1) and solar spectral irradiance (NNLSSI1) models (Lean et al., Earth and Space Science, *in prep*) is developed from the SORCE, TCTE, TSIS-1, CTIM, Aura and, at EUV wavelengths, TIMED and EVE databases of solar irradiance observations. The NNLTSI1 and NNLSSI1 models calculate TSI and SSI from two primary and time-varying inputs, the bolometric facular brightening, $T_F(t)$, and bolometric sunspot darkening, $T_S(t)$. At wavelengths above 115 nm NNLSSI1 calculates SSI using $T_F(t)$ and $T_S(t)$ directly. Solar spectral irradiance changes at EUV wavelengths are determined with an updated version of the Naval Research Laboratory (NRL) EUV model (NRLSSI-EUV; Lean et al., 2011) that uses NASA TIMED SEE and SDO EVE solar EUV irradiance observations and both chromospheric and coronal proxies of facular brightening. The three indices used to determine the EUV spectral irradiance are, $T_F(t)$, the F10.7 cm solar radio flux, $F_{10.7}(t)$, and a temporally smoothed bolometric facular index, $T_F^{sm}(t)$; the $F_{10.7}(t)$ component improves the reproduction of observed solar cycle changes in EUV emissions from the Sun's corona (its highly variable outer atmosphere) and $T_F^{sm}(t)$ improves the reproduction of EUV emissions in the upper chromosphere-transition region.

The variability in solar spectral irradiance over the full spectral range from 0 to 200,000 nm is determined by incorporating the output from updated EUV model calculations into the NNLSSI1 model. The hires SSI model, $I_{hires}(\lambda,t)$, is developed from model coefficients determined from the SORCE and Aura databases of solar irradiance observations following Lean et al. (2022) reformulated to input the bolometric facular and sunspot inputs, $T_F(t)$ and $T_S(t)$, and on the new absolute irradiance scale. Specifically, in CDR V3, $I_{hires}(\lambda,t)$ in each 1-nm bin is scaled to ensure consistency with the independently produced NNRLSSI1 model with improved model inputs and improved knowledge of the absolute irradiance scale; hereafter, the hires SSI model is called NNLSSI1h.

In NNLTSI1 and NNLSSI1, the proxy of solar activity used to reconstruct irradiance from 1610 to 1874 is the total magnetic flux, B_{tot}, determined using a flux transport model that inputs varying numbers of bipolar magnetic flux regions, based on sunspot numbers (Wang and Lean, 2021). Understanding and specification of the historical sunspot number time series has improved since 2015, when the prior CDR V2 was implemented. In the past decade, the Sunspot Index and Long-term Solar Observations (SILSO) center released a new version of the sunspot number record (Clette et al., 2016) that differs notably in the years prior to 1882 from the original Hoyt and Schatten sunspot group number (1998) that had been the standard sunspot number record for over 20 years. While the two sunspot records approximately agree in their representations of solar activity after 1882 (except for their absolute scales), prior solar cycles in the SILSO sunspot number have larger amplitudes than in the Hoyt and Schatten group sunspot number (Lean, 2018). In the last decade, various groups have assessed the new Version 2 SILSO sunspot number record relative to the original as well as assessing various approaches for developing composite records of sunspot numbers (e.g., Svalgaard and Schatten, 2016). Current evidence, based on independent proxies of solar activity extracted from cosmogenic isotope records, suggests that the revised Version 2 SILSO sunspot numbers may be too large prior to 1880 (Usoskin et al., 2016). Lean (2018) showed that an arithmetic average of the original Hoyt and Schatten sunspot group number and the revised Version 2 sunspot number compared favorably with the cosmogenic isotope record, but with considerable uncertainties inherent in the early sunspot records. Wang and Lean (2021) used the average of the two sunspot records to determine the total magnetic flux since 1700 that we use in CDR V3, to reconstruct yearly averaged TSI and SSI prior to 1874. From 1610 to 1700 the sunspot numbers are the Hoyt and Schatten group sunspot number, scaled upwards to be consistent with the adopted sunspot number record after 1700.

Because of the societal and policy importance of estimating the magnitude of future terrestrial and space climate change, CDR V3 also projects solar TSI and SSI from the present to 2100. The basis of the projections is statistical specification of the modulation of bolometric faculae and sunspots by the Schwabe and Gleissberg cycles, with average periods near 11 and 100 years, respectively.

The CDR V3 also provides five (time-invariant) “reference” spectra indicative of the Maunder Minimum period, the 1957 Gleissberg and Schwabe cycle maximum, the 2009 Modern Minimum, the next projected Gleissberg and Schwabe cycle maximum in 2057, and the baseline reference quiet Sun SSI spectrum, $I_{ref}(\lambda)$.The reference quiet Sun SSI is based on NASA SDO EVE

and a hybrid reference spectrum that is based on solar line data and TSIS-1 SIM observations, extended to longer wavelengths with theory (Coddington et al., 2021; 2023) (see Section 3.3.2 and Figure 6). The reference spectra are provided in 200000 bins of equal 1 nm width, from 0.5 to 199999.5 nm. The reference quiet Sun TSI is based on an average of TSIS and CTIM observations.

2.2 Instrument and Model Characteristics

The primary solar irradiance observational dataset for the Solar Irradiance Climate Data Record is that measured by the Total and Spectral Solar Irradiance Sensor (TSIS-1), which a separate ATBD document describes (Coddington et al., 2015).

The present document describes the algorithm that calculates total solar irradiance and solar spectral irradiance using the NASA NOAA LASP (NNL) NNLTSI1 and NNLSSI1 models, respectively, developed from direct solar irradiance observations made by the Total Irradiance Monitor (TIM) on the SORCE, TCTE, TSIS-1 and CTIM spacecraft from 2003 to 2023 and the Solar Irradiance Monitor (SIM) on the SORCE and TSIS-1 spacecraft from 2003 to 2023. The EUV extension of the NNLSSI1 model is developed from direct solar irradiance observations made by the NASA TIMED and SDO missions from 2002 to present day. The high-resolution SSI model, NNLSSI1h, is developed from direct solar irradiance observations made by the SORCE Solar Stellar Irradiance Comparison Experiment (SOLSTICE, Rottman, 2000) instrument and relative solar irradiance observations made by the Ozone Monitoring Instrument (OMI) (Deland and Marchenko, 2013) on the Aura mission.

The technical heritage of the NNLTSI1 and NNLSSI1 models are the suite of Naval Research Laboratory (NRL) NRLTSI and NRLSSI solar irradiance variability models developed over the past two decades. These models input faculae and sunspot proxy indicators to calculate the change in SSI relative to an adopted reference spectrum that these features produce, when present on the solar disc. Lean (2000) describes the basic NRL model approach, Lean et al. (2005) update the approach and compare modeled solar irradiance variability modeled with early SORCE observations, Lean and Woods (2010) provide an overview of the NRLTSI and NRLSSI models, Coddington et al., (2016) describes the 2nd generation models transitioned as the Solar Irradiance CDR Version 2 and Coddington et al. (2019) compare the CDR V2 to SORCE and OMI observations and to independent solar irradiance variability models. Lean et al., (2022) describe the high spectral resolution version of the 2nd generation model, Lean et al. (2020) describe the 3rd generation of the NRL models (NRLSSI3 and NRLTSI3), and Lean et al., Earth and Space Science (*in prep*) and Coddington et al., BAMS (*in prep*) describe the latest evolution of these models, NNLTSI1 and NNLSSI1, that are transitioned as the Solar Irradiance CDR V3. As described earlier, to reflect the agency support and evolving heritage of the predecessor Naval Research Laboratory (NRL) models, they are renamed the NASA NOAA LASP (NNL) solar variability models, Version 1.

The total solar irradiance generated by the NNLTSI1 model is directly comparable with daily average values of the total solar irradiance measured by the TSIS-1 TIM instrument after scaling to the LASP TSI composite composed of SORCE, TCTE, TSIS-1, and CTIM TIM observations and at

the absolute scale defined by the average of CTIM and TSIS-1 TIM TSI (Harber et al., Earth and Space Science, *in prep*). The CTIM flight demonstration (https://lasp.colorado.edu/ctim/data) flew a next-generation TIM instrument from mid-2022 to late-2023. TSIS-1 TIM observations agreed with CTIM observations to within 2-σ standard deviation during their period of overlap. The solar spectral irradiance generated by the NNLSSI1 model is directly comparable with daily average values of the improved SIM instrument on the TSIS platform, after adjustment to match the wavelength bins the TSIS SIM measurements are reported on and after adjustment to the reference spectrum absolute level. The SORCE and TSIS-1 SIM instruments have a single dispersive optical element, a prism, and the spectral resolution is therefore a strong function of wavelength related to the geometry of the prism and the optical dispersion of the fused silica prism material (Richard et al., 2020). The measured SIM spectra are interpolated onto 1 nm wavelength bins for developing the NNLSSI1 model coefficients and for comparison against the modeled data.

Table 2: Solar irradiance products that this CDR provides.

Product	**Type**	**Number of Wavelength Bins**	**Time Range**	**Cadence**
Total Solar Irradiance	Observational composite	1	1978-2023	Daily, single file: quarterly updates
Total Solar Irradiance	NNLTSI1 model	1	1874-2023	Daily, monthly files: quarterly updates
Total Solar Irradiance	NNLTSI1 model	1	1610-2023	Annual files: yearly update.
Solar Spectral Irradiance	NNLSSI1 model	4300 (variable width)	1874-2023	Daily, monthly files: quarterly updates
Solar Spectral Irradiance	NNLSSI1 model	4300 (variable width)	1610-2023	Annual files: yearly update
Hires Solar Spectral Irradiance	NNLSSI1h model (normalized to NNLSSI1 scale)	9700 (variable width)	1874-2023	Daily, monthly files: quarterly updates
Hires Solar Spectral Irradiance	NNLSSI1h model (normalized to NNLSSI1 scale)	9700 (variable width)	1874-2023	Annual files: yearly updates
Solar Spectral Irradiance	Reference Spectra	200000 (1 nm width)	Reference baseline, low, moderate, high and Maunder Minimum solar activity	One observation-based reference spectrum of the indicative of the Maunder Minimum period, the 1957 Gleissberg and Schabe cycle maximum, the 2009 Modern Minimum, the next

				projected Gleissberg and Schabe cycle maximum in 2057, and the baseline reference quiet Sun SSI spectrum. Single file, no update cadence
Bolometric facular brightening and sunspot darkening values; F10.7 cm flux	NNL1 model inputs	N/A	1874-2023	Daily, monthly files: quarterly update
Projected annually averaged total and spectral solar irradiance	NNLTSI1 and NNLSSI1 models and flux transport calculations	1 for TSI; 1 each for SSI integrated in these wavelength bands (0-100 nm, 100-200 nm, 200-300 nm, and 300-400 nm)	1610-2100 (projection data since 2024)	Updated annually, if indicated from ongoing comparisons of prior predictions with observations.

3. Algorithm Description

3.1 Algorithm Overview

The Solar Irradiance Data Record algorithm uses the NNLTSI1 and NNLSSI1 models (newly constructed from recent measurements by TIM and SIM on the TSIS-1 mission, as part of NASA's Solar Irradiance Science Team activities), to calculate the total and spectral solar irradiance when supplied with two inputs; the bolometric facular brightening and sunspot darkening functions, each of which varies with time. The facular and sunspot components of total solar irradiance variability are added to a reference value of TSI (the average of CTIM and TSIS-1 TIM TSI for 1-7 December 2019) to produce the Total Solar Irradiance CDR.

The same time-dependent bolometric components are input to the NNLSSI1 model which calculates the solar spectral irradiance changes that accompany the modeled total solar irradiance change. The time-varying F10.7 cm solar radio flux is additionally input to NNLSSI1 to better model the coronal component of EUV irradiance at λ < 115 nm. The spectral facular and sunspot components are then added to a reference spectrum to produce the Solar Spectral Irradiance CDR. The reference spectrum is the HSRS constructed by normalizing solar line data to the irradiance level of TSIS-1 SIM measurements in 1-7 December 2019, extended to EUV wavelengths using EVE and SEE observations. The reference spectrum integrates to the reference TSI value. Solar spectral irradiance is specified in 4,300 variable-width wavelength bins on a wavelength grid from 0.5 to 199,875 nm, such that at any given time the integral over wavelength of the Solar Spectral Irradiance CDR equals the Total Solar Irradiance CDR

Table 2 summarizes the outputs of the CDR V3.

3.2 Processing Outline

Figure 1 is a flow diagram of the overall algorithm processing steps of the total solar irradiance, $T(t)$ and solar spectral irradiance, $I(\lambda,t)$, calculations at a specified time, t. The basic algorithm assumes that bright faculae and dark sunspots present on the solar disc alter the baseline (reference) total solar irradiance, T_{ref}, by amounts $T_F(t)$ and $T_S(t)$, respectively, so that:

$$T(t) = T_{ref} + T_F(t) - T_S(t)$$

where $T_S(t)$ is specified as positive. Similarly, the faculae and sunspots alter the baseline solar spectral irradiance, $I_{ref}(\lambda)$, from 115 to 200,000 nm, $I_F(\lambda,t)$ and $I_S(\lambda,t)$, so that

$$I_{115\,nm}^{200{,}000\,nm}(\lambda,t) = I_{ref}(\lambda) + I_F(\lambda,t) - I_S(\lambda,t)$$

At λ < 115 nm, the sunspot contribution to spectral irradiance change is negligible whereas the facular contribution has both chromospheric, $I_F(\lambda,t)$, and coronal, $I_{F10.7}(\lambda,t)$, components. An additional smoothed chromospheric component, $I_F^{sm}(\lambda,t)$, is shown to better reproduce solar cycle changes in observations of EUV emission from the upper chromosphere-transition region of the solar atmosphere. The NNLSSI1 model determines solar spectral irradiance at λ < 115 nm according to

$$I_{0\ nm}^{115\ nm}(\lambda,t) = I_{ref}(\lambda) + I_F(\lambda,t) + I_F^{sm}(\lambda,t) + I_{F10.7}(\lambda,t).$$

The integrated spectral irradiance from 0 nm to 200,000 nm equals the corresponding total irradiance:

$$T(t) = \int_{\lambda_0}^{\lambda_\infty} I(\lambda,t)\, d\lambda$$

$$T_{ref} = \int_{\lambda_0}^{\lambda_\infty} I_{ref}(\lambda)\, d\lambda$$

The first step in the algorithm is acquiring the solar facular brightening, $F(t)$, and sunspot darkening, $S(t)$, indices and determining from them the corresponding bolometric facular brightening, $T_F(t)$, and sunspot darkening, $T_S(t)$, functions at time, t. These quantities then quantify the changes in total solar irradiance:

$$T_F(t) \propto F(t)$$

$$T_S(t) \propto S(t)$$

The Solar Irradiance CDR is robust to the unavailability of a single model input, but not both, at time, t. In the advent of a missing facular brightening or sunspot darkening index, its value is approximated using the *observed* (by the TSIS-1 mission) total solar irradiance and the available input, i.e.,

$$T_F(t) = T(t) - T_{ref} + T_S(t)$$

and

$$T_S(t) = -\left(T(t) - T_{ref}(t) - T_F(t)\right)$$

The change in total solar irradiance due to faculae and sunspots, $T_F(t)$ and $T_S(t)$, at time, t, are used in conjunction with the *wavelength-dependent* model coefficients to specify incremental changes in solar spectral irradiance from 115 nm to 200,000 nm.

$$I_F(\lambda,t) \propto T_F(t)$$

$$I_S(\lambda,t) \propto T_S(t)$$

At λ < 115 nm, where the sunspot contribution to EUV irradiance change is negligible, the incremental changes in solar spectral irradiance are expressed by three indices, at time, t: facular contribution to TSI change, $T_F(t)$, it's temporally-smoothed value, $T_F^{sm}(t)$, and the F10.7 cm flux, $F_{10.7}(t)$:

$$I_{EUV}(\lambda,t) = I_{ref,EUV}(\lambda) + T_F(t) + T_F^{sm}(t) + F_{10.7}(t)$$

The NNLSSI1 model is constructed such that the facular and sunspot components of the integrated spectral irradiance equal the corresponding facular and sunspot components of total solar irradiance, specifically:

$$T_F(t) = \int_{\lambda_0}^{\lambda_\infty} I_F(\lambda, t)\, d\lambda$$

$$T_s(t) = \int_{\lambda_0}^{\lambda_\infty} I_S(\lambda, t)\, d\lambda$$

An additional model of SSI variability at higher spectral resolution at wavelengths from 115 to 500 nm, denoted NNLSSI1h, uses a separate set of wavelength-dependent model coefficients developed from SORCE SOLSTICE and Aura OMI observations that produce changes in solar spectral irradiance for a given bolometric facular and sunspot input;

$$I_{hires}(\lambda, t) = I_{ref,hires}(\lambda) + I_{F,hires}(\lambda, t) - I_{S,hires}(\lambda, t)$$

To ensure consistent irradiance variability and consistent irradiance magnitude between NNLSSI1h with the more accurate NNLSSI1 model, time- and wavelength-dependent normalization factors, $\psi(\lambda, t)$, are then computed. These normalization factors ensure that the magnitude and variability of $I_{hires}(\lambda, t)$, from 115 to 500 nm after binning into 1-nm bins and at time, *t*, matches the magnitude and variability of $I(\lambda, t)$ of the NNLSSI1 model in the same wavelength bin and at the same time:

$$I_{hires}(\lambda, t) \text{ [binned into 1-nm bins] * } \psi(\lambda, t) = I(\lambda, t)$$

Because the facular and sunspot components of $I(\lambda,t)$ are constructed such that their *integrals* equal the bolometric facular and sunspot components of $T(t)$, as shown above, it follows that facular and sunspot contributions to the variability of the (scaled) $I_{hires}(\lambda, t)$ are similarly consistent, in 1-nm bins, with those components of $I(\lambda,t)$ from λ = 115 to 500 nm:

$$I_{F,hires}(\lambda, t) \text{ [after binning to 1-nm bins]} \propto I_F(\lambda, t)$$

$$I_{S,hires}(\lambda, t) \text{ [after binning to 1-nm bins]} \propto I_S(\lambda, t)$$

The index of facular brightening in the NNLTSI1 and NNLSSI1 models is the space-based Mg II index, obtained by downloading the operational GOES Mg II index available at https://data.ngdc.noaa.gov/platforms/solar-space-observing-satellites/goes/goes16/l2/data/euvs-l2-avg1d_science/. The F10.7 cm solar radio flux is available from the Dominion Radio Astrophysical Observatory (DRAO) near Penticton, Canada at http://www.spaceweather.gc.ca/.

The sunspot darkening index in the NNLTSI1 and NNLSSI1 models is extracted from more than 50 white light solar images per day (approximately 12 images made in the 676.8 nm photospheric Nickel line, near local solar noon at as many as six sites situated around the globe) made by the operational Global Oscillation Network Group (GONG) available at https://gong.nso.edu. In practice, because of the large quantity of data, GONG personnel prepare zipped files of specific images for download. For comparison and quality control, the sunspot darkening index used in the CDR V2 is also constructed using information about the areas, A_S, and locations, μ, of individual sunspot active regions present on the solar disk on any given day as obtained from the Air Force Solar Observing Optical Network (SOON) sites.

Values of the (invariant) total solar irradiance reference level, T_{ref}, and the corresponding solar irradiance reference spectrum, $I_{ref}(\lambda)$, correspond to the minima in solar activity between solar cycles 24 and 25 (specifically, 1-7 December 2019).

Adding the total irradiance increments due to faculae and sunspots to the baseline reference total solar irradiance, T_{ref} , determines the total irradiance at time, $T(t)$. Adding the spectral irradiance increments due to bolometric faculae and sunspots to the baseline reference spectrum in 1-nm bins, I_{ref} , determines the solar spectral irradiance for λ > 115 nm at the same time, $I(\lambda,t)$. For λ < 115 nm, adding the spectral irradiance increments due to bolometric faculae (and its temporally smoothed value) and the F10.7 cm solar radio flux to the baseline reference spectrum determines the solar spectral irradiance at EUV wavelengths for the same time, *t*.

The hires spectral irradiance, computed over a subset of the spectrum between 115 nm and 500 nm, is provided at 9,700 central wavelengths reported every 0.025 nm for λ < 310 nm and every 0.1 nm for λ > 310 nm.

Output files are generated separately for total solar irradiance, solar spectral irradiance, and the hires solar spectral irradiance. The TSI is one daily value per input bolometric facular brightening and sunspot darkening function values. The units are W m^{-2}. The SSI is one daily spectrum per input incremental change in the facular and sunspot contributions to TSI change, and the F10.7 cm flux. The hires SSI is one daily partial spectrum from 115-500 nm per input incremental change in the facular and sunspot contributions to TSI change. The SSI and TSI irradiances have associated uncertainties that are included in the files delivered to NCEI. Uncertainties for the hires SSI, after binning to 1-nm bins, are those of the SSI for the same bin and day. NCEI also archives, in perpetuity, the earlier CDR V2. The LASP LISIRD server continues to provide an additional data access source for V3 of the CDR.

Figure 1: Flow diagram of the algorithm processing.

3.3 Algorithm Input

3.3.1 Primary Input Data

Adopted for the facular brightening index, $F(t)$, is the ratio of the global (disk-integrated) emission in the core of the Mg II Fraunhofer line, from the Sun's chromosphere, to the emission in the wings of the Fraunhofer line, from the Sun's photosphere. Variations in the Mg core-to-wing ratio reflect changes in the chromospheric extensions of photospheric faculae. The ratio of core emission in Fraunhofer lines to emission in the nearby continuum is called the Mg II index; it is a proxy for the bright faculae that alter solar irradiance because the core emission is enhanced in magnetically active bright regions, and the indices are sensitive indicators of the total (net) emission from all bright regions on the solar disk (Skupin et al., 2004; Snow et al., 2005). Furthermore, as the ratio of absolute fluxes, the Mg II index is, in principle, less susceptible to instrumental sensitivity changes that potentially contaminate the temporal fidelity of the facular index time series.

For use in the CDR V3, a composite Mg index, *MgComp*, is constructed by combining cross-calibrated observations from multiple space platforms after 1978, then extending the index

back to 1874 using various ground-based solar records. The Mg II index for the period after 2017 is that measured operationally by the Extreme UltraViolet Sensor (EUVS) instrument on the Geostationary Operational Environmental Satellite (GOES) mission. From 2000 to 2017, the Mg II index is the University of Bremen composite scaled to the GOES EUVS level by the relationship: $Mg_{Bremen\_at\_GOES\_level} = 0.101077 + Mg_{Bremen} * 1.070052$. From 1996 to 2000 the facular index is the chromospheric proxy that Lean et al. (2000) constructed by cross calibrating and combining multiple Mg II datasets, consistent with the analogous Ca II index at 393 nm, scaled to the GOES EUVS level. From 1954 to 1976, the facular brightening time series is constructed from the F10.7 cm solar radio flux (both smoothed and daily values) using a multiple linear regression relationship to the facular brightening composite derived at lags of 0, 27, and 54 days. From 1874 to 1954, the facular brightening time series is constructed from the SILSO V2 sunspot number record (smoothed and daily values) using a multiple linear regression relationship to the facular brightening composite also derived at lags of 0, 27, and 54 days.

The cycle minima of this initial composite facular brightening time series is adjusted prior to 1954 based on a relationship between the composite facular brightening time series since 1954 with updated magnetic flux transport calculations (Wang and Lean, 2021).

The facular brightening time series, *MgComp*, thus constructed, transforms to the bolometric facular index according to,

$$T_F(t) = (MgComp(t) - 0.2629949) * 117.5332052$$

For use in the CDR V3, a composite sunspot darkening index, *S*(*t*), is also constructed from multiple sources. For the period after March 2001, it is the near-noon average intensity reduction of white light images made at 676.8 nm relative to the local emission (which varies from the center of the Sun to the disc limb) reported by all National Solar Observatory (NSO) Global Oscillation Network Group (GONG) stations. Figure 2 shows two GONG images typical of solar maximum (2002) and solar minimum (2009) activity that illustrate the variation in intensity of the disc pixel as a function of the pixel's radial distance from disc center; pixels with reduced intensity are clearly exposed relative to the local emission. Figure 3 compares the sunspot darkening indices over a 6-month period from 6 different GONG sites.

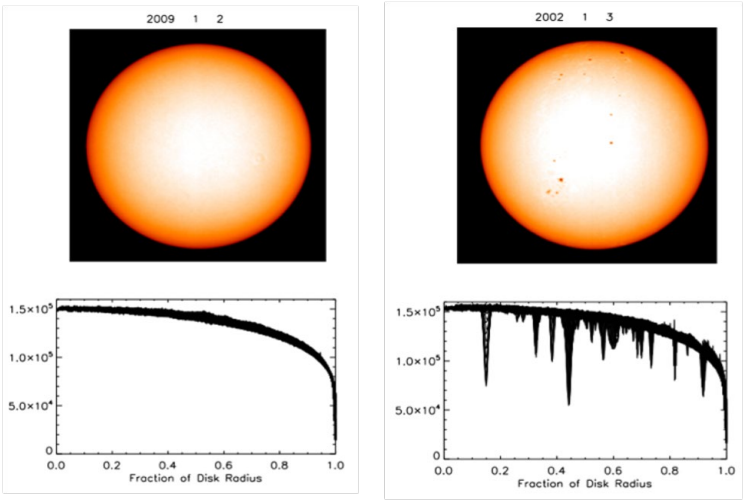

Figure 2: Solar white light images made by the GONG instrument at the Big Bear Solar Observatory during solar cycle maximum in 2002 (left) and during solar cycle minimum in 2009. In the bottom panels, the intensity of each pixel is plotted as a function of the radial position of that pixel from disk center.

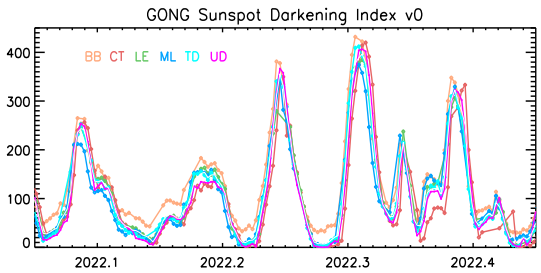

Figure 3: Sunspot darkening indices calculated from six difference GONG sites.

From 1976 to 2001, the sunspot darkening index is derived from direct observations of the areas, A_S, and heliocentric locations, μ, of N_{spot} individual sunspot regions that the Air Force SOON (and other ground- and space-based) sites observe daily as discussed in Lean et al. (1998). The calculation sums the projected area of sunspots on the solar hemisphere visible at Earth and multiplies this by the contrast of sunspots relative to the background (reference) Sun, accounting for variations with limb position on the solar disk. The SOON sunspot darkening index was implemented in the Solar Irradiance CDR v02r00 and CDR V02r01. Prior to 1977, the sunspot darkening is 65% of the value measured by the Royal Greenwich Observatory (RGO). The scaling accounts for systematic area differences between Greenwich and Air Force SOON measurements and is determined by using the sunspot numbers for cross calibration. Summing over all sunspots, the SOON sunspot darkening index for the pre-2001 period is computed as

$$S(t) = \sum_{n}^{N_{spot}} 1.3193[0.2231 + 0.0244 + \log_{10} A_s]A_S\, L(\mu)\mu \times \frac{1}{0.3939}$$

Where

$$L(\mu) = 0.308658 + 0.89026\mu - 0.357926\mu^2 + 0.161633\mu^3$$

and

$$\int_0^1 L(\mu)\mu d\mu = 0.3939$$

The area-dependent sunspot contrast is $1.3193[0.2231 + 0.0244 + log_{10} A_s]$ *and* μ = *cos*(latitude) × *cos*(longitude) is the spot latitude (adjusted for the B_o angle of the Sun's axis to the ecliptic plane) and longitude in heliocentric coordinates. Sunspot darkening values in the pre-2001 period are scaled to merge seamlessly with GONG-derived intensity reductions after 2001.

The following expressions translates the composite sunspot darkening time series, *GONGcomp*, as described above to the bolometric sunspot input quantity,

$$T_S(t) = (GONGcomp(t) - 0.0142832) * 1.0000115$$

The coronal component of the facular brightening index, $F_{10.7}(t)$, is the solar radio flux emission at 10.7 cm measured by ground telescopes and adjusted for the changing distance between the Sun and the Earth to an average distance of 1 astronomical unit (AU). The F10.7 cm solar radio flux is a disk-integrated measure of the Sun's chromospheric emission with added coronal component and has thermal bremsstrahlung and gyrosynchronous emission mechanisms (Tapping, 2013). Therefore, while the F10.7 cm solar radio flux approximately tracks the Mg II

index over the solar cycle, it has larger day-to-day variability than the Mg II index. For the CDR V3, the F10.7 cm solar radio flux since 1947 is the near noon-time observations from the Dominion Radio Astrophysical Observatory (DRAO) near Penticton, Canada (available online from http://www.spaceweather.gc.ca/). Prior to 1 May 2018, the NOAA Space Weather Prediction Center (SWPC) operationally removed radio bursts from the DRAO record by determining if the noon-time value differed by more than 15% from the data values taken shortly before or after noon. If the noon-time value is determined to be affected by radio burst, a different value (either before- or after-noon) is used instead. For all DRAO F10.7 cm solar flux data since 1 May 2018, the Solar Irradiance CDR team operationally removes the radio bursts from the DRAO data by following the NOAA SWPC approach described above. An historical estimate of F10.7 cm solar radio flux for the period from 1874 to 1947 is produced by multiple linear regression of smoothed and daily sunspot numbers (at lags of 0, 27, and 54 days). The cycle minima of this composite F10.7 cm flux time series is adjusted prior to 1947 using a relationship between the cycle minima values of the composite F10.7 cm flux time series after 1947 with cycle minima levels of the Sun's total magnetic flux simulated by a magnetic flux transport model (Wang and Lean, 2021).

Figure 4 shows time series of the bolometric facular brightening and sunspot darkening and the F10.7 cm solar radio flux computed as described above, since 1978, illustrating their evolution during the solar cycle as active regions emerge, evolve, and disappear from the solar disk.

Figure 5 shows variations of these same variables during 2022-2023, illustrating their shorter-term modulation arising from solar rotation, which alters the population of faculae and sunspots on the Sun's disk projected towards the Earth. The Solar Irradiance Climate Data Record algorithm uses these time-varying inputs to parameterize solar irradiance and, therefore, they therefore require careful calculation, validation, and quality-control with possible erroneous values flagged for investigation (see Table 8). For this purpose, all the input indices are routinely compared with various related but independent solar records including the University of Bremen Mg II index (https://www.iup.uni-bremen.de/gome/gomemgii.html), the solar radio flux emission at 3.2, 8, 15, and 30 cm by the Collecte Localisation Satellites (CLS; https://spaceweather.cls.fr/services/radioflux/), the composite Lyman-alpha irradiance time series (Machol et al., 2019) from multiple instruments and models (https://lasp.colorado.edu/data/timed_see/composite_lya/lyman_alpha_composite.nc), and the Mg II index and the Calcium II Potassium (Ca II K) index by the Ozone Monitoring Instrument on the Aura mission (https://sbuv.gsfc.nasa.gov/solar/omi/lisird/readme_omi_index.txt). Additional independent irradiance observations and solar activity indicators used in the Quality Assurance analysis for the Solar Irradiance CDR include the facular and sunspot indices from ground observatory measurements by the San Fernando Observatory (http://www.csun.edu/SanFernandoObservatory/), and the sunspot area, number, and location reports from the Air Force Solar Observing Optical Network (SOON) network stations (http://www.ngdc.noaa.gov/stp/spaceweather.html).

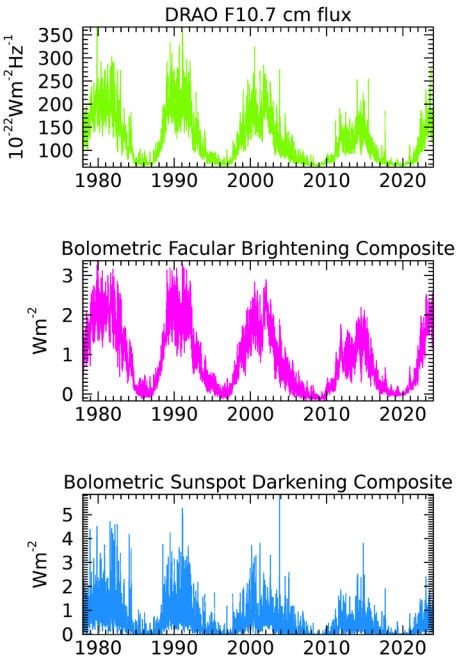

Figure 4: Time series of the DRAO Penticton F10.7 cm solar radio flux (proxy of coronal facular brightening), the bolometric facular brightening composite and the bolometric sunspot darkening composite (inverted to be shown as a positive value) as input to the algorithm during the space-era.

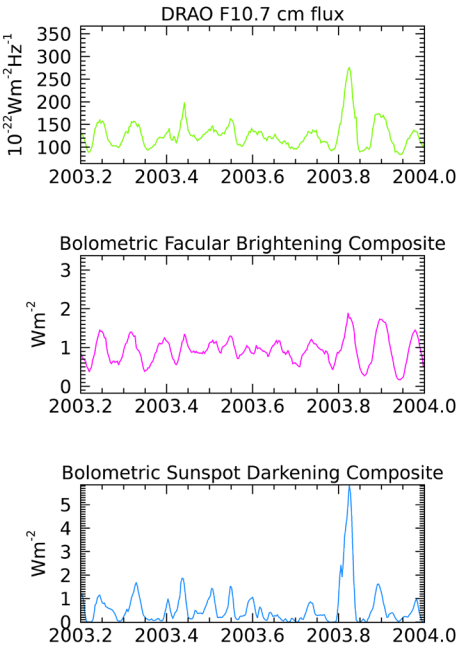

Figure 5: As in Figure 2 but during solar rotation during a period of high solar activity.

3.3.2 Ancillary Data

The algorithm that the Solar Irradiance CDR uses to construct solar spectral irradiance at a given time requires a constant baseline solar spectral irradiance reference spectrum, $I_{ref}(\lambda)$. Figure 6 shows the CDR V3 solar reference spectrum and compares it with the prior CDR V2 reference spectrum. The integral of the reference solar spectral irradiance equals that of the adopted reference total solar irradiance, T_{ref} = 1361.2549 $\pm$ 0.27 Wm^{-2}, which is consistent with the average of direct observations made by CTIM and TSIS-1 TIM in 2019. The T_{ref} is also consistent with the reference TSI value of the CDR V2 (1360.8 $\pm$ 0.5 Wm^{-2}) reported by Kopp and Lean (2011) for the SORCE TIM mission during the extended 2008-2009 solar minimum of the previous solar cycle.

The baseline solar spectral irradiance of the quiet sun (on a 1 nm-binned wavelength grid) composes the TSIS-1 Hybrid Reference Spectrum (HSRS) reference spectrum compiled from TSIS-1 SIM and independent solar line observations (Coddington et al., 2021) and extended from 115-200 nm with SORCE SOLSTICE observations and with theory from 2700 to 200,000 nm (Coddington et al., 2023). The reference spectrum is extended to the shorter extreme ultraviolet wavelength range (from ~ 0 nm to 115 nm) using direct observations made by the

Extreme Ultraviolet Variability Experiment (EVE) on SDO during 2019. A final, additional wavelength-dependent scaling factor adjusts (reduces) the full-spectrum TSIS-1 HSRS from 0 nm to 200 microns by 0.99888 such that its integral equals T_{ref}. Coddington et al. (2021) gives ratios of the TSIS-1 HSRS with other independently acquired solar reference spectra.

Constant wavelength-dependent coefficients, shown in Figure 7, linearly scale the bolometric facular brightening and sunspot darkening functions and the F10.7 cm solar radio flux shown in Figure 4, to produce corresponding irradiance increments that adjust the baseline irradiance, either increasing or decreasing spectral irradiance depending on the wavelength-dependent strengths of the facular and sunspot influences at that time. Irradiance changes at EUV wavelengths, as described above, are estimated from a 3-component model; the EUV coefficients for these three scalings are shown separately in Figure 7. The integral of the facular brightening and sunspot darkening scaling coefficients are equal to 1, and these are the coefficients used to scale incremental change in model inputs to equivalent TSI change. All coefficients are included as part of the algorithm.

A new version of the model may be generated when, and if, the coefficients and/or the input facular and sunspot indices are determined to need revision, based on statistical metrics of additional observations and analysis that indicate significantly improved model performance.

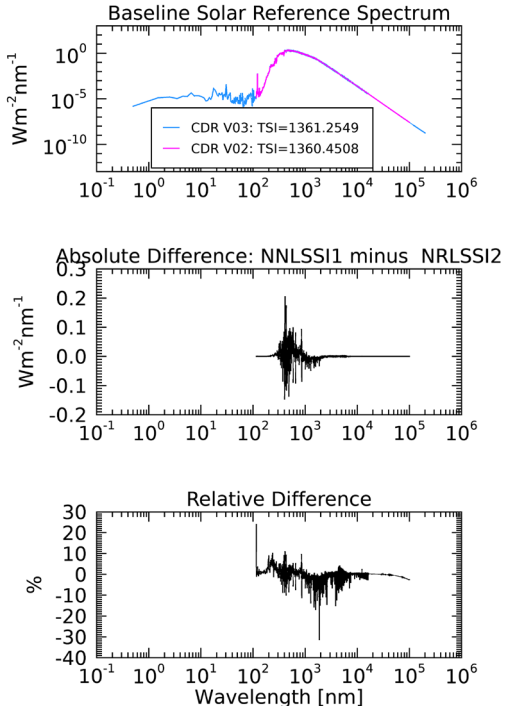

Figure 6: The adopted baseline reference spectra of the CDR V3 (NNLSSI1) and CDR V2 (NRLSSI2) irradiance variability models and their wavelength-dependent absolute and relative differences.

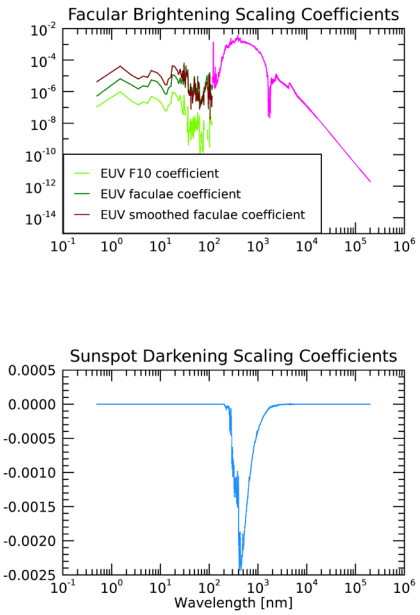

Figure 7: Shown are the model scaling coefficients that convert changes in the bolometric facular brightening and sunspot darkening functions and the F10.7 cm solar radio flux to SSI change, in energy units.

3.3.3 Derived Data

Once the bolometric facular brightening and sunspot darkening inputs are prescribed (as described in Section 3.2), their changes, added to the reference total solar irradiance, determine TSI at time *t*. The facular component of TSI change, plus an 81-day smoothed value of the facular component of TSI, and the F10.7 cm solar radio flux are linearly scaled by wavelength-dependent coefficients to convert them to equivalent changes in solar EUV spectral irradiance. Similarly, the sunspot and facular components of TSI change are linearly scaled by wavelength-dependent coefficients to convert them to equivalent spectral irradiance change at wavelengths longer than 115 nm. The spectral irradiance changes are then added to the baseline (reference) solar spectral irradiance to determine SSI at time *t*. Irradiance changes to the reference spectral irradiance are implemented in 1 nm bins on 0.5 nm grid centers. The 1-nm spectral irradiance thus calculated is then averaged into 4300 wavelength bins of varying width:

1 nm bins on wavelengths grid centers from 0.5 to 749.5 nm	(750 bins)
5 nm bins on wavelength grid centers from 752.5 to 4997.5 nm	(850 bins)
10 nm bins on wavelength grid centers from 5005.0 to 9995.0 nm	(500 bins)
50 nm bins on wavelength grid centers from 10025.0 to 99975.0 nm	(1800 bins)
250 nm bins on wavelength grid centers from 100125.00 to 199875.00 nm	(400 bins)

To determine the corresponding high spectral resolution SSI, NNLSSI1h, a separate set of wavelength-dependent coefficients convert the facular brightening and sunspot darkening indices into equivalent irradiance change in 9,700 central wavelengths reported every 0.025 nm for $\lambda < 310$ nm and every 0.1 nm for $\lambda > 310$ nm. An additional step scales the high-resolution SSI so that its mean value, over 1-nm bins, is equivalent to that of the 1-nm binned SSI product of the NNLSSI1 model. This additional processing step ensures the magnitude and variability of the high spectral resolution SSI, and the 1-nm data products, are self-consistent.

There are no further processing steps; the calculated total, spectral, and high-resolution spectral irradiance are then written to output files in netCDF format. A time series of the output total solar irradiance since 1978 is shown in Figure 8. Figure 9 illustrates the high spectral resolution solar spectral irradiance data compared to the 1-nm NNLSSI1 product on the same day and Figure 10 shows time series of NNLSSI1 binned in broad wavelength bands since 1978. Fig 11 compares percentage of solar cycle energy variability estimated between high and low solar activity levels in the NNLSSI1 and NNLSSI1h products. Because validation of the facular brightening and sunspot darkening inputs are crucial for reliable solar irradiance calculations, a separate file is delivered to the CDR program with the time series of the indices and their bolometric representations (e.g., Figure 4) used in the algorithm to facilitate validation with independent datasets.

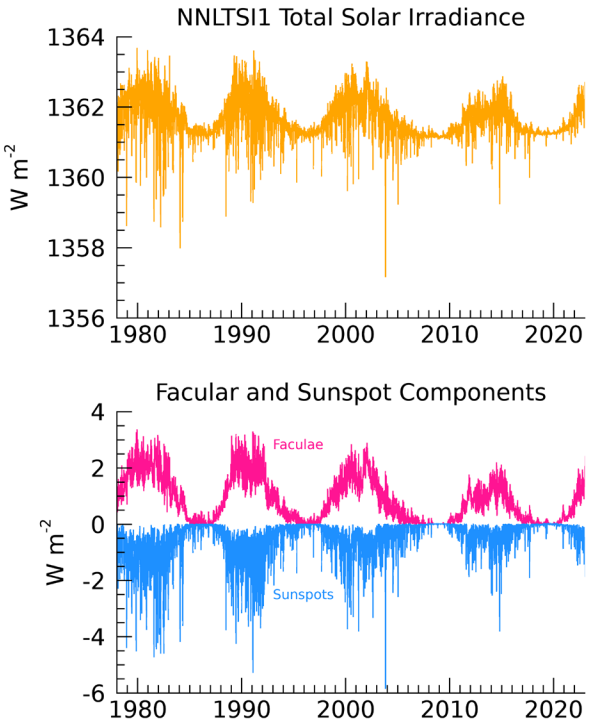

Figure 8: Total solar irradiance reconstructed with the NNLTSI1 model algorithm (upper), and the corresponding bolometric facular and sunspot contributions to the total solar irradiance variations (lower). The reference baseline total solar irradiance is 1361.2549 W m^{-2}.

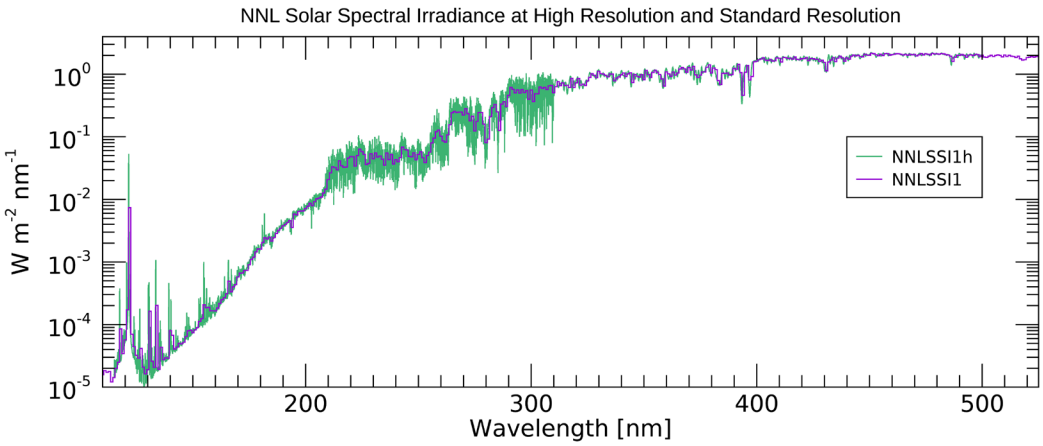

Figure 9: An example solar spectral irradiance spectrum from 115-500 nm calculated by the NNLSSI1 model in 1- nm bins (purple) and the high-resolution NNLSSI1h model, after the online algorithm normalizing has been applied to scale the high-resolution output to the match the irradiance scale and variability of the higher accuracy NNLSSI1 output (green).

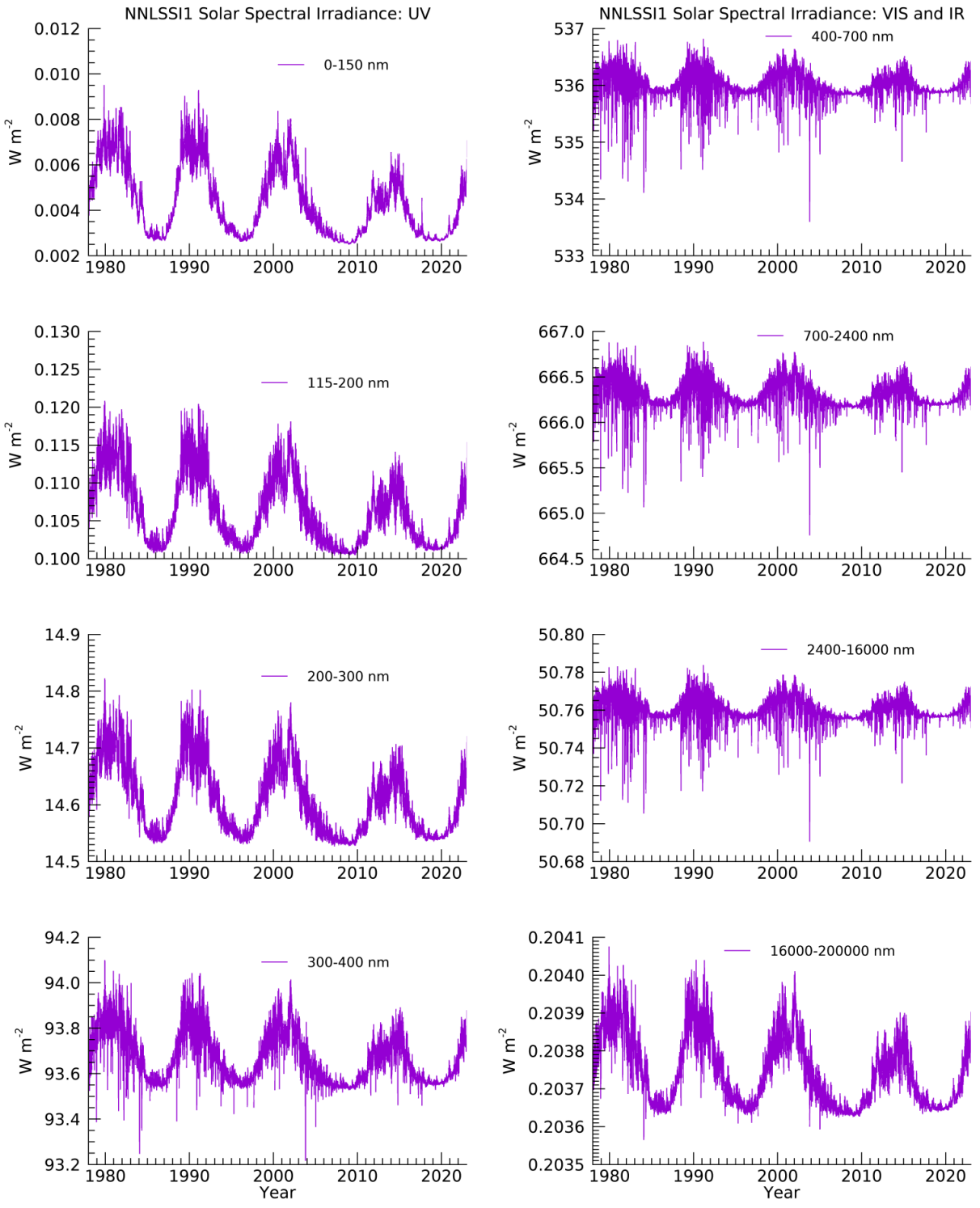

Figure 10: As in Figure 8 but for solar spectral irradiance reconstructed with the NNLSSI1 model algorithm. Shown are time series of SSI in eight broad bands spanning the full spectral range of the model output from the far ultraviolet through the far-infrared. The reference baseline solar spectrum is shown in Figure 6.

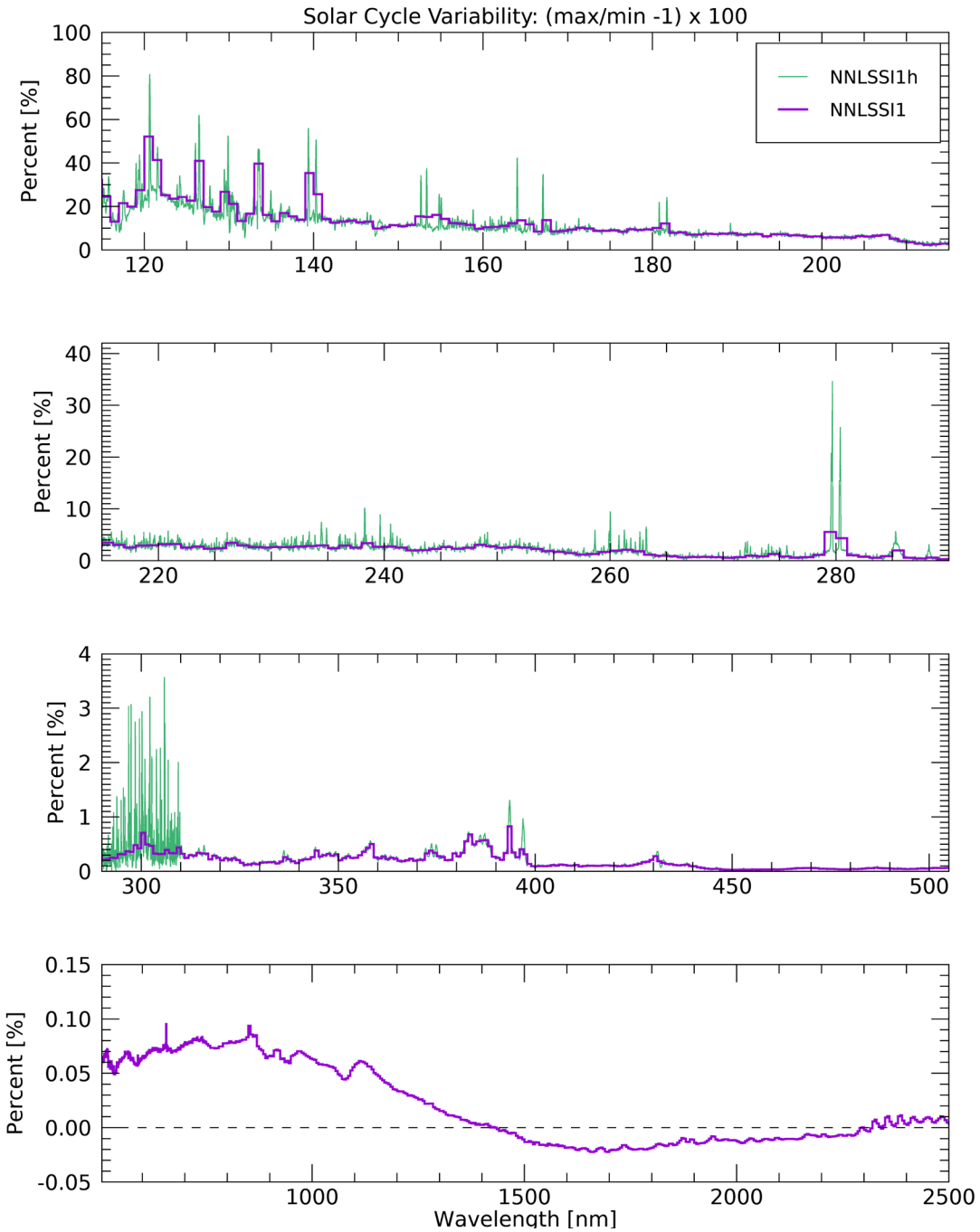

Figure 11: The wavelength-dependence of solar cycle energy change (shown as a percentage) between moderately high activity levels in June 2023 and low solar activity levels in December 2019 as estimated by the NNLSSI1 and NNLSSI1h models.

3.3.4 Forward Models

Not applicable.

3.4 Theoretical Description

The overall approach of the Solar Irradiance Climate Data Record algorithm builds on, and advances, the original NRLTSI and NRLSSI models described in Lean (2000), Lean et al. (2005) and summarized in Lean and Woods (2010). The NRLTSI and NRLSSI models were first developed over two decades ago, prior to the launch of the Solar Radiation and Climate Experiment (SORCE) spacecraft (Rottman et al., 2005), although the formal adoption of the acronyms for these models did not occur until afterward. NRLTSI and NRLSSI have been widely used for a variety of model simulations of climate and atmospheric change, including for the IPCC reports (e.g., Schmidt et al., 2011), and compared as well with other solar spectral irradiance variability models and observations (Thuillier et al., 2013). Since then, new, improved versions of the NRL solar variability models have been produced. Specifically, NRLSSI2 and NRLTSI2, were transitioned as Version 2 of the Solar Irradiance CDR.

In 2024, the Naval Research Laboratory (NRL) solar variability models were reformulated, re-named the NASA NOAA LASP (NNL) solar variability models and transitioned as (the current) Version 3 of the Solar Irradiance CDR. This C-ATBD document describes NNLTSI1, NNLSSI1 and the high spectral resolution NNLSSI1h model (from 115-500 nm) that is scaled in magnitude and variability to be consistent with NNLSSI1 model in 1-nm bins.

The following section provides background on the NRL and NNL model heritage.

Original NRLTSI and NRLSSI Models

The NRLTSI model was formulated using a composite of total solar irradiance constructed by Fröhlich and Lean (2004), by combining observations made by Nimbus 7, ACRIM on SMM and UARS and PMOD on SOHO. The corresponding spectral irradiance variability model, NRLSSI, was constructed for wavelengths less than 400 nm from a linear association of spectral irradiance variations observed by the Solar Stellar Irradiance Comparison Experiment (SOLSTICE, Rottman, 2000), relative to a reference spectrum (the average SOLSTICE spectrum during the UARS time period), with corresponding changes in facular brightening and sunspot darkening, also relative to their respective reference values (Lean et al., 1997). The NRLTSI model calculates the total solar irradiance daily since 1882, monthly since 1882, and annually since 1610.

Lacking observations of solar spectral irradiance variability at wavelengths longer than ~400 nm, NRLSSI's spectral irradiance variations in the visible and infrared spectral regions were determined from the wavelength-dependence of the sunspot and facular contributions, according to their respective theoretical contrasts (ratio of emission to the background quiet solar atmosphere) determined in a theoretical solar atmosphere model (Unruh et al., 2000). For the quiet irradiance spectrum, a composite was compiled on a 1 nm grid from space-based observations made by SOLSTICE on UARS (from 120 to 401 nm) and SOLSPEC on the ATLAS shuttle mission (from 401 to 874 nm, Thuillier et al., 1998), and a theoretical spectrum at longer

wavelengths (Kurucz, 1991). The agreement among these three spectra in their regions of overlap is better than 2%, which is well within their absolute measurement uncertainties (Thuillier et al., 1998). The initially compiled composite spectrum was multiplied by 0.99 at all wavelengths to make its integral equal the independently measured total irradiance of the quiet Sun, whose most likely value at that time was considered to be 1365.5 Wm^{-2}.

Neither Lean (2000) nor Lean et al (2005) refer explicitly to the spectral irradiance calculations, described above, as the NRLSSI model. Following the extension of the model to include the extreme ultraviolet spectrum (Lean et al., 2011), the designation NRLSSI was chosen (e.g., as summarized in Lean and Woods, 2010) to collectively describe an empirical capability to specify the entire solar spectral irradiance and its variability from 1 to 100,000 nm. The NRLSSI model calculates the solar spectral irradiance in 1 nm bins across the entire electromagnetic spectrum, daily since 1882, monthly since 1882 and annually since 1610.

The NRLTSI2 and NRLSSI2 Models

The measurements made by the Total Irradiance Monitor (TIM), Solar Irradiance Monitor (SIM) and SOLSTICE instruments on the SORCE spacecraft provided new observations of total and spectral irradiance with unsurpassed (at the time) accuracy and repeatability, throughout the descending phase of solar cycle 23, the minimum between solar cycles 24 and 25 (2008-2009), the entire cycle 24 (2010-2019), and a second subsequent cycle minimum (2019-2020). The SORCE TIM measurements indicate that the actual total irradiance of the quiet sun was ~5 Wm^{-2} lower than in the original NRLTSI (Kopp and Lean, 2011), and the NRLTSI2 and NRLSSI2 models were constructed to be consistent with this new, lower value of total solar irradiance.

SORCE SIM provided the first-ever continuous, space-based observations of solar spectral irradiance variability at wavelengths longer than 400 nm. The NRLSSI2 model incorporated the short-term (rotational) information in the SIM observations plus the longer record of observed UV variability from SIM and SOLSTICE to define and refine the wavelength-dependent contrast of the sunspot and facular contributions from ~200 to 1600 nm, and SORCE SOLSTICE observations at far ultraviolet wavelengths. At wavelengths longer than ~ 1600 nm, the theoretical solar atmosphere model of Unruh et al. (2000) was used. NRLSSI2 adopted for the quiet irradiance spectrum a composite from the SORCE space-based SSI observations designated the LASP Whole Heliosphere Interval (WHI) spectrum (Woods et al., 2009) integrated with a theoretical spectrum at longer wavelengths (Kurucz, 1991). The integral of the LASP WHI spectrum exceeded the total solar irradiance by approximately 1%, so a multiplicative factor was used to make its integral equal to the measured total solar irradiance (Woods et al., 2009). Agreement among these three spectra in their regions of overlap was better than 2%, which is well within their absolute measurement uncertainties (Thuillier et al., 1998).

The NRLTSI2 and NRLSSI2 models were implemented as the Version 2 NOAA/NCEI Solar Irradiance Climate Data Record. The publication by Coddington et al. (2016) and the accompanying C-ATBD document (Coddington and Lean, 2015)) provide more details about NRLTSI2 and NRLSSI2 models. A revised C-ATBD was released in 2017 with v02r01 after improvements were made to the sunspot blocking indice and to a new representation of

historical irradiance estimates based on the updates to the sunspot number time series were incorporated (Coddington and Lean, 2017).

The NRLTSI3 and NRLSSI3 Models

Version 3 of the NRL solar irradiance variability models utilized SORCE observations from 2003 to 2017 (inclusive) to formulate additional, statistically significant, improvements described in Lean et al. (2020). In addition to using an extended observational time period to develop the model coefficients, the NRLTSI3 and NRLSSI3 models investigated how an additional nonlinear facular term might better reproduce concurrent solar cycle and rotational variability, particularly in the total solar irradiance estimates and at ultraviolet wavelengths, and also how the improved representation of the sunspot index derived from the Debrecen sunspot area catalog (Győri et al., 2011) improved the model's performance relative to the USAF Air Force SOON sites used operationally in Version 2 of the NRL models. Unfortunately, the Debrecen sunspot area catalog cannot be used operationally; it has not been updated since 2017 due to the passing of the lead scientist.

The NRLTSI3 and NRLSSI3 models were not transitioned as an operational version of the Solar Irradiance CDR. However, they are used internally by the Solar Irradiance CDR team as part of the quality assurance process.

The NNLTSI1 and NNLSSI1 Models

Version 1 of the NASA NOAA LASP (NNL) models, NNLTSI1 and NNLSSI1, are constructed using solar irradiance measured from multiple space-based platforms to determine and validate the model coefficients. The primary observational databases are the measurements made by the TIM and SIM instruments on the Total and Spectral Solar Irradiance Sensor (TSIS-1) mission since 2019 and by the EVE instrument on SDO since 2010 and the SEE instrument on the TIMED spacecraft since 2001. The reference spectrum, I_{ref} (0 – 200,000 nm), is based on the TSIS-1 HSRS and SDO EVE observations as described previously, adjusted with a wavelength-independent scaling factor such that the spetral integral equals TSI on the absolute scale defined as the average of the CTIM and TSIS-1 TSI values. In addition to its expanded spectral range relative to earlier versions of the NRL models (115-100,000 nm), NNL Version 1 also incorporates a newly constructed sunspot darkening index with higher repeatability than the SOON index to determine model coefficients. The improved sunspot index is derived from white light images made by the National Solar Observatory's (NSO) Global Oscillation Network Group (GONG) network (https://nso.edu/telescopes/nisp/gong/). Using approximately 12 solar images near local noon at six GONG operating sites enables determination of the daily average sunspot darkening index with smaller standard deviation than do the single observations from the 3 operating stations of the USAF SOON network. The uncertainties in the model coefficients of the sunspot darkening index in the Version 1 NNL model are correspondingly reduced. Furthermore, the greater number of sites in the GONG network improves the operational foundation of the Solar Irradiance CDR since days with missing sunspot darkening data is less likely.

As described in Section 3.2 and Figure 1, the basic formulation of time-dependent total and spectral solar irradiance, $T(t)$ and $I(\lambda,t)$, determines their variations arising from faculae and sunspots superimposed on specified, invariant, reference sun reference values, $T_{ref}(t)$ and $I_{ref}(\lambda,t)$ (Figure 6), as,

$$T(t) = T_{ref} + T_F(t) - T_S(t)$$

$$I_{115\,nm}^{200,000\,nm}(\lambda,t) = I_{ref}(\lambda) + I_F(\lambda,t) - I_S(\lambda,t),$$

with the EUV portion of the SSI requiring additional facular indices for higher fidelity representation as,

$$I_{0\,nm}^{115\,nm}(\lambda,t) = I_{ref}(\lambda) + I_F(\lambda,t) + I_F^{sm}(\lambda,t) + I_{F10.7}(\lambda,t).$$

The first step in the algorithm is determining the corresponding values for the bolometric facular brightening, $T_F(t)$, and sunspot darkening, $T_S(t)$, functions at time, t, that are derived from the facular brightening, $F(t)$, and sunspot darkening, $S(t)$, proxy indices. The $F(t)$ and $S(t)$ are calculated using independent solar observations made approximately daily, respectively, the GOES Mg index of global (i.e., disk integrated) facular emission and integrated intensity reduction from sunspots on the solar disk derived from GONG network white light images, as described in Section 3.3.1.

$$T_F(t) = (Mgcomp - 0.2629949)\ X\ 117.5332052$$

$$T_S(t) = (GONGcomp - 0.0142832) * 1.0000115$$

T_F and T_S at time, t, are the bolometric (i.e. W m^{-2}) components of total solar irradiance change attributed to bright faculae and dark sunspots, respectively. Multiple linear regression is used to determine the scaling coefficients of the facular brightening and sunspot darkening indices that best reproduce the total solar irradiance variability measured directly by multiple LASP TIM instruments incorporated in the LASP TIM TSI composite from 2003 to 2023 (Harber et al., Earth and Space Science, *in prep*). The correlation of the observed, T_{TIM} and modeled, T_{mod}, total solar irradiance is 0.976 and the standard deviation of the residuals, $T_{TIM} - T_{mod}$, is 0.1 Wm^{-2}.

The corresponding facular brightening and sunspot darkening components in the NNLSSI1 spectral irradiance variability model for all λ > 115 nm are

$$I_F(\lambda,t) = c_F(\lambda) \times T_F(t)$$

$$I_S(\lambda,t) = c_S(\lambda) \times T_S(t)$$

At EUV wavelengths, λ < 115 nm, the sunspot darkening components to spectral irradiance variability are negligible and the facular brightening components are

$$I_{F,EUV}(\lambda,t) = e_F(\lambda) \times T_F(t) + e_{F10.7}(\lambda) \times \left[F10.7(t) - F10.7_{ref}\right] + e_F^{sm}(\lambda) \times T_F^{sm}(t) + e_{const}(\lambda)$$

where $F_{10.7}(t)$ is sourced from independent solar radio flux at 10.7 cm observed approximately daily as described in Section 3.3.1. $F10.7_{ref}$ (= 62.53) is the value of the solar radio flux corresponding to I_{ref}, i.e., for the reference quiet sun spectrum. $T_F(t)$ is as described above and $T_F^{sm}(t)$ is it's 81-day smoothed value.

The algorithm uses specified $c(\lambda)$, and $e(\lambda)$ coefficients (see Figure 7 for a plot of all wavelength-dependent coefficients).

Numerically, the integral of the spectral irradiance from the NNLSSI1 model is equal to the independently computed total solar irradiance from the NNLTSI1 model. The average difference over the period from 1978 to mid-2023 between the spectrally integrated NNLSSI1 model and the NNLTSI1 model is -0.0018 W m^{-2} and the standard deviation of the differences is 0.0015 W m^{-2}. The average difference and standard deviation between the spectrally integrated facular components of the NNLSSI1 model and the same component in the NNLTSI1 model, over the same period, are $1.3e^{-14}$ and $1.2e^{-14}$ W m^{-2}, respectively. The same analysis for the sunspot component between the NNLSSI1 and NNLTSI1 models shows similar, vanishingly small, differences as the facular component. As such,

$$T(t) = \int_{\lambda_0}^{\lambda_\infty} I(\lambda, t)\, d\lambda$$

$$T_F(t) = \int_{\lambda_0}^{\lambda_\infty} I_F(\lambda, t)\, d\lambda$$

$$T_s(t) = \int_{\lambda_0}^{\lambda_\infty} I_S(\lambda, t)\, d\lambda$$

In formulating the predecessor NRL Version 2 models that specified the previous CDR V2, additional, small increments to the facular and sunspot indices were made to ensure this same internal consistency between TSI and the integral of SSI. That the NNL Version 1 models do not require this correction accrues from their improved fidelity in representing irradiance change arising from sunspots and faculae on the solar disk. This results from the higher repeatability of the TSIS-1 solar irradiance observations (relative to the SORCE SIM observations) and of the sunspot darkening function derived from the GONG network of white light images (relative to the index derived from the SOON sunspot data).

TSIS SIM's calibration is significantly more stable than that of the predecessor SORCE SIM instrument but is still less stable than that of the TSIS TIM instrument. When formulating the NNLSSI1 model, empirical analysis of both direct and detrended TSIS and SORCE SIM observations are used to formulate the model regression coefficients. In the earlier NRLSSI2 models, only detrended observations were used to derive the model coefficients because of residual instrumental trends in the SIM's solar spectral irradiance measurement record (Lean and DeLand, 2012). Instrumental trends are assumed to be smaller over the (much) shorter rotational times scales than during the solar cycle.

The TSIS SIM (Version 12) data from 2018 through 2023 (inclusive) are used to construct the NNLSSI1 model coefficients. Even though the TSIS-1 SIM measurements are more accurate and have higher in-flight repeatability than the SORCE SIM measurements, radiometric technology and operational advances have not completely alleviated instrument trends in the TSIS-1 SIM data, suspected particularly at wavelengths longer than ~ 700 nm, even in the V12 data release that incorporated substantial advances in instrument calibration of this effect relative to the V11 release.

The scaling coefficients that relate time series of bolometric facular and sunspots with solar spectral irradiance are determined from observations at wavelengths longer than 200 nm by the SIM instrument on TSIS since 2018, and at wavelengths from 115 to 200 nm by the SIM instrument on SORCE between 2003 and 2023. The approach uses multiple linear regression to determine the relationships for the time series directly, and for the detrended time series, where detrending is the process of removing a 'smooth', 81-day running mean, from the direct observations.

The wavelength-dependent coefficients for the sunspot component of the NNLSSI1 model are similar whether derived from direct or detrended TSIS-1 observations. This is because sunspots dominate irradiance variability at visible and infrared wavelengths on solar rotation time scales and their signal is readily detected in the observations.

The wavelength-dependent coefficients for the NNLSSI1 facular component are specified by combining both direct and detrended TSIS-1 observations such that the resultant model reproduces the magnitude of observed rotational modulation and the time series of the spectral integral of the facular signal equals that of the bolometric faculae time series. Figure 12 shows the good agreement between the 27-day cycle amplitude in the observed and modeled time series, derived using complex demodulation.

At wavelengths less than about 300 nm, where the sunspot influence is minimal, the faculae signal dominates both solar rotation and solar cycle irradiance variability and the model coefficients derived from direct and detrended observations are typically comparable. At visible and near-infrared wavelengths, the facular influence is submerged by the large sunspot influence during solar rotation, but dominates on solar cycle time scales, requiring that it be separated from multi-year instrument drifts. At wavelengths longer than 400 nm, the range of facular variability in the detrended time series is typically smaller than during the solar cycle because long term instrument drifts can increase the scaling coefficients derived from the direct observations while

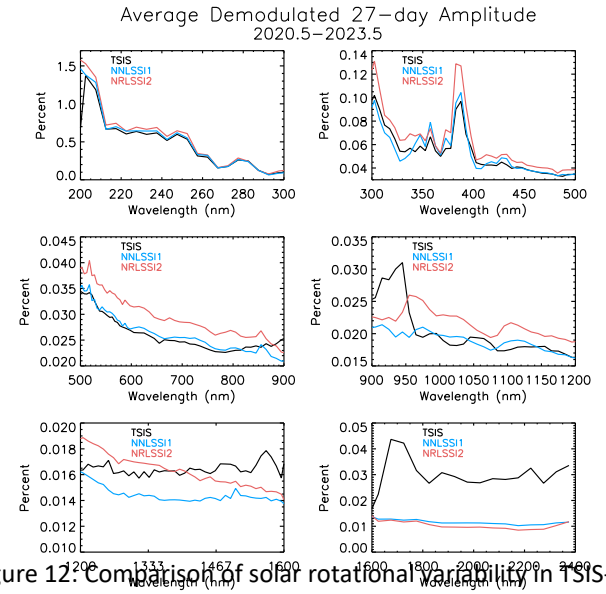

Figure 12: Comparison of solar rotational variability in TSIS-1 SIM measurements and the NRLSSI2 and NNLSSI1 models over the same 3 year period.

instrumental “noise” (lack of short-term repeatability) can decrease the scaling coefficients derived from the detrended time series.

Estimated Solar Irradiance Changes, Daily since 1874, Annually since 1610

As well as being a dominant determinant of solar cycle irradiance variations, changes in faculae in the bright network that comprises the “background” solar emission (i.e. those areas on the Sun’s surface not identified as dark sunspots or bright faculae) are speculated to cause longer-term (decadal to centennial) irradiance changes that manifest from one cycle minimum to the next. Specifying the past evolution of the network facular signal, as well as solar cycle changes in faculae and sunspots, is therefore necessary for reconstructing historical irradiance variations.

Information about sunspots is available from direct observations made by the Greenwich Observatory from 1874 to 1976 and is suggested by direct observations of sunspot numbers since (at least) 1610. In contrast, knowledge of past changes in faculae is highly uncertain and is typically inferred from somewhat ambiguous circumstantial evidence. For example, based on current observations of facular contrast and disk coverage, the disappearance of all faculae from the Sun's surface is estimated to decrease total solar irradiance about 0.1% (Lean et al., 1992). Attempts have been made to translate variations in the chromospheric activity in Sun-like stars to plausible ranges of the facular influence on solar irradiance (Lean et al., 1992, 1995), with results broadly consistent with inferences from the cosmogenic and geomagnetic indices. Changes in solar structure are also considered as possible sources of long-term irradiance variations in addition to, or instead of, facular variations (Hoyt and Schatten, 1993; Tapping et al., 2007) producing levels as much as 0.3% below contemporary solar minima values (e.g., review of Maunder Minimum levels in Lean et al., 2005).

In the original version of NRLSSI (Lean, 2000) the long-term “background” component of the facular index, $F_{BG}(t)$, was specified as a 15-year running mean of annual sunspot group numbers in which the reduction from the quiet Sun to the Maunder Minimum is 92% of the increase in $F_{BG}(t)$ from the quiet Sun to cycle maximum (monthly average for November 1989). These changes mimicked the reduced Ca fluxes in non-cycling Sun-like stars compared with the range of fluxes in cycling Sun-like stars (Radick et al., 1998 and Lean et al., 2001, provide additional details) which at the time of the NRLSSI model formulation were thought to exemplify long-term solar irradiance changes. However, a subsequent reassessment of the stellar data was unable to recover the original bimodal separation of (lower) Ca emission in non-cycling stars (assumed to be in Maunder Minimum type states) compared with (higher) emission in cycling stars (Hall and Lockwood, 2004). Nor do long-term trends in the aa index and cosmogenic isotopes (generated by open flux) necessarily imply equivalent long-term trends in solar irradiance (which track closed flux) according to simulations of the transport of magnetic flux on the Sun and propagation of open flux into the heliosphere (Lean et al., 2002; Wang et al., 2005).

These developments motivated revision of the long-term “background” component of the NRLSSI model using a flux transport model to estimate the plausible magnitude of a long-term

secular facular component. The flux transport model (with variable meridional flow) simulates the eruption, transport, and accumulation of magnetic flux on the Sun's surface from the Maunder Minimum to the present in strengths and numbers proportional to the sunspot number (Wang et al., 2005). The model estimated variations in both open and total flux arising from the deposition of bipolar magnetic regions (active regions) and smaller-scale ephemeral regions on the Sun's surface: The open flux compares reasonably well with the geomagnetic and cosmogenic isotopes, which gives confidence that the approach is plausible. A small accumulation of total flux (and possibly ephemeral regions) produces a net increase in facular brightness that, in combination with sunspot blocking, permits the reconstruction of total solar irradiance.

In 2021, Wang and Lean (2021) updated and revised their original (Wang et al., 2005) simulations of change in the Sun's total magnetic flux since the Maunder Minimum using a magnetic flux transport model, for three main reasons: to incorporate revised sunspot number time series by the Sunspot Index and Long-term Solar Observations (SILSO) that showed a different secular increase in sunspot activity prior to 1880 than in the original group sunspot number record (Hoyt and Schatten, 1998); a longer record of sunspot numbers that spanned the weakest sunspot cycle (cycle 24) and the longest solar minimum period in the observational record (2008-2009); and four decades of climate quality total solar irradiance observations including during the 2008-2009 solar minimum period. Basic elements of the magnetic flux transport model are as described in Wang et al. (2005). A key finding in the Wang and Lean (2021) study, which included TSI observations during four contemporary solar minima, was that TSI and facular brightness during solar minimum increase less steeply with the photospheric magnetic flux (both simulated and observed) than during the 11-year solar activity cycle. This was assumed to be because of the dominance of small-scale ephemeral regions when activity is very low. As a result, the irradiance increase estimated in Wang and Lean (2021) from 1700 to 1964 is 2-3x smaller (0.2 W m^{-2}) than in the earlier Wang et al. (2005) study (an increase of 0.58 W m^{-2}).

The increase in total solar irradiance from the Maunder Minimum to the present-day reference baseline TSI in the NNL1 models are consistent with the Wang and Lean (2021) study and equal to about 0.015%. For comparison, the irradiance increase from the Maunder Minimum to present day was about 0.04% in the NRL2 models, and because of the larger background facular component adopted in Lean (2000), the increase from the Maunder Minimum to the present-day quiet Sun in the original version of the NRLSSI model was about 0.16%, four times larger than that of the NRL V2 models. See Lean et al. (2005) and Wang and Lean (2021) for further details.

The solar total and spectral irradiance changes in the NNLTSI1 and NNLSSI1 models prior to November 1978 are determined from historical reconstructions of the bolometric facular and sunspot indices shown daily since 1874 in Figure 13 and annually since 1610 in Figure 14. The evolution of the bolometric facular index during successive solar cycle minima is consistent with the Wang and Lean (2021) simulated changes in cycle minima total magnetic flux, according to

the relationship between bolometric faculae (determined as observed TS adjusted for bolometric sunspot darkening) and total magnetic flux during the past four solar cycle minima.

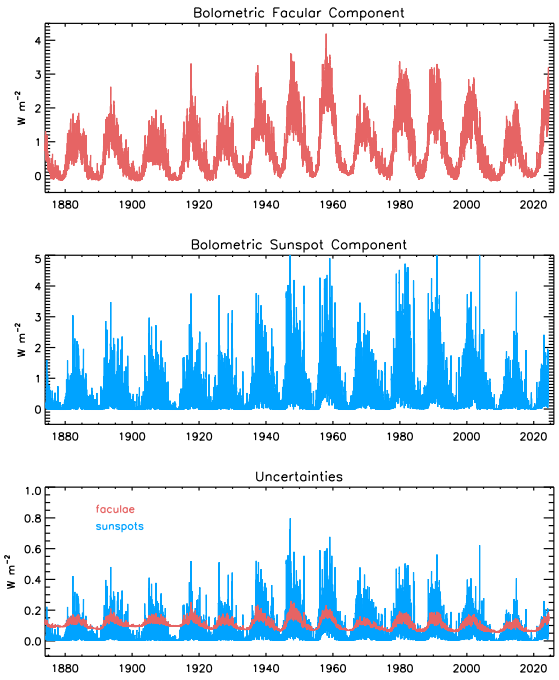

Figure 13: Shown in the upper panel are daily values of the bolometric facular index, in the middle panel of the bolometric sunspot index and in the bottom panel their respective uncertainties, since 1874.

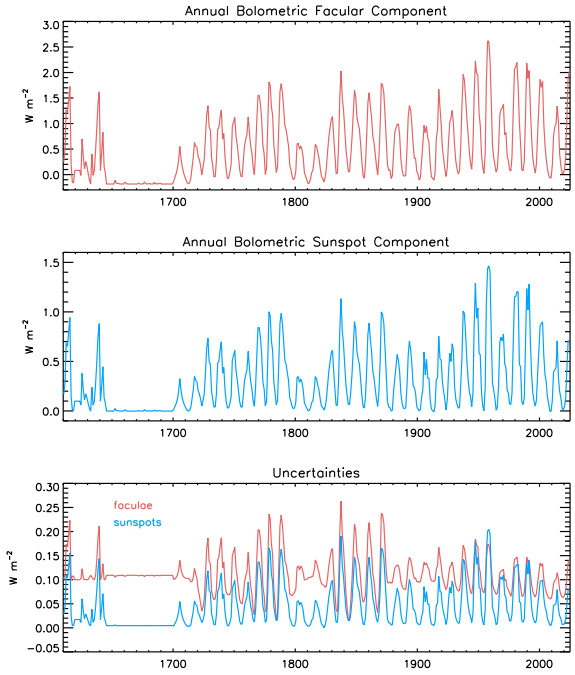

Figure 14: Shown in the upper panel are annual values of the bolometric facular index, in the middle panel of the bolometric sunspot index and in the bottom panel their respective uncertainties, since 1610.

Projected Solar Irradiance Changes to 2100

Evident in the annual time series of the bolometric facular brightening and sunspot darkening indices during the past 300 years (in Figure 14, see also Wang and Lean 2021, Figures 20, 21) are two dominant periods, specifically the 11-year Schwabe cycle and the longer period, ~100-year Gleissberg cycle which modulates Schwabe cycle minima and maxima.

The CDR V3 projections of future solar irradiance, shown in Figure 15, assume the continuation of both the Schwabe and Gleissberg cycles during the next century. The timing of future Schwabe cycles is estimated for a range of periods from 10.7 to 11.1 years, and the Schwabe cycle modulation is estimated by scaling the amplitude of the most recent Gleissberg cycle from 1910-2009. The projections select the most likely Schwabe cycle period and Gleissberg cycle amplitude by comparing statistical representations of the two cycles with independent observations in cycle 25, which is the first Schwabe cycle of the new Gleissberg cycle.

CDR V3 updates the projections of future solar irradiance at most annually, taking into account the performance of the prior year's projections compared with the actual observations during

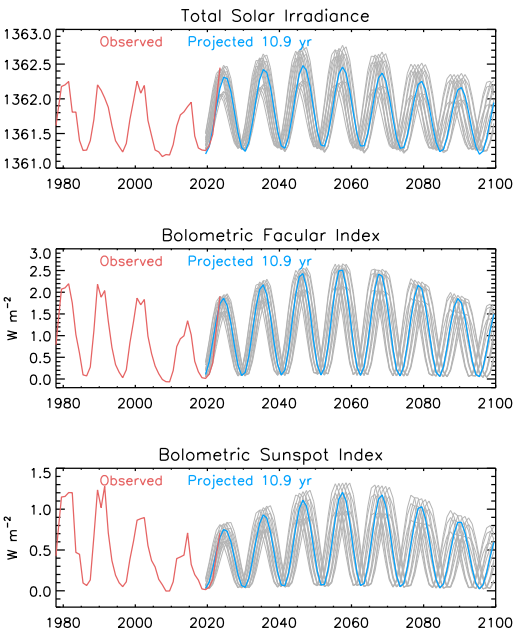

that year. The uncertainties in the irradiance projections reflect the range of projections defined by a plausible range of Schwabe cycle periods and Gleissberg cycle amplitudes.

Figure 15: Projections of TSI and bolometric facular brightening and sunspot darkening indices (blue curves) are shown from 2023 to 2100, compared with the observations (red curves) from 1980 to 2023. The assumed period of the Schwabe cycle is 10.9 years; grey lines indicate uncertainties associated with Schwabe cycle periods from 10.7 to 11.1 years.

3.4.1 Physical and Mathematical Description

The NNLTSI1, NNLSSI1, and NNLSSI1h models, which the V3 Solar Irradiance Climate Data record algorithm utilizes, assume that bright faculae and dark sunspots are the only causes of solar irradiance variability on contemporary time scales. The occurrence of these features on the Sun varies during the Sun's 11-year activity cycle, producing a prominent 11-year cycle in solar irradiance. The rotation of the Sun on its axis alters the population of faculae and sunspots projected to earth, producing an additional 27-day irradiance modulation.

Following the approach of Lean et al. (1998), when the sun is inactive, the "reference baseline" irradiance for a specified solar minimum period at the Earth (at a distance of 215 times the solar radius) is determined by integrating the radiance, $R(\lambda,1)$, at the center of the disk ($\mu = 1$) over the entire disk using the center-to-limb function, $L(\lambda, \mu)$ to define the ratio of $R(\lambda, \mu)$ to $R(\lambda, 1)$ at heliocentric position μ, which ranges from 0 (at the disk's limb) to 1 (at disk center). Thus, the irradiance of the reference sun is

$$I_{ref}(\lambda) = \frac{2\pi R_{ref}(\lambda, 1) \int_0^1 L(\lambda, \mu)\, \mu d\mu}{(215)^2}$$

$$T_{ref} = \int_{\lambda_0}^{\lambda_\infty} I_{ref}(\lambda)\, d\lambda$$

Magnetic features – dark sunspots and bright faculae – when present or absent on the solar disk relative to their (nominally homogeneous) population at the time of the reference (nominally quiet) period alter the distribution of radiance, and hence the irradiance at the Earth, which is at some (non-reference) time, t, given as

$$I(\lambda,t) = \frac{2\pi R_{ref}(\lambda,1)\int_0^1 C(\lambda,\mu)L(\lambda,\mu)\,\mu d\mu}{(215)^2}$$

where

$$C(\lambda,\mu) = \frac{R(\lambda,\mu)}{R_{ref}(\lambda,\mu)}$$

is the ratio of the Sun's radiance at heliocentric location, μ, relative to the radiance of the surrounding quiet Sun. This ratio is termed the contrast.

Separating radiance elements on the solar disk into those that are brighter than, darker than, or equal to the quiet sun radiance permits expression of the irradiance as

$$I(\lambda,t) = I_{ref}(\lambda) + \frac{2\pi R_{ref}(\lambda,1)}{(215)^2}\int_0^1 [C_F(\lambda,\mu)-1]L(\lambda,\mu)\,\mu d\mu + \frac{2\pi R_{ref}(\lambda,1)}{(215)^2}\int_0^1 [C_S(\lambda,\mu)-1]L(\lambda,\mu)\,\mu d\mu$$

where $C_F(\lambda,\mu)$ and $C_S(\lambda,\mu)$ are the contrasts of the faculae and sunspots, respectively. For the number of radiance elements defined as faculae, N_{fac}, and sunspots, N_{spot}, with actual area on the solar surface of A_{fac} and A_{spot}, at a given time, t, the corresponding solar irradiance is (with $A = 2\pi r_{sun}^2 d\mu$ for solar radius r_{sun})

$$I(\lambda,t) = I_{ref}(\lambda) + \frac{2\pi R_{ref}(\lambda,1)}{(215)^2}\sum_1^{N_{fac}} [C_F(\lambda,\mu)-1]L\,(\lambda,\mu)\mu\frac{A_{fac}}{2\pi r_{sun}^2} + \frac{2\pi R_{ref}(\lambda,1)}{(215)^2}\sum_1^{N_{spot}} [C_S(\lambda,\mu)-1]L\,(\lambda,\mu)\mu\frac{A_{spot}}{2\pi r_{sun}^2}$$

which is analogous to the basic formulation used in the Solar Irradiance Climate Data Record algorithm for the solar spectral irradiance:

$$I(\lambda,t) = I_{ref}(\lambda) + I_F(\lambda,t) + I_S(\lambda,t)$$

where

$$I_F(\lambda,t) = \frac{2\pi R_{ref}(\lambda,1)}{(215)^2}\sum_1^{N_{fac}} [C_F(\lambda,\mu)-1]L\,(\lambda,\mu)\mu\frac{A_{fac}}{2\pi r_{sun}^2}$$

$$I_S(\lambda,t) = \frac{2\pi R_{ref}(\lambda,1)}{(215)^2}\sum_1^{N_{spot}} [C_S(\lambda,\mu)-1]L\,(\lambda,\mu)\mu\frac{A_{spot}}{2\pi r_{sun}^2}$$

The Solar Irradiance CDR V3 includes estimates of extreme ultraviolet (EUV) solar irradiance variability from ~ 0 nm to 115 nm. Empirical models of EUV variability (e.g., Lean et al. 2011) have shown that a three-component model best represents observed EUV variability, where proxies of chromospheric and coronal emission come from the Mg II index and the F10.7 cm solar radio flux, respectively. The 3rd component is a smoothed chromospheric proxy

component that is shown to better reproduce EUV solar cycle variability at all wavelengths. The sunspot darkening contribution is negligible at EUV wavelengths.

The GONG sunspot darkening index for the CDR V3 is constructed by extracting sunspot areas, locations and contrasts directly from operational white light images made in the photospheric Ni line at 676.8 nm at six different GONG sites, near noon, around the globe. After processing each GONG image (e.g., identifying disk center, radius, sun-earth distance) the signal in each pixel is plotted versus its distance from the image center to characterize the center-to-limb function. A center-to-limb function is fitted to the local emission devoid of sunspots to determine the dependence of solar radiance with disk position. The locations of sunspots and their emission magnitudes are identified statistically as those regions that deviate from this "limb-darkened background", defined, for example, by the standard deviation of pixel intensities at a specified radial distance. The signal total of all such pixels is the sunspot darkening of the full-disk solar irradiance.

The corresponding total solar irradiance is

$$T(t) = \int_{\lambda_0}^{\lambda_\infty} I_{ref}(\lambda)\, d\lambda$$

$$T(t) = \int_{\lambda_0}^{\lambda_\infty} I_{ref}(\lambda)\, d\lambda + \int_{\lambda_0}^{\lambda_\infty} I_F(\lambda, t)\, d\lambda - \int_{\lambda_0}^{\lambda_\infty} I_S(\lambda, t)\, d\lambda$$

which is analogous to the basic formulation used in the Solar Irradiance Climate Data Record algorithm for the total spectral irradiance:

$$T(t) = T_{ref} + T_F(t) - T_S(t)$$

The calculation of the sunspot darkening index in Section 3.3.1 is physically an estimate of $\frac{T_S}{T_{ref}}$ made using the above theoretical basis with several assumptions and parameterizations, as follows. In NRL V2 and predecessor models, the center-to-limb variation was assumed to be independent of wavelength (i.e. "bolometric") and specified as the 'Delta-Eddington' approximation:

$$L(\mu) = \frac{3\mu + 2}{5}$$

$$\int_0^1 L(\mu)\, \mathrm{d}\mu = \int_0^1 \frac{3\mu + 2}{5}\, \mu \mathrm{d}\mu = \frac{2}{5}$$

For the NNL version 1 models, a theoretical study of the wavelength- and position-dependence of the center-to-limb variation using computed spectral synthesis (i.e. radiative transfer calculations) of a "quiet" solar atmosphere model profile (Fontenla, 1999; 2011) was undertaken. In this analysis, the spectral integral of the center-to-limb variability weighted by the spectral irradiance variability, gave evidence that radiance in the limb regions ($0 < \mu < 0.7$) contributes less to bolometric irradiance chage than the Delta-Eddington approximation.

Therefore, the center-to-limb function assumed for the NNL version 1 models replaces the Delta-Eddington approximation by this cubic polynomial:

$$L(\mu) = 0.308658 + 0.890260\mu - 0.357926\mu^2 + 0.161633\mu^3.$$

The sunspot contrast $C_S(\lambda) = R_S(\lambda) / R_{ref}(\lambda)$ is assumed to be independent of μ and its bolometric (i.e., spectrally integrated) value nominally 0.32. When the USAF SOON network observations are used to source the sunspot information from, the sunspot area, A_S, that is reported is in millionths of the solar hemisphere, i.e.,

$$A_S = \frac{A_{spot}}{2\pi r_{sun}^2} \times 10^6$$

Typically, information about sunspot areas and locations from the USAF SOON network are recorded at different times throughout the day (depending on local time) by three or so different ground-based stations; this number is less than the dozen stations at the peak of the USAF SOON global operations. The declining number, and data quality, from the USAF SOON network since the release of the Version 2 Solar Irradiance CDR, motivated new research into using the National Solar Observatory's (NSO) Global Oscillation Network Group (GONG) network for deriving sunspot darkening proxy instead (as explained further below).

When the USAF SOON stations are used to inform the sunspot darkening index for NNLTSI1 and NNLSSI1, the sunspot index is then the average of all the available SOON information on a given day. With the above assumptions,

$$\begin{aligned}
\frac{T_S(t)}{T_Q} &= \frac{\int_0^\infty \frac{2\pi R_Q(\lambda,1)}{(215)^2} \sum_1^{N_{spot}} A_S[C_S(\lambda)-1]L(\mu)\mu \, d\lambda}{\int_0^\infty \frac{2\pi R_Q(\lambda,1)}{(215)^2} \int_0^1 L(\mu)\mu \; d\mu d\lambda} \\
&= \sum_n^{N_{spot}} A_S L(\mu)\mu \; \frac{\int_0^\infty R_Q(\lambda,1)[C_S(\lambda)-1] \; d\lambda}{\int_0^\infty R_Q(\lambda,1) \; d\lambda} \times \frac{1}{\int_0^1 L(\mu)\mu d\mu} \\
&= \sum_n^{N_{spot}} A_S L(\mu)\mu \; \frac{\int_0^\infty R_Q(\lambda,1)[C_S(\lambda)-1] \; d\lambda}{\int_0^\infty R_Q(\lambda,1) \; d\lambda} \\
&= \sum_n^{N_{spot}} A_S L(\mu)\mu \; (C_S^B - 1) \times \frac{1}{\int_0^1 L(\mu)\mu d\mu}
\end{aligned}$$

where $L(\mu)$ is the cubic polynomial listed above.

Furthermore, empirical evidence shows a size-dependence to the contrast of sunspots (Brandt et al., 1994). For the version 1 NNL models, we impose this size-dependence in the sunspot contrast with the Brandt et al. (1994) modification as shown below:

$$\frac{T_S(t)}{T_Q} = \sum_{n}^{N_{spot}} A_S[0.2231 + 0.0244 + \log_{10} A_S]\, L(\mu)\mu\ (C_S^B - 1) \times \frac{1}{\int_0^1 L(\mu)\mu d\mu}$$

In a final step, we convert the sunspot blocking function to units of irradiance [W m^{-2}] by multiplying by the TSI of the adopted reference Sun in the NNLTSI1 (1361.2549 W m^{-2}) and removing the millionths of a solar hemisphere factor that came from the convention adopted by the USAF SOON network when reporting the sunspot area values (see above).

$$\Delta T_S(t) = \frac{\Delta T_S(t)}{T_Q} \times 1361.2549 \times 10^{-6}\ [units\ Wm^{-2}]$$

The sunspot darkening computed from the white light images of the GONG network is the sum of the intensity reduction in all pixels that are darker than the local intensity in GONG white light images a time, *t*. This process, which automatically accounts for the center-to-limb variation of the background emission and the sunspot contrast relative to the background, produces a more precise TSI model. The availability of the sunspot darkening index from the operational GONG network is also more reliable than the USAF SOON network data currently. The Solar Irradiance CDR team is currently working to operationalize the determination of sunspot darkening from the GONG network. For the NNLTSI1 model, the total irradiance change due to sunspots is calculated as a linear function of a "flux" (i.e. disk-integrated) proxy of GONG sunspot darkening, *S*(*t*). Figures 2 and 3 shows the sunspot darkening computed from the GONG white light images.

The facular brightening can be calculated similarly to the sunspot darkening index, which Lean et al. (1998) demonstrate for the irradiance at 200 nm using histograms of calibrated Ca K solar images to identify bright faculae. However, for practical applications, the characteristics of faculae are in general poorly observed in solar imagery and inadequately specified compared with the more compact, darker and relatively well-defined sunspot regions. Furthermore, whereas sunspot regions are typically discrete and therefore relatively easily quantified, faculae occur with a continuous distribution of sizes and contrasts, so that statistical definitions (which can be ambiguous) are needed for practical quantification. Because of the lack of reliable quantitative data for facular areas, center-to-limb functions and contrasts, the NNL V1 model (like the predecessor original, V2 and V3, NRL models) calculates spectral irradiance change due to faculae as a linear function of a "flux" (i.e., disk-integrated) proxy of facular brightening, *F*(*t*). Figures 4 and 5 shows the facular brightening composite of Mg II core-to-wing ratio. A research activity of the recently convened Solar Irradiance Science Team (SIST-4) is the derivation of a facular area time series from GONG magnetograms that accompany each white light image, after removing the areas of sunspot darkening identified during the white light image analysis as described above.

3.4.2 Data Merging Strategy

No data merging is needed for the NNLTSI1 and NNLSSI1 models to calculate solar irradiance.

3.4.3 Numerical Strategy

The NNLTSI1 and NNLSSI1 models do not include functions that numerically approximate the algorithms described above.

3.4.4 Calculations

The algorithm calculates the total solar irradiance using an IDL procedure to apply the previously derived (and constant in time) model regression coefficients to scale the two bolometric facular brightening and sunspot darkening functions. The algorithm then calculates the solar spectral irradiance from ~0 to 200,000 nm using an IDL procedure that applies the previously derived (and constant in time) wavelength-dependent model regression coefficients to scale three inputs: the F10.7 cm solar radio flux and facular and sunspot components of TSI change; these two latter components are an output of the NNLTSI1 model. The high spectral resolution NNLSSI1h model is calculated using an IDL procedure to apply the previously derived (and constant in time) high-resolution wavelength-dependent coefficients to scale proxies of facular brightening and sunspot darkening. In a follow-on step, the hires irradiances are normalized, in 1-nm bins, such that the magnitude and variability is consistent with the output of the improved NNLSSI1 model, in the same 1-nm bins and at the same point in time.

3.4.5 Look-Up Table Description

There are no designated Look-Up tables, per se, that the algorithm needs to repeatedly access. The NNLSSI1 algorithm does require, as initial input, the spectral irradiance of the baseline reference sun, specified in 1 nm bins from 0.5 to 199,999.5 nm, as well as the coefficients (on the same 1 nm wavelength grid) to convert the facular brightening and sunspot darkening indices to spectral irradiance change at any given time. Similarly, the bolometric baseline reference TSI and model coefficients for faculae and sunspots are required as inputs. In a similar manner, the NNLSSI1h algorithm also has its own set of coefficients (with central wavelengths output on a variably spaced grid) to convert input facular brightening and sunspot darkening indices to irradiance changes at any given time. All bolometric and wavelength-dependent inputs are part of the overall algorithm, but they could be separately formulated and reconsidered as Look Up Tables.

3.4.6 Parameterization

The irradiance magnitude of the NNLSSI1h model is converted so that its mean value and time-dependent variability, in 1-nm bins, is equivalent to the NNLSSI1 model in the same 1-nm bins at the same time, *t*. This time- and wavelength-dependent normalization factor is computed online in the IDL procedure.

3.4.7 Algorithm Output

Total Solar Irradiance (TSI)

The NNLTSI1 model produces a value and associated uncertainty of total solar irradiance on an absolute scale defined by a composite of TSI measurements made by LASP TIM instruments for

given inputs of the bolometric facular brightening and bolometric sunspot darkening functions. These inputs are estimated from ground and space-based solar observations daily when available, as specified in Section 3.4.1.

The total solar irradiance output files in NetCDF4 format have the structure identified in Table 3. The files follow CF-1.6 metadata convections for variable names and attributes. Table 6 provides representative TSI values and uncertainties.

The TSI values are aggregated in several time averaging formats to support the projected needs of the user communities. The initial transition of the Solar Irradiance Climate Data Record to NOAA includes separate, daily and monthly-averaged modeled TSI values from 1874 through 2023, aggregated into yearly files. Additionally provided are annually averaged TSI from 1610 through 2023, aggregated into a single, period of record, file. Preliminary, quarterly updates in the daily and monthly-averaged TSI are produced operationally. At each subsequent year-end, the preliminary files are replaced by final values of daily and monthly-averaged TSI, aggregated into a year-long record. Yearly updates to the annually averaged TSI are incorporated into a new, period of record file.

Table 3: Structure of the algorithm (NNLTSI1) output of Total Solar Irradiance (TSI).

Variable Name	Long Name	Standard Name	Units	Missing Value
TSI	NOAA Climate Data Record of Daily Total Solar Irradiance (W m-2)	solar_irradiance	W m^{-2}	-99.0
TSI_UNC	Uncertainty in daily total solar irradiance		W m^{-2}	-99.0
time		time	days since 1610-01-01 00:00:00.0	-99.0
time_bnds	Minimum (inclusive) and maximum (exclusive) dates included in the time averaging		days since 1610-01-01 00:00:00.0	

The time averaging in the data is identified using the *time_bounds* variable in the netCDF4 output.

The file naming conventions for the TSI data described above is as follows:
<***product***>_<***version***>_<***type***>_s<***YYYYmmdd***>_e<***YYYYmmdd***>_c<***YYYYmmdd***>.nc
where,
<product> is ‘tsi’ for total solar irradiance,
<version> is the product version number (this is ‘v03r00’ for final data, and ‘v03r00-preliminary’ for preliminary version data),
<type> is type of time average (‘daily’ for daily data, ‘monthly’ for monthly averaged data, and ‘yearly’ for annually averaged data)
s<YYYYMMDD> is the start year, month, and day of the data in the file,
e<YYYYMMDD> is the end year, month, and day of the data in the file, and
c<YYYYMMDD> is the creation of processing data of the file.

A file name example is tsi_v03r00_daily_s20010101_e20011231_c20240131.nc.

The start, s<>, and end, e<>, formats vary based on whether the irradiance values are daily, monthly or annually averaged. For example, the time format for daily TSI values follows YYYYMMDD convention, monthly-averaged TSI values follows YYYYMM convention, and annually averaged TSI values follows YYYY convention.

Solar Spectral Irradiance (SSI)

The NNLSSI1 model produces solar spectral irradiance values, and associated uncertainties, on an absolute scale such that the integrated spectral irradiance is equivalent to the average total irradiance observed by the TSIS-1 TIM and Compact TIM (CTIM) (Harber et al., 2019) instruments during December 1-7, 2019. The spectral component is equivalent to the full-spectrum TSIS-1 Hybrid Solar Reference Spectrum (Coddington et al., 2021; 2023) extended to wavelengths below 115 nm using TIMED SEE and SDO EVE observations and then scaled (reduced) in a wavelength-independent manner such that the integral of the reference solar spectral irradiance equates to the reference TSI value. This reference spectrum is modulated according to given inputs of sunspot darkening and chromospheric and coronal facular brightening, estimated daily using data from ground and space-based solar observations when available, as specified above.

The solar spectral irradiance output files in NetCDF4 format have the structure identified in Table 4. The files follow CF-1.6 metadata convections for variable names and attributes. Table 7 provides representative SSI values and uncertainties. The science product for solar spectral irradiance also contains the value of TSI, and its associated uncertainty, because users interested in SSI (for example, climate modelers) also require the integrated quantity to constrain the total incoming solar irradiance. By including the TSI with the SSI science product, we provide the user community the necessary values in a single file.

The initial transition of the Solar Irradiance Climate Data Record to NOAA includes separate, daily and monthly-averaged modeled SSI values from 1874 through 2023, aggregated into yearly files. Additionally provided are annually averaged SSI from 1610 through 2023, aggregated into a single, period of record, file. Preliminary, quarterly updates in the daily and monthly-averaged SSI are produced operationally. At each subsequent year-end, the preliminary files are replaced by final values of daily and monthly-averaged SSI, aggregated into a year-long record. Yearly updates to the annually averaged SSI are incorporated into a new, period of record file.

The time averaging in the data is identified using the *time_bounds* variable in the netCDF4 output.

The file naming conventions for the SSI data described above is as follows:
<***product***>_<***version***>_<***type***>_s<***YYYYmmdd***>_e<***YYYYmmdd***>_c<***YYYYmmdd***>.nc
where,
<product> is ‘ssi’ for solar spectral irradiance,

<version> is the product version number (this is 'v03r00' for final data, and 'v03r00-preliminary' for preliminary version data),
<type> is type of time average ('daily' for daily data, 'monthly' for monthly averaged data, and 'yearly' for annually averaged data)
s<YYYYMMDD> is the start year, month, and day of the data in the file,
e<YYYYMMDD> is the end year, month, and day of the data in the file, and
c<YYYYMMDD> is the creation of processing data of the file.

A file name example is ssi_v03r00_daily_s20010101_e20011231_c20240131.nc.

Table 4: Structure of the algorithm (NNLSSI1) output for values of Solar Spectral Irradiance (SSI).

Variable Name	Long Name	Standard Name	Units	Missing Value
SSI	NOAA Climate Data Record of Daily Solar Spectral Irradiance (W m^{-2} nm^{-1})	solar_irradiance_per_unit_wavelength	W m^{-2} nm^{-1}	-99.0
SSI_UNC	Uncertainty in Solar Spectral Irradiance		W m^{-2} nm^{-1}	-99.0
wavelength	Wavelength grid center	radiation_wavelength	nm	N/A
Wavelength_Band_Width	Wavelength band width. Centered on wavelength.		nm	N/A
TSI	NOAA Climate Data Record of Daily Total Solar Irradiance (W m^{-2})	toa_total_solar_irradiance	W m^{-2}	-99.0
TSI_UNC	Uncertainty in Daily Total Solar Irradiance (W m^{-2})		W m^{-2}	-99.0
time		time	days since 1610-01-01 00:00:00.0	
time_bnds	Minimum (inclusive) and maximum (exclusive) dates included in the time averaging		days since 1610-01-01 00:00:00.0	

High Spectral Resolution Solar Spectral Irradiance (SSI)

The NNLSSI1h model produces high spectral resolution solar spectral irradiance values. A normalization is applied online so that the NNLSSI1h output is on the same absolute scale of the NNLSSI1 model and consistent with the variability prescribed by the improved NNLSSI1 model.

The hires solar spectral irradiance output files in NetCDF4 format have the structure identified in Table 5. The files follow CF-1.6 metadata convections for variable names and attributes.

Irradiances and uncertainties for the hires SSI are consistent, after binning to 1-nm bins, to the uncertainties of the standard SSI product for the same time (see Table 7).

The initial transition of the Solar Irradiance Climate Data Record to NOAA includes separate, daily and monthly-averaged modeled high spectral resolution SSI values from 1874 through 2023, aggregated into yearly files. Additionally provided are annually averaged SSI from 1610 through 2023, aggregated into a single, period of record, file. Preliminary, quarterly updates in the daily and monthly-averaged high-resolution SSI are produced operationally. At each subsequent year-end, the preliminary files are replaced by final values of daily and monthly-averaged SSI, aggregated into a year-long record. Yearly updates to the annually averaged SSI are incorporated into a new, period of record file.

The time averaging in the data is identified using the *time_bounds* variable in the netCDF4 output.

The file naming conventions for the high-resolution SSI data described above is as follows:
<***product***>_<***version***>_<***type***>_s<***YYYYmmdd***>_e<***YYYYmmdd***>_c<***YYYYmmdd***>.nc
where,
<product> is 'hires-ssi for high spectral resolution solar spectral irradiance,
<version> is the product version number (this is 'v03r00' for final data, and 'v03r00-preliminary' for preliminary version data),
<type> is type of time average ('daily' for daily data, 'monthly' for monthly averaged data, and 'yearly' for annually averaged data)
s<YYYYMMDD> is the start year, month, and day of the data in the file,
e<YYYYMMDD> is the end year, month, and day of the data in the file, and
c<YYYYMMDD> is the creation of processing data of the file.

A file name example is hires-ssi_v03r00_daily_s20010101_e20011231_c20240131.nc.

Table 5: Structure of the algorithm (NNLSSI1h) output for values of High-resolution Solar Spectral Irradiance (SSI), scaled to NNLSSI1 absolute level and variability.

Variable Name	Long Name	Standard Name	Units	Missing Value
SSI	NOAA Climate Data Record of Daily High Spectral Resolution Solar Spectral Irradiance ($W\ m^{-2}\ nm^{-1}$)	solar_irradiance_per_unit_wavelength	$W\ m^{-2}\ nm^{-1}$	-99.0
wavelength	Wavelength grid center	radiation_wavelength	nm	N/A
time		time	days since 1610-01-01 00:00:00.0	
time_bnds	Minimum (inclusive) and maximum (exclusive) dates included in the time averaging		days since 1610-01-01 00:00:00.0	

4. Test Datasets and Outputs

4.1 Test Input Datasets

As a first test that the algorithm is performing as expected, the total solar irradiance is compared numerically with the integral of the solar spectral irradiance, and the individual faculae and sunspot components of irradiance change are also compared. Over the satellite-era period from 1978 through 2023, the residual difference between the total solar irradiance and the integral of the solar spectral irradiance is -0.0018 $\pm$ 0.0016 W m^{-2}. Over the same period, the residual difference between the facular component of TSI variability and the spectral integral of the facular component of SSI variability are essentially negligible ($1.3e^{-14} \pm 1.2e^{-14}$ W m^{-2}). Similarly, the residual difference between the sunspot component of TSI variability and the spectral integral of the sunspot component of SSI variability are also negligible ($-4.2.90e^{-15} \pm 7.0e^{-15}$ W m^{-2}).

A second test for algorithm performance is comparison of selected time series of the NNLTSI1 and NNLSSI1 irradiance values that the algorithm calculates with the corresponding time series of the NRLTSI2 and NRLSSI2 models, which formed Version 2 of the CDR and have, themselves, been widely compared with available observations. Figure 16 shows such a comparison for the total solar irradiance. NNLTSI1, constructed directly from the series of LASP TIM observations, has a slightly higher absolute scale that represents an evolving understanding of absolute solar irradiance level, than that of NRLTSI2 formulated from the first LASP TIM instrument on the SORCE platform. The residual difference between the NNLTSI1 and NRLTSI2 (after scaling NRLTSI2 to match NNLTSI1 in Dec 2019) shows negligible change in long-term irradiance trend during the satellite era but greater differences on short-term scales. Figure 17 shows another comparison of NNLTSI1 to NRLTSI2, but for the period since 1880 and after 365-day smoothing has been applied to each dataset. Figure 17 demonstrates that the differences from Version 2 of the CDR grow in the historical era. This is attributed to the improved understanding of historical irradiance change based on updated flux transport calculations applied to ever-lengthening record of satellite solar irradiance observations and ground- and space-based magnetic flux observations (Wang and Lean, 2021). The NNLTSI1 model estimates smaller irradiance change between the historical era and present day than the NRLTSI2 model.

Figures 18 shows similar comparisons to Figure 16 but for solar spectral irradiance in selected broad wavelength bands. NNLSSI1 also benefits from a higher-accuracy irradiance scale and, as evident in the left-hand column of Figure 18 (as well as Figure 6), the absolute scale differences from NRLSSI2 are wavelength dependent. Notably, the enhanced irradiance magnitude in the visible wavelengths below 700 nm is almost completely balanced by the reduction in irradiance magnitude in the near-infrared wavelengths longer than 700 nm (Richard et al., 2019, Richard et al., 2024). The right-hand column of Figure 18, which depicts the residual differences between NNLSSI1 and NRLSSI2 models after NRLSSI2 has been adjusted to the absolute irradiance scale of NNLSSI1 during December 2019, illustrates that the magnitude of the variability of the NNLSSI1 model also differs from NRLSSI2 in wavelength dependent ways. This is attributed to changes in model regression coefficients derived from the higher-precision TSIS-

1 SIM observations that inform changes in the wavelength-dependent impacts of facular and sunspots on spectral irradiance change. Also evident is the transition in facular brightening proxy from the Bremen Mg II index (used in NRL, Version 2) to the GOES operational Mg II index (used in NNL, Version 1) in early 2017, primarily at ultraviolet and near-ultraviolet wavelengths where the net irradiance change is dominated by faculae and the sunspot contribution is negligible. Figure 19 demonstrates that the spectral irradiance differences from Version 2 of the CDR grow in the historical era. As was the case in TSI, the historical changes in SSI are attributed to the improved understanding of historical irradiance change based on updated flux transport calculations applied to ever-lengthening record of satellite solar irradiance observations and ground- and space-based magnetic flux observations (Wang and Lean, 2021). The NNLSSI1 model also estimates smaller irradiance change between the historical era and present day than the NRLSSI2 model, consistent with NNLTSI1 estimates.

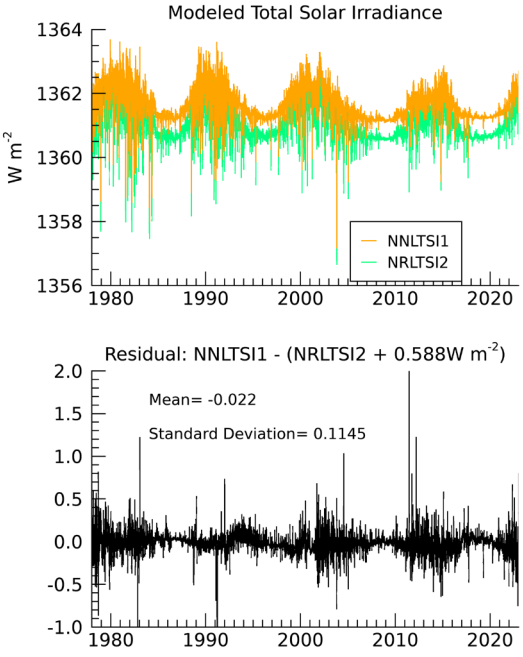

Figure 16: Comparison of NNLTSI1 total solar irradiance variations calculated by the algorithm with the earlier NRLTSI2 model of the Solar Irradiance CDR V02. At bottom is the residual difference between the datasets, after NRLTSI2 output is scaled to the more accurate NNLTSI1 level during solar minimum conditions in December 2019. NRLTSI2 scaling factor is listed in the plot title.

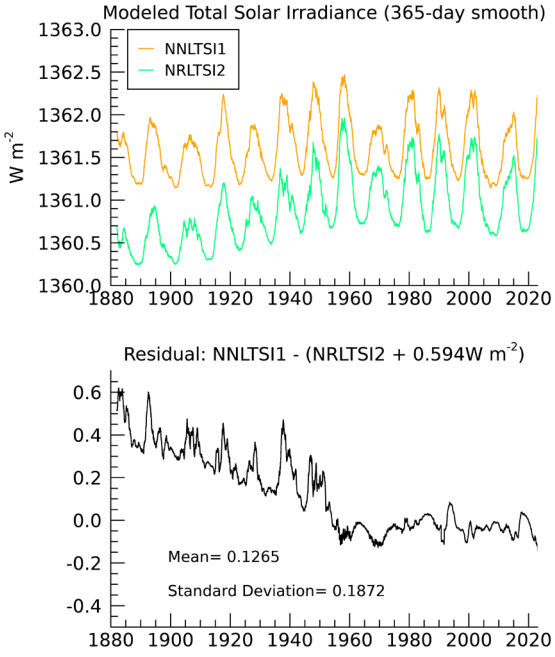

Figure 17: As in Figure 16, but for the period 1880-2023 and after 365-day smoothing applied to each data set to highlight the solar cycle variability.

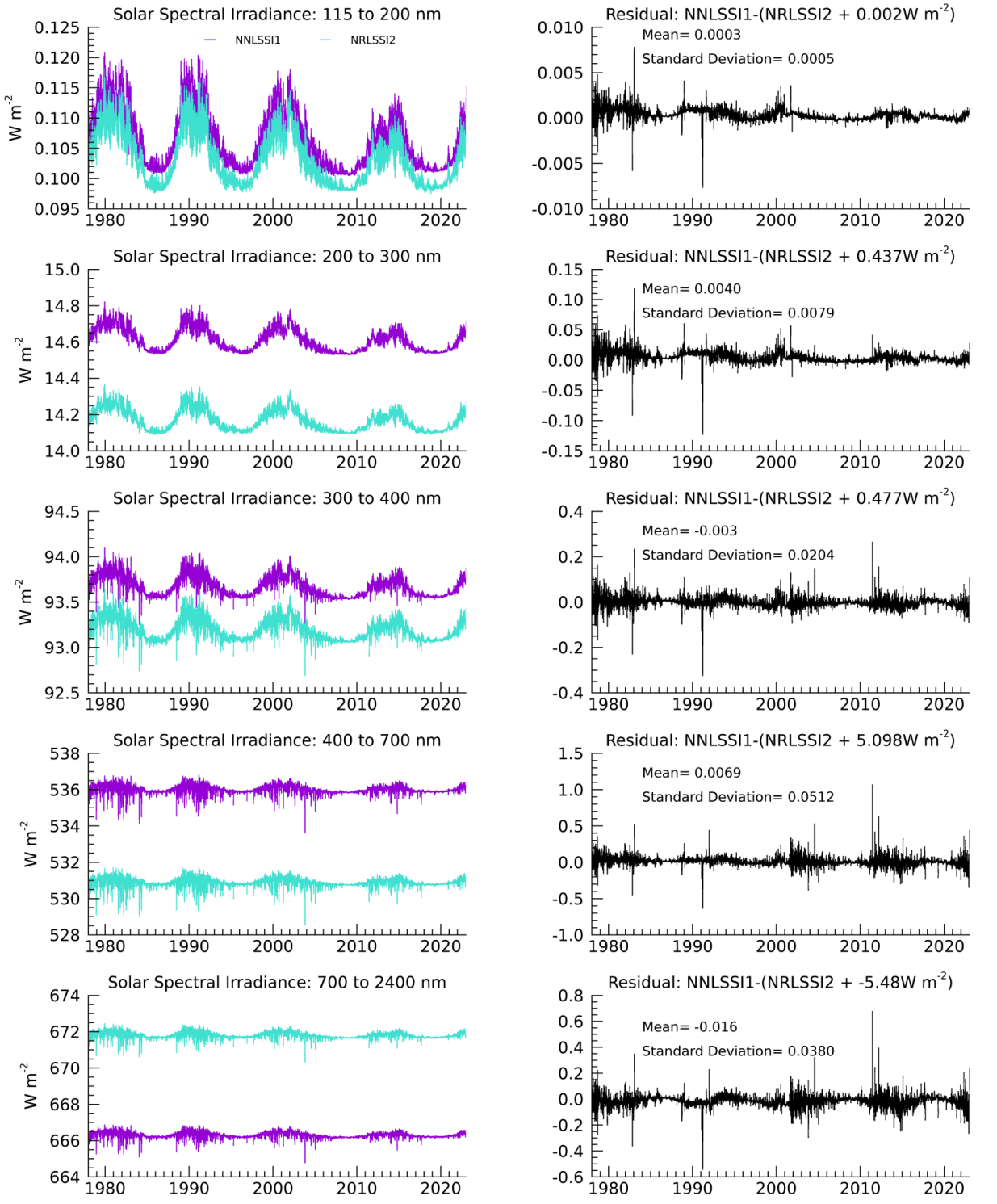

Figure 18: As in Figure 16 but for comparisons of NNLSSI1 solar spectral irradiance variation calculated by the algorithm and binned in selected broad wavelength bands with the earlier model, NRLSSI2. On the left are the time series in energy units. On the right are the residual differences between NNLSSI1 and NRLSSI2 (after NRLSSI2 offsets as listed in the subtitles); the mean and standard deviation of the residual differences from 1978-2023 are listed on each plot.

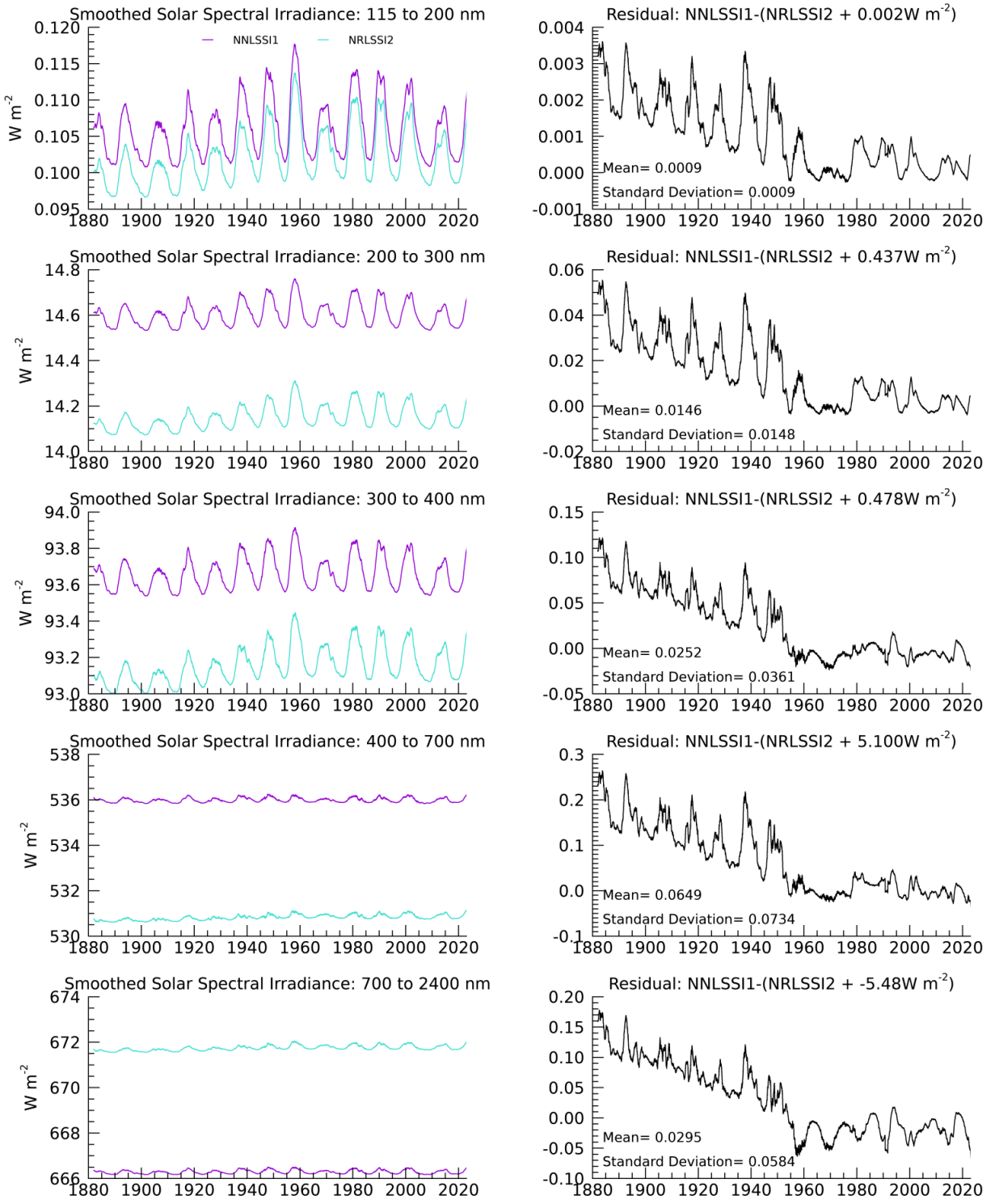

Figure 19: As in Figure 18, but for the period 1880-2023 and after 365-day smoothing applied to each data set to highlight the solar cycle variability.

4.2 Test Output Analysis

4.2.1 Reproducibility

The algorithm's calculation of total and spectral irradiance is 100% numerically reproducible given identical sunspot darkening and facular brightening inputs.

4.2.2 Precision and Accuracy

Numerically, the algorithm itself precisely and accurately calculates the total and spectral irradiance according to the specified sunspot darkening and facular brightening inputs, the baseline (quiet) reference irradiance values and the bolometric and wavelength-dependent scaling factors. An immediate verification of the algorithm performance is the numerical comparison of the total solar irradiance, $T(t)$, with the integral of the solar spectral irradiance. In CDR V3 $\int_{\lambda_0}^{\lambda\infty} I(\lambda,t)\,d\lambda$ and $\int_{\lambda_0}^{\lambda\infty} I(\lambda,t)\,d\lambda$ agree to better than 1.e-3. As well, the separate facular and sunspot components that the algorithm calculates for the total irradiance and the integrated spectral irradiance agree , i.e., $\Delta T_F(t) = \int_{\lambda_0}^{\lambda\infty} I_F(\lambda,t)\,d\lambda$ and $T_S(t) = \int_{\lambda_0}^{\lambda\infty} I_S(\lambda,t)\,d\lambda$ to better than 1.e-13. Verification of the high spectral resolution solar spectral irradiance is performed differently because it spans only a subset of wavelengths from 115-500 nm which precludes verifying the integral against the TSI. Instead, because the high resolution solar spectral irradiance is normalized to NNLSSI1 in 1-nm bins at their spectral range of overlap, we assume that the NNLSSI1h product is independently verified against NNLTSI1 via the highly consistent NNLSSI1 model performance.

The precision and the accuracy of the derived solar irradiance depend on:

1) uncertainties in the absolute scale of the reference solar irradiance, which are obtained from direct solar irradiance measurements made by instruments whose calibration is traceable to National Institute of Standards and Technology (NIST) standards (Harber et al., 2019; Richard et al., 2020; White et al., 2022; Kopp and Lean, 2011).

2) uncertainties in the input bolometric facular brightening and bolometric sunspot darkening functions, including those related to measurements of the indices, and to assumptions about the indices' representations of facular brightening and sunspot darkening.

3) statistical uncertainties of the coefficients, which are derived from regression against direct observations, that scale the facular and sunspot inputs to equivalent irradiance increments.

4) assumptions used to formulate the basic algorithm equations (as discussed in Section 6).

4.2.3 Error Budget

Error budgets for the total solar irradiance CDR V3 are time dependent and those for the solar spectral irradiance CDR V3 are time and wavelength dependent; when the bolometric facular brightening and bolometric sunspot darkening contributions are zero (i.e., the bolometric indices have their minimum values, $T_F(t) = T_{F,ref}$ and $T_S(t)=T_{S,ref}$, the error budget reduces to that

of the absolute uncertainty of the adopted irradiance of the reference baseline sun. But when the bolometric facular brightening and sunspot darkening contributions do not equal their reference values, which is typically the case, the estimation of these additional components produces additional uncertainties that increase the error budget.

Tables 6 and 7 provide uncertainty estimates typical of daily total irradiance and solar spectral irradiance, respectively, during high solar activity conditions (specifically, on 30 October 2023) arising from the first three sources of uncertainty identified in Section 4.2.2. Relative uncertainties in the absolute scale of the irradiance (see second to last row in Tables 6 and 7) are based on those reported for the direct measurements.

Uncertainties in the coefficients that transform the input indices to irradiance are obtained from the statistical output of the regression analyses used to construct the model that the algorithm uses (taking into account autocorrelation of the time series which decreases the number of degrees of freedom). The accuracy and stability of the input solar indices are monitored by comparisons with other independent proxies of solar indices that are not utilized in the algorithm.

The uncertainties in solar irradiance are written to output. Users of the Solar Irradiance CDR can compute the additive contribution due to the relative uncertainty in the absolute irradiance scale (the 1st source of uncertainty) in post-analysis with a user-guided value of the relative uncertainty in the absolute irradiance scale (multiplied by the reference baseline sun irradiance to convert to irradiance units). For example, in Tables 6 and 7 we list the contribution to the modeled total and spectral irradiance associated with the uncertainty in the absolute irradiance scale, $\sigma_{T_{ref}}$ and $\sigma_{I_{ref}}(\lambda)$.

Uncertainties arising from the assumptions used to formulate the algorithm are more difficult to assess objectively and establish quantitatively. Future work in support of ongoing efforts to produce a robust solar irradiance climate data record may extend the initial error estimates for the NNLTSI1 and NNLSSI1 modeled solar irradiance given in Tables 6 and 7. The future uncertainty estimates will also incorporate an understanding of the impacts of the assumptions in the algorithm's theoretical basis on the derived solar irradiance (itemized in Table 8). This future understanding will reflect previous peer-reviewed studies and statistical results from the operational production of the modeled solar irradiance.

Total Solar Irradiance

The total solar irradiance is determined (Section 3.4) as

$$T(t) = T_{ref} + T_F(t) - T_S(t)$$

The total uncertainty in $T(t)$ is

$$\sigma_T^{tot}(t) = \sqrt{\left(\sigma_{T_{ref}}\right)^2 + \left(\sigma_{T_F}(t)\right)^2 + \left(\sigma_{T_S}(t)\right)^2}$$

and the uncertainty in TSI variability relative to the reference value is

$$\sigma_T^{rel}(t) = \sqrt{\left(\sigma_{T_F}(t)\right)^2 + \left(\sigma_{T_S}(t)\right)^2}$$

Uncertainties in the bolometric facular brightening and bolometric sunspot darkening functions used to construct the TSI and SSI changes relative to their reference levels for TSI after 1978 (i.e., in the era of direct irradiance observations) are specified as

$$\sigma_{T_F}(t) = 0.0628 + 0.03841(t)$$

and

$$\sigma_{T_S}(t) = 0.0045 + 0.1056(t)$$

Lean et al. (2020) established these dependencies of the bolometric facular and sunspot uncertainties on the magnitude of quantities at time, *t*, using statistical analysis of an ensemble of models of TSI variability using 42 combinations of different TSI observations and facular and sunspot indices.

Figure 20 shows time series of total solar irradiance with time-dependent uncertainties indicted by grey shading. Table 6 lists values of the quantities used to estimate the uncertainty in total solar irradiance on 30th October 2003, a day when facular brightening and sunspot darkening values were relatively high (see Figures 4 and 5).

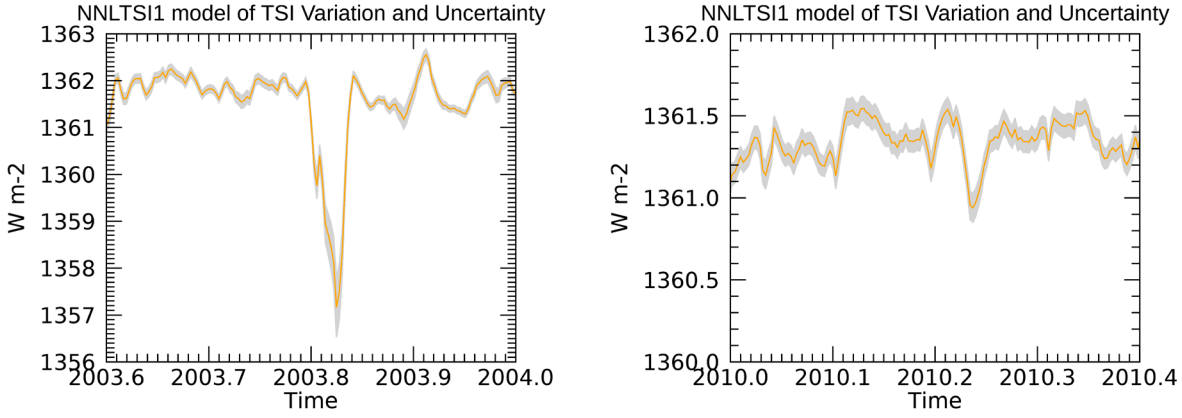

Figure 20: Examples of NNLTSI1 total solar irradiance variations and estimated uncertainties in the relative changes (i.e., excluding the ±0.27 W m^{-2} uncertainty in the total solar irradiance absolute scale) that the algorithm calculates during epochs of high solar activity (left) and moderate solar activity (right).

Table 6: Representative quantities and their uncertainties, used to estimate 1-σ relative uncertainties in the daily value of total solar irradiance produced by the algorithm on 30th October 2003, when facular brightening and sunspot darkening values were relatively high.

Quantity	Value and Uncertainty
$T_F(t)$ Bolometric facular change	1.769± 0.131 W m^{-2}
$T_S(t)$ Bolometric sunspot index change	5.534 ± 0.589 W m^{-2}
$T(t) - T_{ref}$ TSI change from quiet sun	-3.765 ± 0.603 W m^{-2}
T_{ref}	1361.2549 ± 0.272 W m^{-2}
$T(t)$ absolute value	1357.490 ± 0.662 W m^{-2}

Solar Spectral Irradiance

Solar spectral irradiance at wavelength λ and time *t* is determined (Section 3.4) as

$$I(\lambda,t) = I_{ref}(\lambda) + I_F(\lambda,t) - I_S(\lambda,t)$$

$$I_F(\lambda,t) = c_F(\lambda) \times T_F(t)$$

$$I_S(\lambda,t) = c_S(\lambda) \times T_S(t)$$

where $c_F(\lambda)$ and $c_S(\lambda)$ are scaling coefficients of the bolometric facular and sunspot components of T(t) that account for the wavelength-dependence of the facular and sunspot contrasts.

The total uncertainty in spectral irradiance at time, t, is

$$\sigma_I^{tot}(\lambda,t) = \sqrt{\left(\sigma_{I_{ref}}(\lambda)\right)^2 + \left(\sigma_{I_F}(\lambda,t)\right)^2 + \left(\sigma_{I_S}(\lambda,t)\right)^2}$$

and the uncertainty relative to the reference spectrum is

$$\sigma_I^{rel}(\lambda,t) = \sqrt{\left(\sigma_{I_F}(\lambda,t)\right)^2 + \left(\sigma_{I_S}(\lambda,t)\right)^2}$$

where

$$\left(\frac{\sigma_{I_F}(\lambda,t)}{I_F(\lambda,t)}\right)^2 = \left(\frac{\sigma_{c_F}(\lambda)}{c_F(\lambda)}\right)^2 + \left(\frac{\sigma_{T_F}(t)}{T_F(t)}\right)^2$$

and

$$\left(\frac{\sigma_{I_S}(\lambda,t)}{I_S(\lambda,t)}\right)^2 = \left(\frac{\sigma_{c_S}(\lambda)}{c_S(\lambda)}\right)^2 + \left(\frac{\sigma_{T_S}(t)}{T_S(t)}\right)^2$$

where $T_F(t) \pm \sigma_{T_F}(t)$ and $T_S(t) \pm \sigma_{T_S}(t)$ are the bolometric facular brightening and sunspot darkening indices and their uncertainties. Figure 21 shows $c_F(\lambda), c_S(\lambda), and\ \frac{\sigma_{c_F}(\lambda)}{c_F(\lambda)}\ and\ \frac{\sigma_{c_S}(\lambda)}{c_S(\lambda)}$.

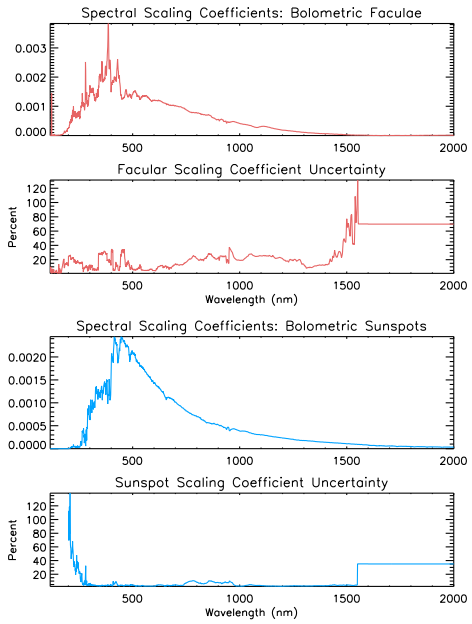

Figure 21: Wavelength dependence of percent uncertainties of the facular brightening and sunspot darkening coefficients, that the algorithm uses to calculate solar spectral irradiance variability.

The coefficients c_F and c_S are determined by multiple regression of the bolometric facular and sunspot indices against direct spectral irradiance observations, using both directly observed and detrended (with 81 day running means). The estimated uncertainties take into account autocorrelation in the time series (which reduces the number of degrees of freedom) and differences between the coefficients derived using the direct versus detrended time series.

Shown in Figure 22 are the changes in solar spectral irradiance estimated by the algorithm for 30th October 2003, a day when facular brightening and sunspot darkening are relatively high (see Figures 4 and 5), with associated wavelength-dependent uncertainties indicated by the gray shading. This is the spectral irradiance change that accompanies the large total solar irradiance decrease seen in 2003 in Figure 20. Figure 23 shows time series of the solar spectral irradiance during 2003 at 4 wavelengths. The numerical values in Table 7 for the spectral irradiance change and uncertainties on 30 October 2003 correspond to the same four wavelengths shown in Figure 23.

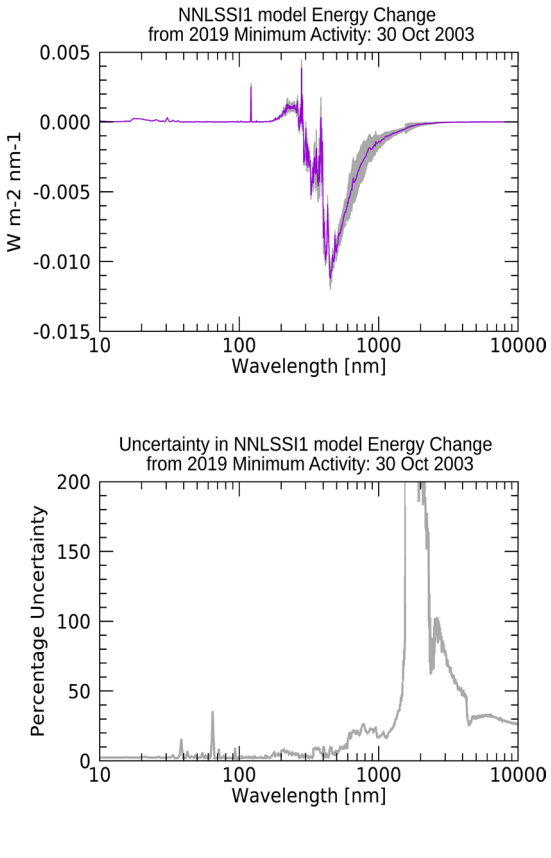

Figure 22: NNLSSI1 modeled solar spectral irradiance change typical of high solar activity and percentage uncertainties. Uncertainties shown are relative and exclude the additional uncertainty in the solar spectral irradiance absolute scale.

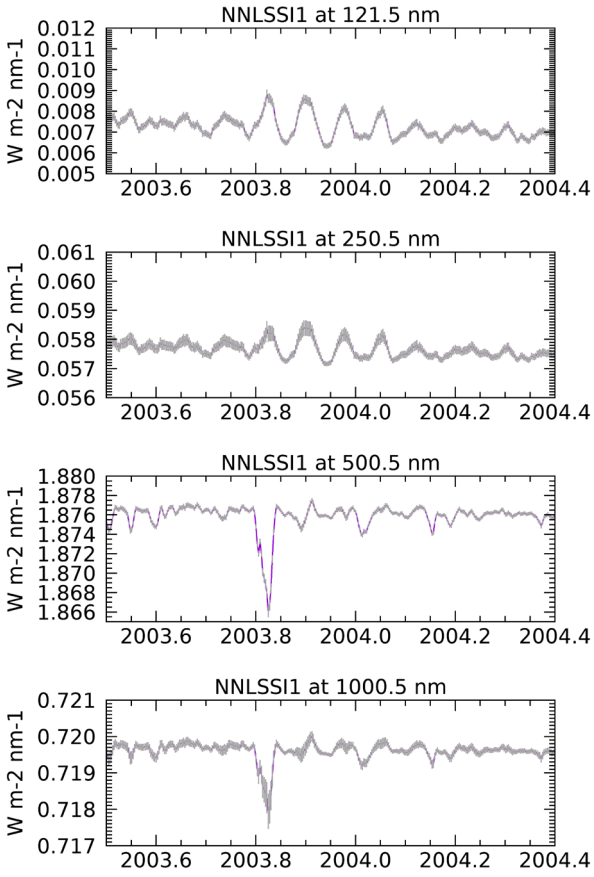

Figure 23: Solar spectral irradiance variations calculated by the algorithm during an epoch of relatively high solar activity for the four wavelengths listed in Table 7. Uncertainties shown are relative.

Table 7: Representative quantities and their uncertainties, used to estimate 1-σ uncertainties in daily values of solar spectral irradiance produced by the algorithm on 30th October 2003, when bolometric facular brightening and sunspot darkening indices were relatively high and equal to the values specified in Table 6.

Quantity	Value and Uncertainty 121.5 nm	Value and Uncertainty 250.5 nm	Value and Uncertainty 500.5 nm	Value and Uncertainty 1000.5 nm
$c_F(\lambda)$ scaling coefficient of bolometric facular index	0.0014±0.00003	0.0008±0.00013	0.0014±0.00011	0.0004±0.00008
$c_S(\lambda)$ scaling coefficient of bolometric sunspot index	0.0±0.00001	-0.0001±0.00001	-0.0021±0.00008	-0.0004±0.00001
$I_F(\lambda, t)$ facular index change	0.0026±0.0002 W m^{-2} nm^{-1}	0.0015±0.0003 W m^{-2} nm^{-1}	0.0025±0.0003 W m^{-2} nm^{-1}	0.0007±0.0002 W m^{-2} nm^{-1}
$I_S(\lambda, t)$ sunspot index change	0.0±0.0 W m^{-2} nm^{-1}	-0.0003±0.0 W m^{-2} nm^{-1}	-0.0115±0.0004 W m^{-2} nm^{-1}	-0.0021±0.0004 W m^{-2} nm^{-1}
$I(\lambda,t) - I_{ref}(\lambda)$ SSI change from quiet sun	0.0026±0.0002 W m^{-2} nm^{-1}	0.0012±0.0003 W m^{-2} nm^{-1}	-0.0090±0.0005 W m^{-2} nm^{-1}	-0.0014±0.0005 W m^{-2} nm^{-1}
$I_{ref}(\lambda)$	0.0061±0.0002 W m^{-2} nm^{-1}	0.0570±0.0007 W m^{-2} nm^{-1}	1.876±0.0060 W m^{-2} nm^{-1}	0.7311±0.0023 W m^{-2} nm^{-1}
$I(\lambda,t)$ absolute value	0.0086±0.0003 W m^{-2} nm^{-1}	0.0582±0.0008 W m^{-2} nm^{-1}	1.867±0.0060 W m^{-2} nm^{-1}	0.7300±0.0024 W m^{-2} nm^{-1}

5. Practical Considerations

5.1 Numerical Computation Considerations

The Solar Irradiance Climate Data Record algorithm uses basic algebra. There are no matrix inversions or extrapolations in the algorithm itself, which leads to a computationally rapid, efficient and repeatable algorithm. The computation of EUV SSI applies an 81-day temporal smoothing to the daily bolometric facular change to improve the representation of solar cycle change at all extreme ultraviolet wavelengths. This is performed with the IDL ts_smooth.pro function. Prior to 1874, when only annually-averaged values for the bolometric facular change are available, the computation of yearly-averaged EUV SSI does not apply this separate smoothing step, instead incorporating the (already smoothed) annually-averaged facular component of TSI change to represent this component.

The Solar Irradiance Climate Data Record processing utilizes LaTiS (formerly known as the LASP Time Series Server), an Application Programming Interface. This processing system accesses data files of reductions in sunspot intensity derived from NSO's GONG network images. The processing system also operationally accesses the composite Mg II index record made by the GOES satellite mission, the F10.7 cm solar radio flux made by the Dominion Radio Astrophysical Observatory and irradiance measurements as observed by the TSIS-1 mission using the same underlying LaTiS time series server. An automated routine downloads files to LASP's Interactive Solar Irradiance Datacenter (LISIRD) for access by the NNLTSI1, NNLSSI1, and NNLSSI1h solar irradiance algorithms.

The Solar Irradiance Climate Data Record is provided to NOAA NCDC as NetCDF4 data files (Section 3.4.7). LaTiS provides a second user access to the Solar Irradiance Climate Data Record for a user-specified time range and desired variables.

5.2 Programming and Procedural Considerations

Execution speed is rapid, and optimization is not needed. Given the facular and sunspot indices, the algorithm calculates the corresponding total and spectral irradiance and high-resolution spectral irradiance in 2.5 seconds (on a 2021 MacBook Pro with an M1 Max CPU (10 cores) and 32 GB RAM).

5.3 Quality Assessment and Diagnostics

The quality assurance (QA) process utilizes both the science analysis and the data quality assurance. The Solar Irradiance Climate Data Record team oversees this process, which involves regular, careful examination of all solar and proxy data, and assesses the veracity and quality of the data to be released. The quality assurance takes several different forms based on: 1) the confidence in the calibration and performance of the instruments providing solar and proxy observations, 2) comparisons of model output with previous and simultaneous measurements, taking into account the calibration and performance of the direct, independent solar irradiance observations, and 3) understanding of the Sun and its variability – an

understanding based on a broad range of solar models and on multiple solar observations at other wavelengths.

The Solar Irradiance Climate Data Record production system supports both automatic and manual diagnostic statistical analyses of the science products. Deviations from expected or predicted values, flagging of anomalous and/or duplicated values, and trends of the bolometric sunspot darkening function and bolometric facular brightening function, as well as final science values, are all incorporated into the assessment of the stability in the final science data products. The Solar Irradiance CDR V3 benefits from automated processes already developed, tested, and implemented during the production of the earlier Solar Irradiance CDR V2. However, the quality assurance for the CDR V3 continues to involve manual quality assurance particularly for the physical representativeness of the bolometric facular brightening and sunspot darkening functions.

Physical and statistical relationships between the bolometric facular index, the GOES Mg II index, and independent metrics including the Mg II index acquired from non-GOES platforms, ground-based observations of the Ca K index, the F10.7 cm solar radio flux and other solar indices are used to identify and flag outliers in the Mg II index value that is used to derive the bolometric facular brightening function. In addition, the time series of GONG sunspot intensity reductions is monitored against the sunspot blocking derived from the SOON sunspot area, number, and location records. The CDR V3 also provides the ability to derive either the bolometric facular brightening or sunspot darkening indices using the direct TSI observations and the other input; these derived bolometric properties can also be compared with independent metrics as another quality assurance check.

Table 8 lists the assumptions in the algorithm. The operational steps to monitor time series of algorithm inputs and the output solar irradiance are also noted.

5.4 Exception Handling

The processing code is not currently robust when it comes to exception handling. Error conditions are unlikely, assuming the processing environment is adequately prepared. Future enhancements will ensure that appropriate error messages are returned.

5.5 Algorithm Validation

In addition to the checks on the algorithm performance described in Section 4, the algorithm is validated by comparing the total and solar spectral irradiance times series that it produces with direct observations where available, and with other models of irradiance variability.

Figures 24 compares the NNLTSI1 total irradiance time series with the observations made by a composite record from a series of LASP TIM TSI instruments on SORCE, TCTE, TSIS-1 and CTIM platforms, the NRLTSI2 model (of the Solar Irradiance CDR V2), and the original NRLTSI model. The comparisons highlight the differences in absolute irradiance scale (Figure 24 top and middle) and the variability for high and low solar activity conditions (Figure 24 bottom).

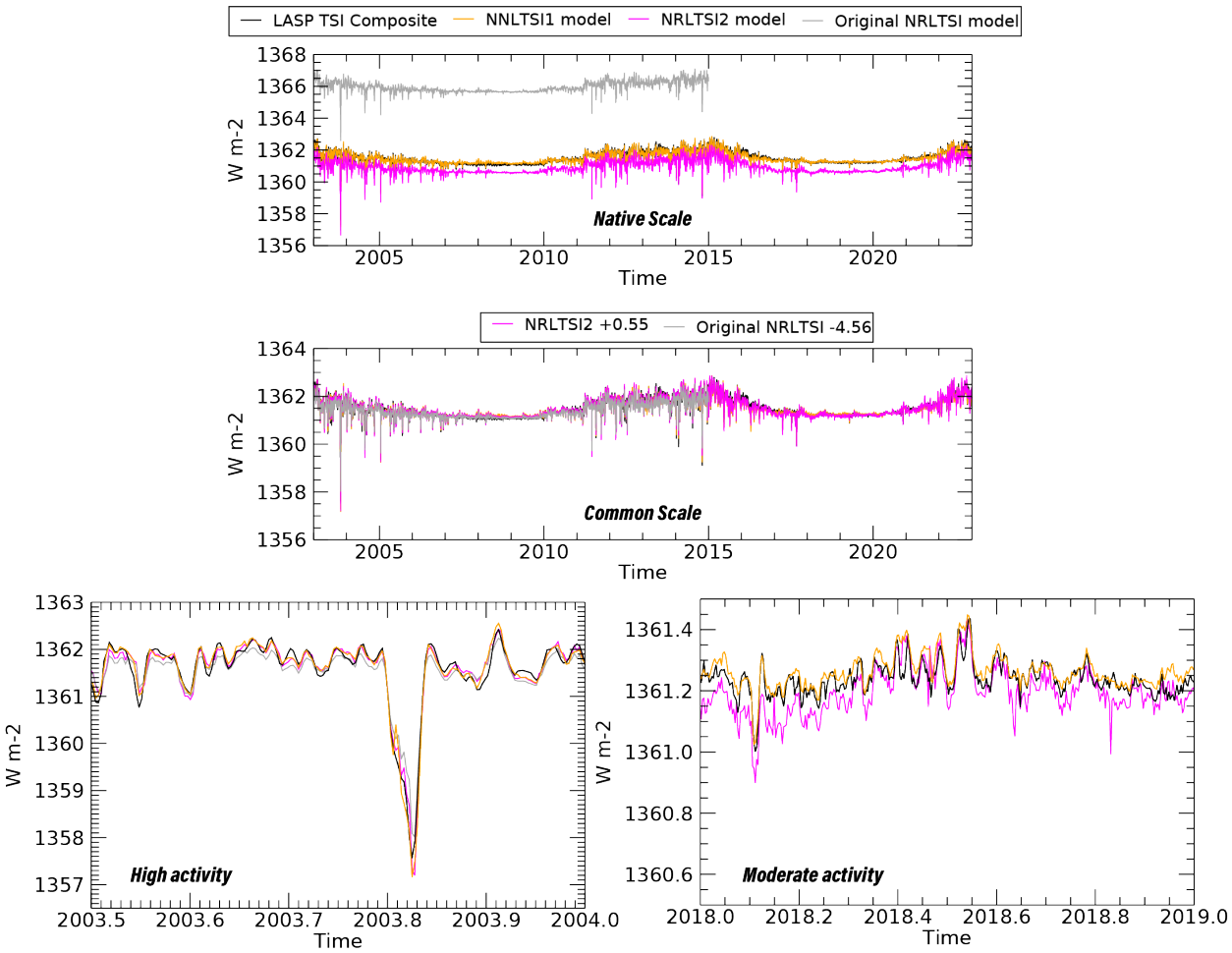

Figure 24: (top) The total solar irradiance time series calculated by the algorithm (NNLTSI1 model), the earlier CDR V2 (NRLTSI2 model), and the original NRLTSI2 model are compared with the CDR V3 TSI observational composite comprised of the LASP TSI composite since 2003 and the PMOD composite prior to 2003 after adjustment to the absolute irradiance scale of the LASP TSI composite. The comparisons are shown on the native scales of the dataset and after normalization to the LASP TSI composite (normalization factors are listed in legend). (bottom) The comparisons are shown during solar rotation at high and moderate activity conditions.

Figure 25 shows the residual difference of daily TSI in the CDR V3 observational TSI composite and estimated by the NNLTSI1 and NRLTSI2 models since 1978. The NNLTSI1 model better estimates observed daily variability as evidenced by smaller mean and standard deviation of the difference relative to the earlier NRLTSI2 model. The improved reproduction of TSI in the NNLTSI1 model is particularly noticeable after 2003 where the CDR V3 TSI composite is the LASP TSI composite developed from highly accurate and stable TIM instruments. The NNLTSI1 model-data residuals have a mean of 0.012 W m^{-2} and a standard deviation of 0.181 W m^{-2} from 1978-2023 compared with 0.022 W m^{-2} mean difference and a standard deviation of 0.197 W m^{-2} for the NRLTSI2 model, after accounting for absolute scale difference. Between 2003 and 2023, the slope of the NNLTSI1 model-data residual is 1.27 part per million (ppm) per year.

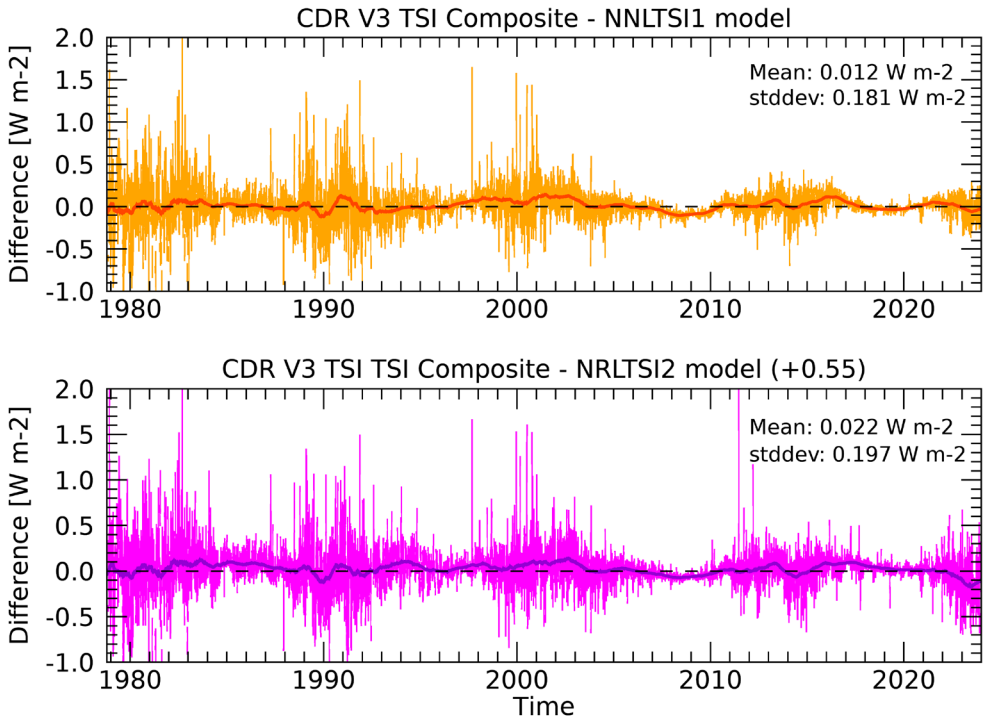

Figure 25: Differences in daily total solar irradiance that the algorithm calculates (according to NNLTSI1) with the CDR V3 TSI composite (upper) and the NRLTSI2 model of the CDR V2 (lower).

The NNLTSI1 model explains 95.2% of the observed daily variability (correlation coefficient 0.976) in the LASP TSI composite (2003-2023) relative to the NRLTSI2 model performance that explained 92.0% of the observed daily variability in the LASP TSI composite (correlation coefficient 0.963) over the same period.

Figure 26 compares time series of solar spectral irradiance binned in selected broad wavelength bands, calculated by the NNLSSI1 model algorithm, compared with observations made by TSIS-1 Spectral Irradiance Monitor (SIM) instrument and with equivalent time series of the NRLSSI2 model after accounting for absolute scale differences relative to TSIS-1 SIM. The comparisons show spectral irradiance modulation associated with the Sun's 27-day rotation. On these relatively short (compared with the solar cycle) time scales, instrumental effects in the observations are assumed to be modest compared with true solar irradiance variability. Improvements in model inputs, particularly the bolometric sunspot darkening derived from the NSF GONG network are evident in the NNLSSI1 spectral irradiance output. For wavelengths > 300 nm, where sunspots contribute to irradiance reductions, the estimated variability of the NRLSSI2 model is noisier than that of NNLSSI1.

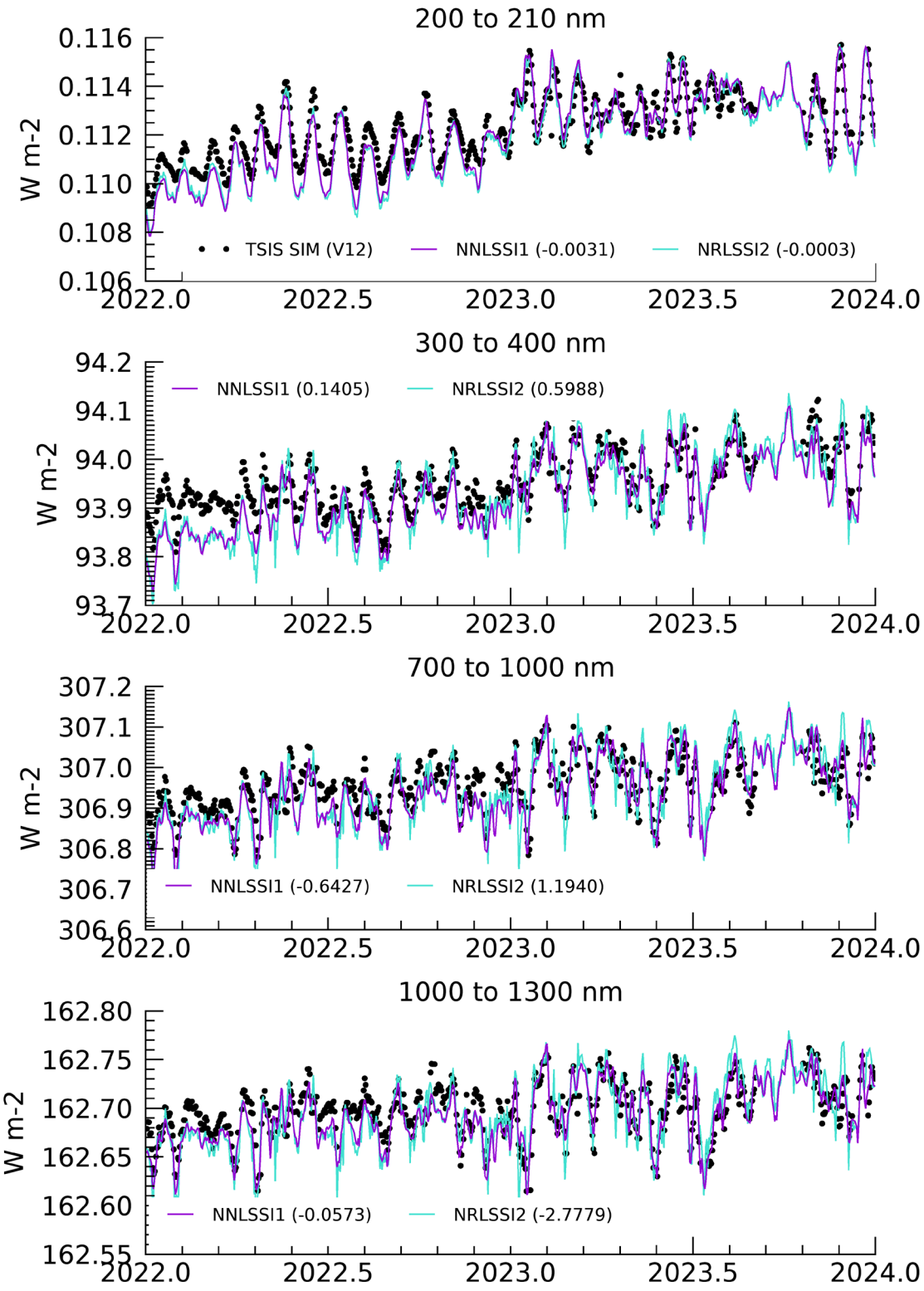

Figure 26: Shown are time series of solar spectral irradiance variations that the algorithm calculates (i.e., the NNLSSI1 model) and binned in broad wavelength bands compared with TSIS SIM (V12) observations from 2022 to 2024. For comparison, also shown are NRLSSI2 model output of the CDR V2. The primary variations are associated with the Sun's 27-day rotation.

The TSIS-1 SIM record is more stable than the predecessor SORCE SIM record. Thus, actual solar cycle spectral irradiance changes are less-ambiguous with the TSIS-1 SIM record than they were for the SORCE SIM record that ended in 2020. However, observed solar spectral irradiance cycle changes remain more uncertain than that of the total solar irradiance record. Figure 27 shows solar cycle changes in spectral irradiance estimated by the NNLSSI1 algorithm, compared with the changes estimated by NRLSSI2.

The Solar Irradiance Climate Data Record Team will continue to validate the solar irradiance CDR algorithm, with ongoing tests, statistical characterizations and self-consistency checks, and comparisons with observations.

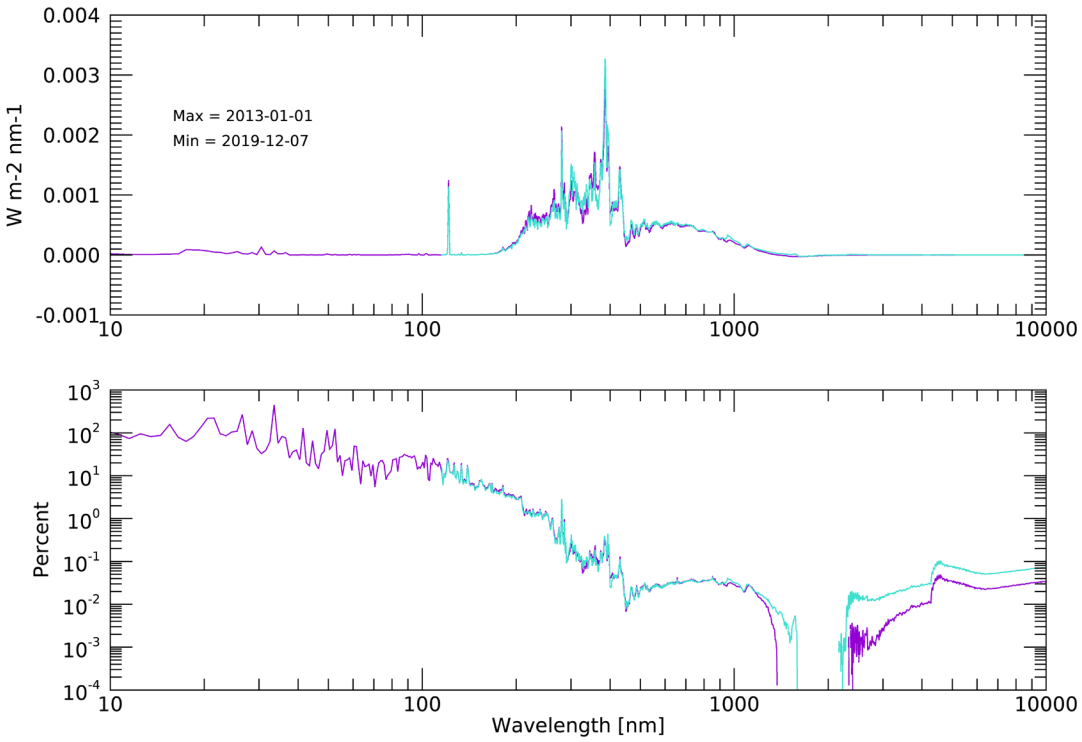

Figure 27: Shown are the solar spectral irradiance changes during the descending phase of solar cycle 24, in both energy units (upper) and percentages (lower), that the algorithm calculates (using the NNLSSI1 model) from solar minimum at the end of 2019 to high solar activity at the start of 2013, compared with corresponding changes estimated using the NRLSSI2 model.

5.6 Processing Environment and Resources

The processing code is written in IDL and requires version 8.6 or later. It runs on commodity hardware (e.g. 10 cores 32GB RAM) with modest computation time, taking less than one minute to process one day. In principle the code could run on any OS with IDL, although it was developed on Unix-based systems. All the processing routines and utility routines are included in the code repository. The only (unlikely) storage concerns are for the final output products.

LaTiS, an Open Source software framework developed at LASP to provide uniform access to datasets, provides the primary data access layer. The GONG sunspot intensity reduction or the sunspot area data, the F10.7 solar radio flux from DRAO, and the MgII index data from GOES or from the University of Bremen (adjustment to GOES scale applied) are converted to bolometric facular brightening and sunspot darkening quantities, which are then provided to the IDL processing code from a LaTiS server running at LASP. Other input files are included in the code repository and read directly by the IDL code.

6. Assumptions and Limitations

The assumptions in the algorithm's theoretical basis are detailed in Section 3. Table 8 summarizes these assumptions and the approach, where possible, to quantifying and monitoring their impacts on the modeled solar irradiance. The accuracy of the modeled solar irradiance also depends on the inputs (bolometric facular brightening and sunspot darkening indices) and the measurements used to derive these inputs (the Mg II index from GOES EUVS solar spectrum observations and sunspot intensity reductions from GONG white light solar images) and the reference Sun measurements have uncertainties themselves. In addition, there are uncertainties in the representativeness of the indices to the true (wavelength-dependent) facular brightening and sunspot darkening that produce irradiance changes. Also contributing to the uncertainty in the modeled irradiance, and possibly the easiest to quantify, are statistical uncertainties in the coefficients obtained by multiple regression of the input indices to the measured solar irradiance (total and spectral).

Several validation studies have been performed, as illustrated in Section 5.5. The uncertainty estimates given in Tables 6 and 7 account for uncertainties in the input indices and in the multiple regression coefficients, and how these translate to equivalent irradiance uncertainties. But these estimates do not account for scientific assumptions in the algorithm. Work is ongoing to estimate more realistic uncertainties in the NNLTSI1 and NNLSSI1 modeled solar irradiances, by incorporating better quantification of the algorithm's assumptions, such as those that Table 8 identifies.

Table 8: Summary of assumptions in the theoretical basis for modeled solar irradiance, model inputs and the potential validation approaches. Validation approaches that can be monitored over time (i.e. statistical) to provide an estimate in the uncertainty in the modeled solar irradiance are labeled '*Operational*'.

Assumptions & Scientific Support/Citation(s)	Validation Approach
The adopted value of the reference baseline Sun (total and spectral) is not invariant from minimum-to-minimum (Wang and Lean., 2021).	Comparison to irradiance measurements at solar minimum conditions. Comparison of magnetic flux at solar minimum conditions.
Faculae brightening and sunspot darkening are the only modulators of *contemporary* solar irradiance and their respective impacts on irradiance are represented by linear adjustments of baseline, reference, conditions (Lean et al., 1998, 2005; Lean, 2000; Lean and Woods, 2010; Lean, 2018, Wang and Lean, 2021).	The derived bolometric facular and sunspot functions are imperfect indicators of the sunspot darkening and facular brightening sources and their uncertainties are derived from the statistical spread from 42 different irradiance model combinations. ***Operational***: Monitor the correlation between contemporary modeled and measured solar irradiance, and the standard deviation of residuals between modeled and measured solar irradiance.
The background, facular brightening during *historical*, longer-term time scales (decade, centennial) remains speculative (Lean et al., 1992, 1995, 2000, 2002, 2005;	Improvements to the plausible magnitude of facular brightening, as simulated from a flux-transport model that simulates eruption, transport, and accumulation of magnetic flux from Maunder Minimum to present, has

Hoyt and Schatten, 1993; Tapping et al., 2007; Radick et al, 1998; Hall and Lockwood, 2004; Wang et al., 2005). However, longer irradiance and magnetic flux records, combined with advanced flux transport models, have identified a solar cycle-phase specific dependency to the historical facular brightening (Wang and Lean, 2021); this has been implemented in NNLTSI1/NNLSSI1 models.	been evaluated in conjunction with a new, reproduction of the sunspot number.
	• The rise in solar irradiance since the Maunder Minimum is estimated as 2-3x smaller than estimated in the NRLSSI2 model, which was by itself 4x smaller than the original NRLSSI estimate.
	• Monitor circumstantial evidence of facular impacts on irradiance trends:
	  ○ Reduction in measured TSI corresponding with disappearance of faculae.
	  ○ Variations in chromospheric activity of Sun-like stars.
	  ○ Inferences with cosmogenic and geomagnetic indices.
	  ○ Inferences with changes in solar structure.

The bolometric reduction in intensity due to sunspot darkening can be computed using operational NSO GONG white light images. The derived sunspot blocking is an improved representation of the sunspot blocking derived from using sunspot areas, heliocentric locations, and number of individual sunspot regions (Allen, 1979; Lean et al., 1998; Brandt, Stix and Weinhart, 1994).
• The relative contrast of sunspots to baseline Sun irradiance is known with these assumptions:
  ○ The center-to-limb variation is dependent on wavelength and sunspots at the limbs contribute less to irradiance variability than assumed by the Delta-Eddington approximation.
  ○ Sunspot contrast is independent of position on solar disk and has an experimental bolometric (integrated) value of 0.32.
  ○ Sunspot darkening function is the average of all sunspot areas and locations over the day.
  ○ The reduction in white light intensity from sunspots is highly correlated with the sunspot darkening function derived from sunspot areas and locations.
	The solar rotation axis, ecliptic plane (beta angle) are known throughout the year and are used to adjust the projection of sunspot areas to the direction of the Earth, as it orbits the Sun.
	• Sunspot areas prior to 1977 are corrected for a systematic 35% high bias (measurement error).
	• ***Operational***: Monitor mean and standard deviation of time series of sunspot darkening function derived from the GONG white light images and the SOON network.
	• ***Operational***: Implement quality flags for the sunspot blocking function. Flag:
	  ○ Missing station data
	  ○ Duplicate records
	  ○ Larger (or smaller) than expected variability.
	• ***Operational***: Monitor relationship between sunspot intensity reduction, and sunspot areas and sunspot number. If sunspot number is zero, a physically plausible result of sunspot area is 0 (i.e. “positive” result). If sunspot number is non-zero, a physically implausible result is a sunspot area of 0 (i.e.“negative” result).

The facular brightening function is a linear function of a flux "proxy" of facular brightening (Lean et al., 1998). • The Mg II index is a proxy for chromospheric variability, which is an extension of photospheric faculae (Snow et al., 2005). • The Mg II index is (relatively) free of instrumental sensitivity (drifts). • The operational GOES EUVS Mg II index record is ensured through the mid-2030's.	Faculae are poorly observed in solar imagery and inadequately specified. • ***Operational***: Monitor mean and standard deviation of time series of facular brightening function. o For single, and multiple (i.e. overlapping in time) instruments. • ***Operational***: Monitor relationship between time series of Mg II index and the 10.7 cm radio flux. The relationship is expected to be consistent; a deviation is expected to be indicative of outlier in the Mg II record. • ***Operational***: Implement quality flags for facular brightening based on Mg II record. Flag: o Time gaps. o Larger (or smaller) than expected variability. o Outliers (when compared to F10.7 cm flux). • **Operational**: Filter the Penticton F10.7 cm flux data for one daily, near-noon value, free of radio bursts. • Future, quantitative record of facular brightening could be derived from the operational GONG magnetograms and white light images (after intensity reductions from sunspots are removed) • Future, reliable and quantitative, observations can be used to define statistical definitions of spectral irradiance changes due to faculae.
A LASP composite TSI record of measurements from 2003 through 2023 is the total solar irradiance standard used to compute scaling coefficients of facular brightening and sunspot darkening for NNLTSI1 using a multiple linear regression technique. • TSI adopted reference solar irradiance is 1361.2549 Wm-2 (Harber et al, 2019), based on the average of TSIS TIM and Compact TIM measured TSI during December 2019.	***Operational***: Monitor the correlation between contemporary modeled and measured total solar irradiance, and the standard deviation of residuals between modeled and measured total solar irradiance.
TSIS SIM measurements contain fewer instrumental trends than SORCE SIM but known temperature and instrumental artifacts remain (Richard et al., 2019). • Facular brightening coefficients derived from detrended (with 81 day running mean removed) or non-	Differences in facular and sunspot contrasts from theory and observation are not well understood. Compare wavelength-dependent scaling coefficients of facular brightening and sunspot darkening derived from observation to their respective theoretical contrasts (ratio of emission to quiescent solar atmosphere).

detrended TSIS SIM data differ at some wavelengths. o Prescribed uncertainties for facular brightening are larger at wavelengths where the coefficients differ depending on the approach. • Sunspot darkening coefficients derived from detrended or non-detrended TSIS SIM observations are consistent.	

The most probable cause of the algorithm generating incorrect irradiance values lies with the determination of the bolometric facular brightening and sunspot darkening indices, which rely on ground- and space-based observations of global intensity reduction from sunspots and global facular brightness. The accuracy and precision of these ground-based observations is essentially unknown, and spurious inputs could produce unrealistic irradiance values. The algorithm flags input values that are missing and/or deemed implausible, outside the range of current observed values.

Quality assurance algorithms will be improved to validate concurrent sunspot darkening and facular brightening inputs from multiple sensors that will aid in securing a more robust algorithm. For input to NNLTSI1/NNLSSI1 calculations of sunspot blocking are made for concurrent days using two independent sources, the USAF/SOON and the GONG network. Additionally, the operational GOES Mg II index is compared with the independently produced Bremen Mg II index research product and a TSIS-1 Mg II index on concurrent days.

6.1 Algorithm Performance

There are no assumptions made concerning algorithm performance. The algorithm is designed to compute modeled solar irradiance, using basic algebra, over a user-defined time range, and this input time range can be of arbitrary length. The algorithm is free of matrix inversions or parameter extrapolations and the execution is rapid and repeatable. A temporal smoothing of the facular component of TSI variability is accomplished with the IDL ts_smooth.pro function.

6.2 Sensor Performance

The solar irradiance reconstructions that this C-ATBD describes compliment the direct measurements of total and spectral solar irradiance made by the Total and Spectral Solar Irradiance Sensor (TSIS-1) instrument, documented in the TSIS ATBD (Coddington et al., 2014). The TSIS-1 ATBD describes the algorithms used to produce all data levels of solar and spectral irradiance for the TSIS instrument complement, which consists of the Total Irradiance Monitor (TIM) and Spectral Irradiance Monitor (SIM). The TSIS-1 ATBD also describes the predicted science and housekeeping operation modes, measurement error budgets, and the plan to monitor and correct for instrument degradation. TSIS-1 SIM instrument papers (Richard et al.,

2019; 2020) and a separate SIM instrument degradation paper (Mauceri et al., 2018) provide further details.

For solar irradiance, variations of less than 0.1% per decade are typical of the kinds of signals that must be extracted from "noisy" time-series measurements. The calibration approach adopted for TSIS TIM characterizes the flight instrument as an "absolute sensor". TSIS SIM is also characterized as an absolute sensor, followed by end-to-end absolute calibration to reach final uncertainties of < 1% (Richard et al., 2019). This involves characterizing each term in the measurement equation and tabulating a list of individual uncertainties and root sum square errors for overall measurement uncertainty.

Accuracy and Long-term Stability of the TSIS Instrument Complement

The TSIS TIM instrument is more accurate than the SORCE TIM due to engineering advances in the optical and electrical sensors and to the end-to-end validation of the radiometer at the TSI Radiometer Facility (TRF) at the Laboratory for Atmospheric and Space Physics (LASP). The Compact TIM demonstration instrument, and advances in room-temperature ground irradiance reference standards (White et al., 2022), provide even further accuracy advances.

Lessons learned from the first-ever measurements of daily spectral solar irradiance longward of 400 nm made by the SORCE SIM were incorporated into the TSIS SIM to meet climate-quality measurement requirements. Specific TSIS SIM capability improvements relative to SORCE SIM include reduced uncertainties in the prism degradation correction to meet long-term stability requirements, improved noise characteristics of the electrical substitution radiometer (ESR) and photodiode detectors to meet the measurement precision requirement, and improved absolute accuracy through pre-launch calibration using the novel, Spectral Radiometer Facility (SRF) at LASP. The SRF was not designed and built at the time of SORCE launch. The TSIS TIM observations are more stable and accurate than the TSIS SIM observations.

The TSIS-1 TIM measures 4x daily total solar irradiance with an absolute accuracy of ~150 ppm and a relative accuracy of 10 ppm per year. The TSIS-1 SIM measures 2x daily solar spectral irradiance at variable resolution from 200-2400 nm with an absolute accuracy of 0.41% < 460 nm and 0.24% > 460 nm, a relative accuracy of 0.05% (500 ppm) at the shortest wavelengths near 200 nm and 0.01% (100 ppm) at all other wavelengths, and long-term relative stability of 0.02% per year (for wavelengths shortward of ~250 nm) and <0.01% per year for wavelengths longward of 400 nm (Richard et al., 2024).

Degradation Monitoring and Correction of the TSIS Instrument Complement

The sensitivities of all instruments on TSIS are assumed to degrade as the mission progresses and solar exposure accumulates. There are general assumptions that the degradation will monotonically decrease with time, although not linearly, and that a primary cause of the decreased sensitivity is related to the exposure to the harsh radiation environment from the Sun and the presence of on-orbit contaminants. However, there is no guarantee these assumptions will be met and other changes that are strictly time-dependent, or aging effects, must also be considered. The possibility that instrument sensitivity may increase cannot be ruled out, and the degradation analysis does not preclude this condition (Mauceri et al., 2018).

Exposure and time-dependent degradation is a challenging problem that requires refinements throughout the mission as well as considerable analyses effort by the TSIS instrument scientists. In addition, initial correction parameterization may need evaluation and modification during the mission (see TSIS-1 release notes, https://lasp.colorado.edu/tsis/data/ssi-data/sim-ssi-release-notes/ and https://lasp.colorado.edu/tsis/data/tsi-data/tim-tsi-release-notes/). Unexpected changes to the thermal stability of the spacecraft environment may require offsets in the analysis of certain data, and electronics and detector functionality can be impacted by energetic particles in major solar storms. Such impacts may require discontinuous changes in the science product rather than parameterized functions.

The Solar Irradiance Climate Data Record Team maintains close contact with the TSIS instrument science team to secure robust understanding of observed long-term solar irradiance variations. The technique used to understand instrument degradation for the TSIS TIM and SIM instruments is to have completely independent instrument channels, to use each channel with a varying duty cycle, and then to compare their observations of the Sun (Mauceri et al., 2018; Richard et al. 2019, 2020, 2024). The degradation in the instruments is assumed to be primarily dependent on the exposure of the optics and detectors to solar radiation. With the assumption that exposure-dependent degradation will proceed proportionally faster for the normal channel, an exposure-dependent model of degradation is developed.

7. Future Enhancements

Planned for the future are improved determinations of the sunspot darkening and facular brightening inputs and their wavelength-dependent contrasts. In the future, the algorithm may be revised and updated with a new formulation framework and coefficients, to reflect improved understanding of solar irradiance absolute scale and variability from ongoing analysis and recalibration of existing irradiance (and other) datasets, as well as the availably of reprocessed and new irradiance databases, such as from TSIS-1, TSIS-2, and beyond.

Because solar irradiance is an essential, universal input for models of the terrestrial environment, we have provided a new high resolution solar spectral irradiance product to accommodate the needs of the atmospheric chemistry user community. Additionally, we have provided an extended solar spectral irradiance for an enhanced wavelength range from ~ 0 nm to 200,000 nm. Future enhancements will include validation and verification of the high resolution solar spectral irradiance, which we plan to monitor closely, and extension to EUV wavelengths. Thus, the Solar Irradiance CDR will also serve evolving needs of the space weather community, who utilize extreme ultraviolet solar irradiance in models of thermospheric satellite drag, for example.

7.1 Enhancement 1: Improved Facular Brightening Index

The operational GONG network provides a superior record of the sunspot darkening function. Because the solar irradiance climate data record algorithm is formulated from multiple regression of the facular brightening and sunspot darkening indices with the LASP composite of TIM observations, changes in either index necessarily affect the proportion of irradiance variability that the model ascribes to each. As such, an improved sunspot darkening index enables superior assessment of limitations in the current facular index. A newly funded Solar Irradiance Science Team (SIST-4; PI: J. Lean) will investigate an alternative facular brightening index derived from the GONG network of concurrent magnetograms and white light images. The approach to attain improvements to the bolometric facular index involves removing the sunspots from the magnetograms (via the white light intensity images) and analyzing the residual magnetic flux relative to some baseline value as “facular enhancements”.

The alternative facular enhancement will be assessed against the various Mg indices produced by different groups. To date, securing a facular index that has robust long-term (solar cycle time scale) stability has proven challenging because there are distinct and reported differences among various Mg indices produced by different groups. In particular, changes from the successive 1996 to 2008 solar minima are not consistent (within current understanding) among various solar proxy indices (Snow et al., 2014). Analysis and study by the solar irradiance community is ongoing to secure the most reliable, long term facular index possible, including newly developed composite records of the Ca K enhancement. We will test the effect of new indices in the model formulation and algorithm, as well as compare different indices to better

quantify irradiance uncertainties arising from this index. This future analysis of various facular brightening indices will enable improved uncertainties for this input to the algorithm.

7.2 Enhancement 2: Improved Model Formulation

The solar irradiance algorithm uses coefficients that require three databases for their determination: a time series of observed solar irradiance, a time series of the facular brightening index and a time series of sunspot darkening index. Significant (or even modest) changes in any of these time series result in altered algorithm coefficients that may warrant a new algorithm version. The facular time series may change as a result of Enhancement 1 and the new sunspot intensity reductions derived from the GONG network have resulted in changes to the sunspot time series. The solar irradiance dataset may change as a result of reprocessing existing observations or by the addition of new observations. In another case, the introduction of additional terms to the regression analysis would result in a new model formulation and CDR algorithm. The overall consistency of the magnitude of solar irradiance variability estimated by the NNL1 (CDRV3) and NRL2 (CDRV2) models in the current era suggests that the algorithm coefficients are robust within their stated uncertainties.

The CDR V3 is more robust to missing indices than the previous CDR V2. In the case of a single missing model input, it is possible to derive the value from the other model input and from the observed TSI (see Section 3.2).

7.3 Enhancement 3: Improved Exception Handling

The processing code is not currently robust when it comes to exception handling. Error conditions are unlikely, assuming the processing environment is adequately prepared. Future enhancements will ensure that appropriate error messages are returned.

7.4 Enhancement 4: Improved Quality Flagging

The current implementation of the data quality flags remains relatively immature. While substantial improvements were made to quality flagging of the USAF/SOON network sunspot area observations for the CDR V2, the CDR V3 is incorporating new model inputs. As the operational production of the CDR V3 advances, opportunities will arise to make enhancements in implementing a bit mask for multiple flags, improving the QA record to identify suspected outliers and duplicate or missing records in the input facular brightening and sunspot darkening indices, as well as outliers in the modeled total and spectral solar irradiance time series. The flagging of outliers in the input data will be assessed by comparison to independent but correlated data sets. The flagging of outliers in the modeled total and spectral solar irradiance will be based on comparisons to the measurement record. A second SIST-4 team (PI: O. Coddington) is producing a gap-filled TSIS-1 SIM record with CDR V3 data. This activity will result in a robust understanding of the performance of the measurements and the CDR V3. This, concurrent with knowledge of modeled irradiance developed since the original NRL and NRL2 models, will advance knowledge and definition of an outlying irradiance data point.

As noted in Sections 5.3 and 6, initial manual monitoring of the Solar Irradiance Data Record, particularly of the input data sets, will ultimately lead to improved operational implementation of the Solar Irradiance Climate Data Record algorithm and confidence in the quality flagging.

8. References

Allen, C. W. 1981, Astrophysical Quantities (3d ed.; London: Athlone)

Brandt, P, N., M. Stix, M., and H. Weinhardt (1994). Modelling solar irradiance variations with an area dependent photometric sunspot index. *Solar Phys*. 152:119-124.

Clette, F. and L. Lefèvre (2016). The New Sunspot Number: Assembling All Corrections, *Solar Physics,* 291, https://doi.org/10.1007/s11207-016-1014-y.

Coddington, O., and J. Lean (2015), V02R00 Total Solar Irradiance and Solar Spectral Irradiance Climate Algorithm Theoretical Basis Document Coddington, CDRP-ATBD-0612, DSR-788.

Coddington, O., and J. Lean (2017), V02R01 Total Solar Irradiance and Solar Spectral Irradiance Climate Algorithm Theoretical Basis Document Coddington, CDRP-ATBD-0612, DSR-1171.

Coddington, O., P. Pilewskie, E. Richard, G. Kopp, J. Lean, D. Harber, E. Hartnett, and S. Beland (2013). TSIS Algorithm Theoretical Basis Document (ATBD).

Coddington, O., J. Lean, P. Pilewskie, M. Snow, and D. Lindholm (2016), A solar irradiance climate data record, *Bull. Amer. Meteor. Soc.*, doi:10.1175/BAMS-D-14-00265.1.

Coddington, O., Lean, J., Pilewskie, P., Snow, M., Richard, E., Kopp, G., et al. (2019). Solar Irradiance variability: comparisons of models and measurements. *Earth and Space Science*, 6, 2525–2555. https://doi.org/10.1029/2019EA000693

Coddington, O. M., Richard, E. C., Harber, D., Pilewskie, P., Woods, T. N., Chance, K., et al. (2021). The TSIS-1 Hybrid Solar Reference Spectrum. *Geophysical Research Letters*, 48, e2020GL091709. https://doi.org/10.1029/2020GL091709

Coddington, O. M., Richard, E. C., Harber, D., Pilewskie, P., Woods, T. N., Snow, M., et al. (2023). Version 2 of the TSIS-1 Hybrid Solar Reference Spectrum and extension to the full spectrum. *Earth and Space Science*, 10, e2022EA002637. https://doi.org/10.1029/2022EA002637

DeLand, M., & Marchenko, S. (2013). The solar chromospheric Ca and Mg indices from Aura OMI. *Journal of Geophysical Research: Atmospheres*, **118**, 3415–3423. https://doi.org/10.1002/jgrd.50310

Fontenla, J. M., White, O. R., Fox, P. A., Avrett, E. H., & Kurucz, R. (1999). Calculation of Solar Irradiance. I. Synthesis of the Solar Spectrum, *ApJ*, 518, 480, DOI 10.1086/307258

Fontenla, J. M., J. Harder, W. Livingston, M. Snow, and T. Woods (2011). High-resolution solar spectral irradiance from extreme ultraviolet to far infrared, *J. Geophys. Res.*, 116, D20108, doi:10.1029/2011JD016032.

Fröhlich, C., and J. Lean (2004). Solar irradiance variability and climate. *Astron. Astrophys. Rev*., 12 (4), 273-320, doi: 10.1007/s00159-004-0024-1

Győri, L., Baranyi, T., & Ludmány, A. (2011). Photospheric data programs at the Debrecen Observatory. Proc. Of the Intern. Astron. Union, 6, Symp. S273, https://doi.org/10.1017/S174392131101564X

Hall, J. C. and G. W. Lockwood (2004). The Chromospheric Activity and Variability of Cycling and Flat Activity Solar-Analog Stars. *Astrophys. J.*, 614:942, doi:10.1086/423926.

Harber, D., Castleman, Z., Drake, G., Van Dreser, S., Farber, N., Heuerman, K., Miller, M., et al. (2019). Compact total irradiance monitor flight demonstration. Proc. SPIE 11131, CubeSats and SmallSats for Remote Sensing III, 111310D https://doi.org/10.1117/12.2531308

Hoyt, D. V., and K. H Schatten (1993). A discussion of plausible solar irradiance variations, 1700-1992. *J. Geophys. Res*., 98.A11: 18895-18906.

Hoyt, D. V., & Schatten, K. H. (1998). Group sunspot numbers: A new solar activity reconstruction. *Solar Physics*, **181**(2), 491–512. https://doi.org/10.1023/A:1005056326158

Kopp, G., and J. L. Lean (2011). A new low value of Total Solar Irradiance: evidence and climate significance. *Geophys. Res. Lett*., 38, L01706, doi:10.1029/2010GL045777 2011

Kurucz, R.L. (1991). The solar spectrum. *The University of Arizona Press*, Tucson, pp. 663-669.

Lean, J., A. Skumanich, and O. R. White (1992). Estimating the Sun's Radiative Output During the Maunder Minimum. *Geophys. Res. Lett*., 19:1591-1495.

Lean, J., J. Beer, and R. Bradley (1995). Reconstruction of solar irradiance since 1610: Implications for climate change. *Geophys. Res. Lett*., 22:3195-3198.

Lean, J. L., G. J. Rottman, H. L. Kyle, T. N. Woods, J. R. Hickey, and L. C. Puga (1997). Detection and parameterization of variations in solar mid and near ultraviolet radiation (200 to 400 nm). *J. Geophys. Res*., 102:29939-29956.

Lean, J. L., J. Cook, W. Marquette, and A. Johannesson (1998). Magnetic modulation of the solar irradiance cycle. *Astrophys. J*., 492: 390-401.

Lean, Judith (2000). Evolution of the Sun's Spectral Irradiance since the Maunder Minimum. *Geophys. Res. Lett*., 27:2425-2428.

Lean, J. L., O. R. White, W. C. Livingston, and J. M. Picone (2001) Variability of a composite chromospheric irradiance index during the 11-year activity cycle and over longer time period. *J. Geophys. Res*., 106, 10,645-10,658.

Lean, J., Y.-M. Wang, and N. R. Sheeley, Jr. (2002). The effect of increasing solar activity on the Sun's total and open magnetic flux during multiple cycles; Implications for solar forcing of climate. *Geophys. Res. Lett*., 29, doi:10.1029/2002GL015880.

Lean, J., G. Rottman, J. Harder, and G. Kopp (2005). SORCE contributions to new understanding of global change and solar variability. *Solar Phys*., 230, 27-53, DOI: 10.1007/s11207-005-1527-2

Lean, J. L., and T. N. Woods (2010). Solar spectral irradiance measurements and models, in *Evolving Solar Physics and the Climates of Earth and Space*, Karel Schrijver and George Siscoe (Eds), Cambridge Univ. Press.

Lean, J. L., T. N. Woods, F. Eparvier, R. R. Meier and D. J. Strickland, Solar EUV Irradiance, Past, Present and Future (2011). *J. Geophys. Res*., 116, A01102, doi:10.1029/2010JA015901.

Lean, J. L., and M. T. Deland (2012). How does the Sun's spectrum vary? *J. Climate*, 25: 2555-2560, doi: http://dx.doi.org/10.1175/JCLI-D-11-00571.1.

Lean, J. L. (2018). Estimating solar irradiance since 850 CE. *Earth and Space Science*, 5, 133–149. https://doi.org/10.1002/2017EA000357.

Lean, J. L., Coddington, O., Marchenko, S. V., Machol, J., DeLand, M. T., & Kopp, G. (2020). Solar irradiance variability: Modeling the measurements. *Earth and Space Science*, 7, e2019EA000645. https://doi.org/10.1029/2019EA000645.

Lean, J. L., Coddington, O., Marchenko, S. V., & DeLand, M. T. (2022). A new model of solar ultraviolet irradiance variability with 0.1–0.5 nm spectral resolution. *Earth and Space Science*, 9, e2021EA002211. https://doi.org/10.1029/2021EA002211

Machol, J., Snow, M., Woodraska, D., Woods, T., Viereck, R., & Coddington, O. (2019). An improved lyman-alpha composite. *Earth and Space Science*, 6, 2263–2272. https://doi.org/10.1029/2019EA000648.

Mauceri, S., Pilewskie, P., Richard, E. *et al.* (2018). Revision of the Sun's Spectral Irradiance as Measured by SORCE SIM. *Sol Phys* **293**, 161. https://doi.org/10.1007/s11207-018-1379-1

Radick, R. R., G. W. Lockwood, B. A. Skiff, and S. L. Baliunas (1998) Patterns of Variation among Sun-like Stars. *Astrophys. J. Suppl*. 118:239 doi:10.1086/313135.

Richard E, Harber D, Drake G, Rutkowski J, Castleman Z, et al. 2019. Compact spectral irradiance monitor flight demonstration mission. In: Vol. **11131** of *Proc SPIE*: *CubeSats and SmallSats for Remote Sensing*, SPIE. p. 1113105. https://doi.org/10.1117/12.2531268.

Richard E, Harber D, Coddington O, Drake G, Rutkowski J, et al. 2020. SI-traceable spectral irradiance radiometric characterization and absolute calibration of the TSIS-1 spectral irradiance monitor (SIM). *Remote Sens* **12**, 1818. https://doi.org/10.3390/rs12111818.

Richard, E., O. Coddington, D. Harber, M. Chambliss, S. Penton, K. Brooks, et al. (2024). Advancements in solar spectral irradiance measurements by the TSIS-1 spectral irradiance monitor and its role for long-term data continuity, JSWSC, 14, 10. https://doi.org/10.1051/swsc/2024008.

Rottman, G. J. (2000). Variations of solar ultraviolet irradiance observed by the UARS SOLSTICE — 1991 to 1999. *Space Sci. Rev*., 94 (1-2), 83-91, DOI: 10.1023/A:1026786315718.

Rottman, G. J., J. Harder, J. Fontenla, T. Woods, O. R. White and G. M. Lawrence (2005). The Spectral Irradiance Monitor (SIM): Early observations. *Solar Phys*., 230:7-25, DOI: 10.1007/s11207-005-8112-6.

Schmidt, G. A., J. H. Jungclaus, C. M. Ammann, E. Bard, P. Braconnot, T. J. Crowley, G. Delaygue, F. Joos, N. A. Krivova, R. Muscheler, B. L. Otto-Bliesner, J. Pongratz1, D. T. Shindell, S. K. Solanki, F. Steinhilber, and L. E. A. Vieira (2011). Climate forcing reconstructions for use in PMIP simulations of the last millennium (v1.0). *Geosci. Model Dev*., 4:33–45, doi:10.5194/gmd-4-33-2011.

Skupin, J., M. Weber, H. Bovensmann, and J. P. Burrows (2004). The Mg II solar activity proxy indicator derived from GOME and SCIAMACHY. *Proceedings of the ENVISAT & ERS Symposium* (SP-572), ESA Publications Division.

Snow, M., W. E. McClintock, T. N. Woods, O. R. White, J. W. Harder, and G. Rottman (2005). The Mg II Index from SORCE, *Solar Phys.*, 230:325-344.

Snow, M. J., M. Weber, J. Machol, R. Viereck, and E. Richard (2014). Comparison of Magnesium II core-to-wing ratio observations during solar minimum 23/24. *Space Weather Space Clim*. **4**:A04, http://dx.doi.org/10.1051/swsc/2014001.

Svalgaard, L., Schatten, K.H. (2016). Reconstruction of the Sunspot Group Number: The Backbone Method. *Sol Phys* **291**, 2653–2684, https://doi.org/10.1007/s11207-015-0815-8

Tapping, K. F., D. Boteler, P. Charbonneau, A. Crouch, A. Manson, and H. Paquette (2007). Solar magnetic activity and total irradiance since the Maunder Minimum. *Sol. Phys*., 246,:309–326, doi:10.1007/s112070079047x.

Tapping, K. F., (2013) The 10.7 cm solar radio flux ($F_{10.7}$). *Space Weather*, **11**, 394-406, doi:10.1002/swe.20063.

Thuillier, G., M. Hersé, P. C. Simon, D. Labs, H. Mandel, D. Gillotay, and T. Foujols (1998). The visible solar spectral irradiance from 350 to 850 nm as measured by the SOLSPEC spectrometer during the ATLAS I mission. *Solar Phys.,* 177:41-61.

Thuillier, G., Melo, S. M. L., Lean, J. L, Krivova, N. A., Bolduc, C., Fomichev, V. I., Charbonneau, P., Shapiro, A. I., Schmutz, W., and Bolsée, D. (2013). Analysis of Different Solar Spectral Irradiance Reconstructions and Their Impact on Solar Heating Rates. *Solar Phys*., DOI 10.1007/s11207-013-0381-x.

Unruh, Y.C., S. K. Solanki, and M. Fligge (2000). Modelling solar irradiance variations: Comparison with observations, including line-ratio variations. *Space Sci. Rev.*, 94 (1-2):145-152, DOI: 10.1023/A:1026758904332.

Usoskin, I.G., Kovaltsov, G.A., Lockwood, M. *et al.* (2016). A New Calibrated Sunspot Group Series Since 1749: Statistics of Active Day Fractions. *Sol Phys* **291**, 2685–2708, https://doi.org/10.1007/s11207-015-0838-1

Wang, Y.-M., J. L. Lean, and N. R. Sheeley, Jr. (2005). Modeling the Sun's magnetic field and irradiance since 1713. *Astrophys. J.*, 625:522–538.

Wang, Y.-M., and J. L. Lean, (2021), A New Reconstruction of the Sun's Magnetic Field and Total Irradiance since 1700, *Astrophys. J.*, 920, DOI 10.3847/1538-4357/ac1740.

White, M., Heuerman, K., Shaw, P. S., Stephens, M. S., Tomlin, N. A., Yung, C., Lehman, J., Rice, J., Rutkowski, J., & Straatsma, C. (2022). Decadal validation of the LASP TRF cryogenic radiometer by NIST, and establishment of a replacement room temperature standard, Metrologia, 59, https://doi.org/10.1088/1681-7575/ac89f5

Woods, T. N., S. M. Bailey, F. G. Eparvier, G. M. Lawrence, J. Lean, W. E. McClintock, R. G. Roble, G. J. Rottman, S. C. Solomon, W. K. Tobiska, and O. R. White (2000), The TIMED solar EUV experiment, *Physics and Chemistry of the Earth, Part C: Solar, Terrestrial & Planetary Science*, *25*, 5-6, 393-396, doi:10.1016/S1464-1917(00)00040-4.

Woods, T. N., P. C. Chamberlin, J. W. Harder, R. A. Hock, M. Snow, F. G. Eparvier, J. Fontenla, Wi. E. McClintock, and E. C. Richard (2009). Solar irradiance reference Spectra (SIRS) for the 2008 Whole Heliosphere Interval (WHI), *Geophys. Res. Lett.,* 36, L01101, doi:10.1029/2008GL036373.

Appendix A. Acronyms and Abbreviations

Acronym or Abbreviation	Meaning
λ	Lambda; wavelength (nm)
μ	Heliographic position
ACRIM	Active Cavity Radiometer Irradiance Monitor
C-ATBD	Climate Algorithm Theoretical Basis Document
Ca K	Calcium K Fraunhofer line in the solar spectrum
CDR	Climate Data Record
F(t)	Facular Brightening Function (time-dependent)
F10.7	Solar radio flux at 10.7 cm
GOME	Global Ozone Monitoring Experiment
GOME-2	Global Ozone Monitoring Experiment 2
I(t)	Solar Spectral Irradiance (time-dependent)
I_Q	Solar Spectral Irradiance of the Quiet Sun
ISS	International Space Station
LASP	Laboratory for Atmospheric and Space Physics
LaTiS	Formerly LASP Time Series Server, no longer an acronym
LISIRD	LASP Interactive Solar Irradiance Data Center
m	meter
Mg II	Magnesium II index
MDI	Michelson Doppler Imager
NCEI	National Centers for Environmental Information
NCDC	National Climatic Data Center
netCDF4	Network Common Data Format
NIMBUS	Series of NASA satellites, first launched in 1964; NIMBUS-7 was the last in the series.
NOAA	National Oceanographic and Atmospheric Administration
NGDC	NOAA National Geophysical Data Center
NNL	NASA NOAA LASP
NNLTSI1	NASA NOAA LASP Total Solar Irradiance model
NNLSSI1	NASA NOAA LASP Solar Spectral Irradiance model
NNLSSI1h	NASA NOAA LASP Solar Spectral Irradiance model – High resolution

NRL	Naval Research Laboratory
NRLSSI	Naval Research Laboratory Solar Spectral Irradiance model (original)
NRLSSI2	Naval Research Laboratory Solar Spectral Irradiance model (version 2, this C-ATBD)
NRLTSI	Naval Research Laboratory Total Solar Irradiance model (original)
NRLTSI2	Naval Research Laboratory Total Solar Irradiance model (version 2, this C-ATBD)
nm	nanometer
NOAA	National Oceanic and Atmospheric Administration
PMOD	Physikalisch-Meteorologisches Observatorium Davos
ppm	Part per million
QA	Quality Assurance (Analysis)
R	Radiance
S(t)	Sunspot Darkening Function (time-dependent)
SCIAMACHY	Scanning Imaging Absorption SpectroMeter for Atmospheric ChartographY
SIM	Spectral Irradiance Monitor
SMM	Solar Maximum Mission
SOHO	Solar and Heliospheric Observatory
SOLSPEC	SOLar SPECtral Irradiance Measurements; French instrument that measured irradiance from the ISS
SOLSTICE	Solar Stellar Intercomparison Experiment
SOON	Solar Observing Optical Network (US Air Force)
SORCE	Solar Radiation and Climate Experiment
SRF	Spectral Radiometer Facility (LASP)
SSD	Space Science Division (Naval Research Laboratory, Washington, DC)
SSI	Solar Spectral Irradiance
STARA	Sunspot Tracking and Recognition Algorithm
T(t)	Total Solar Irradiance (time-dependent)
T_Q	Total Solar Irradiance of the Quiet Sun
TCTE	TSI Transfer Calibration Experiment
TIM	Total Irradiance Monitor
TRF	TSI Radiometer Facility (LASP)

TSI	Total Solar Irradiance
TSIS	Total and Spectral Solar Irradiance Sensor
UARS	Upper Atmosphere Research Satellite
USAF_MWL	US Air Force Mount Wilson Observatory
UV	ultraviolet
W	Watt